Title
Chlamydia trachomatis effectors specifically modulate the landscape of the host cell: Dre1 interacts with dynactin to reposition host organelles during infection.

Author
Sherry, Jessica Lynne

Publication Date
2021

Chlamydia trachomatis effectors specifically modulate the landscape of the host cell: Dre1 interacts with dynactin to reposition host organelles during infection.

by
Jessica Sherry

DISSERTATION
Submitted in partial satisfaction of the requirements for degree of
DOCTOR OF PHILOSOPHY

in

Cell Biology

in the

GRADUATE DIVISION
of the
UNIVERSITY OF CALIFORNIA, SAN FRANCISCO

Approved:

DocuSigned by:
Shaeri Mukherjee
7AA908684B40471...

Shaeri Mukherjee

Chair

DocuSigned by:
Joanne Engel

Joanne Engel

DocuSigned by:
Anita Sil
DocuSigned by:

Anita Sil

DocuSigned by:
Adam Frost
2BFC3B4CEA6C478...

Adam Frost

Committee Members

For Mom and Dad,

I carry you with me in all I do.

Thank you.

ACKNOWLEDGEMENTS

I have had the unbelievable privilege of being surrounded by amazing people throughout my life, and I am filled with gratitude for the unconditional support I have received. All of the best parts of me come from the people around me; I am truly indebted.

I must first thank Joanne Engel for being an extraordinary mentor and role model. She is a fierce supporter of her trainees, and has worked hard to build an incredibly bright and supportive community of scientists in her lab and in her department. I deeply admire her drive, her sharp mind, and her ability to rise to any challenge. I thank her for helping me grow as a scientist and find confidence in myself. The Engel lab will always be the first place where I felt like a scientist.

I thank the members of the Engel lab, past and present, for somehow always giving me exactly what I need (whether that's a listening ear or a kick in the pants). I have so many perfect memories and can't imagine sharing this experience with any other group of people. Cheri, Kat, Yuki, Henriette, Khavong, Clara, Ramiro, Ellie, Cindy, and Travis – their friendship and guidance has meant everything to me. I also thank Carol for keeping the lab running and for bringing sunshine to even the foggiest SF days. I especially want to thank Cheri for being Ultimate Best; her unwavering support gave me the courage I needed to climb the steepest sections of graduate school. There aren't words for the gratitude and love I feel.

My thesis committee Shaeri Mukherjee, Anita Sil, and Adam Frost have inspired me in many ways. Throughout my projects, they provided the perfect mix of excitement and critical thinking, and demonstrated their investment in my development as a scientist and a person. Shaeri brought an infectious curiosity to our meetings, and always took the time to both ask the hard questions and work with me to answer them. Anita's patience and genuine kindness helped me feel strong enough to ask myself the hard questions. Adam's excitement reminded me, in the toughest moments, of the joy there is in shining light on the still dark corners of our world.

Other UCSF members who were invaluable guides throughout my project include: Sophie Dumont, who dove into a brand-new field of biology in order to be able to help me when I needed advice, and who was just as generous with sharing reagents as she was sharing her time and expertise; Rick McKenney, who helped me learn about motor proteins for quals and has been a part of my project as long as I have; Robyn Kaake, who has enthusiastically helped me build a whole second project and a team of amazing collaborators; and the 4th Floor MPHD crew, who have been insightful science sounding boards, co-conspirators during grad student "unhappy hours", and have always been down to participate in freezer-thaw snowball fights late at night.

Graduate school brought me some of the most rewarding and sincere friendships of my life. Han and Susan, who introduced me to the Bay Area, fed me ridiculous quantities of food, wore matching animal onesies with me while we creeped ourselves to sleep, and who suffered through me attempting to explain every meme I came across, will always

be my roomies-of-the-heart. From crying in the Parnassus cafeteria during quals, to adventuring across the bay in search of baby goats, to struggling through genetics (cell bio ftw!); from being way too invested in a neighborhood noodle shop, to supporting my long-distance running habit with lots of pickles, from monthly pilgrimages to Fort Funston, to being there through every low and sharing the joy of every win, Alex, Noah, Han, Anne, and Susan have become family. Rachel has kept me sane through precision meme-sharing, has kept me from using way too many exclamation points in emails, and is an unparalleled champion at pouring a sucrose gradient. Down-hill runs and watching cheesy holiday movies with Pallavi brought me joy through the hard times. I am also truly thankful for the friendship and memories shared with Frances, Dan, Leeanne, Melanie, Delsy, Kevin, Betsy, Jade, Sumitra, and Allison.

Raphael Valdivia and his research group at Duke University have been generous, creative and supportive advisors and collaborators at different stages of my project. I especially would like to thank Lee Dolat, Robert Bastidas, and Anusha Gopalakrishnan both for helping me with experiments, but also for their exuberance and kindness – they make the Chlamydia research community the wonderful, welcoming place that it is.

There have been many mentors along the way that have helped me discover my love for science, and have fostered my curiosity. I would like to acknowledge the teachers at Sand Creek and Colonie Central High, especially Mr. Cat, Mr. Collins, Mrs. Gerlach, Mrs. LaBrake, and Mr. Kach. I would particularly like to thank Jay Goldberg, whose perfect mix

of sarcasm and enthusiasm for science inspired me to care a little less about grades and a lot more about the rewards of asking the kinds of questions that are not yet answered.

From Wesleyan, I must thank David Beveridge, who encouraged me to apply to UCSF; Amy MacQueen for inspiring my on-going love for microscopy; and Andrea Roberts, who infused STEM education at Wesleyan with joy and gave me the opportunity share that joy with my own mentees. For his mentorship, and for giving me the opportunity to take on my first independent research project, I must thank Fred Cohan. In my own research career, I can only hope to emulate his sincere delight in science, his omnivorous hunger for knowledge, his kindness and optimism, and his desire to use his expertise to fight for positive change in the world.

I am indescribably grateful for the people in my life who keep me whole: Sarah, Nicole, Nellie, Chris, Karley, Rosie, Chloe, Julia, Ceili, Hannah, Bryan, Jamie, Sammy K., Cassie, Joy, Jenna, Katlin, Amy, Mike R., Sheila, Brian, Jess, and Alysia. Thank you for always being there – so much of my strength comes from your friendship.

I do not think that it is possible to describe how much my family means to me. Their unconditional love, unremitting joy, and unfaltering support keep me aloft. They are the magic. They are the foundation. They taught me how to laugh when the lights go out, how to fight when it feels too hard, how to dance and stay warm in the cold, how to build a rocket ship, how to find beauty in everything, and how to be curious. They are my courage and my reason.

I thank Kevin, Meg, and Ronan for being an oasis during the hardest parts of grad school, and for bringing me an abundance of family, philosophy, adventures, and delicious food. I thank: Nina for reminding me to use my imagination; Jenny for showing me how to balance grace, courage, and humor; Barbara for giving me the keys to The Land of the Great Beyond, for her compassion and altruism, and for nurturing my curiosity; Alex for showing me how to do an Ollie and reminding me to not be too grounded; Graham for racing hurricanes for me and for always being up for an adventure. I thank my brother, Michael, for being a safe port in a storm, for understanding and appreciating even my strangest quirks, for his loyalty and sense of humor, and for loving me even when I'm prickly. I thank my grandmother, Sarah, for showing me how to achieve the unexpected, how to find poetry and adventure at every turn, how to never lose one's thirst for knowledge, how to weather the most turbulent storms, and most importantly, how to find the sunshine hidden on the other side of the clouds. I carry her stories and songs in my heart, and they bring me comfort when I most need it.

I am forever grateful for my parents, Tami and Robert. I would not be anywhere without them. They have been at my side through it all, supporting me, fostering my independence and curiosity, teaching me how to dream and how to be a good person, introducing me to reading and putting distant worlds within reach, doing whatever they could to bring their family happiness, and making impossible things possible. As they have carried me in loving arms these many years so that I never feared hitting the ground, I carry them with me, always. Thank you.

STATEMENT REGARDING AUTHOR CONTRIBUTIONS

Chapter 2 is a manuscript draft intended for publication:

Jessica Sherry, Lee Dolat, Eleanor McMahon, Danielle Swaney, Robert Bastidas, Jeffrey Johnson, Raphael Valdivia, Nevan Krogan, Cherilyn Elwell, Joanne Engel. *Chlamydia trachomatis* effector Dre1 interacts with dynactin to reposition host organelles during infection. Submitted to biorxiv.

I conceived, designed, and performed the experiments and wrote the manuscript under the guidance of Joanne Engel. Lee Dolat performed the mouse infections. Eleanor McMahon assisted with preparing infected samples for Mass Spectrometry (MS). Danielle Swaney and Jeffrey R Johnson ran the MS samples, and Danielle Swaney performed analysis on the resulting data set.

Chapter 3 is unpublished work using cross-linking Mass Spectrometry (MS) and cryo-electron microscopy (EM) to identify where Dre1 binds within the dynactin complex, and whether this complex differs structurally from published cryo-EM structures of dynactin. I conceived and designed the experiments described under the guidance of Robyn Kaake (UCSF) and Joanne Engel (UCSF). I performed the Dre1:dynactin purifications, the *C. trachomatis* infections, and the experiments involving in-vivo cross-linking. Robyn Kaake performed the chemical cross-linking, prepared samples for MS, and analyzed the resulting data sets. Komal Pawar (UCSF) and Kliment Verba (UCSF) assisted with the cryo-EM experiments and analysis of the resulting data.

Chapter 4 contains a reprint of an *Antimicrobial Agents and Chemotherapy* article:

Hanh Lam, Tannia Lau, Adam Lentz, Jessica Sherry, Alejandro Cabrera-Cortez, Karen Hug, Annalyse Lalljie, Joanne Engel, R. Scott Lokey, Victoria Auerbach. (2021). Developing Cyclic Peptomers as Broad-Spectrum Type III Secretion System Inhibitors in Gram-Negative Bacteria. Vol. 65, No. 7: e01690-20.

Hanh Lam conceived, designed, and performed the majority of the biological experiments and drafted the manuscript under guidance of Victoria Auerbach. Tannia Lau was responsible for the chemical aspects of the work. Adam Lentz assisted with biological experiments. I conceived, designed, and performed the biological experiments relevant to *Chlamydia trachomatis*, and I revised the sections of the manuscript relevant to *C. trachomatis*. For the paper, I contributed Figures 4.8A, 4.8B, and 4.8C. Karen Hug and Annalyse Lalljie both assisted with biological experiments and data analysis. I authored the original section of this thesis chapter detailing future directions for this project; I designed and performed the experiments to select *C. trachomatis* mutants resistant to a novel type III secretion system inhibitor under the guidance of Victoria Auerbach and Joanne Engel.

ABSTRACT

C. trachomatis effectors specifically modulate the landscape of the host cell.

Jessica Sherry

This thesis presents work toward understanding how the obligate intracellular pathogen, *Chlamydia trachomatis,* modulates the host cell to establish a protected replicative niche. In order to evade host-cell innate immune surveillance, internalized *Chlamydia* develop within a membrane-bound compartment referred to as the inclusion. Given that *C. trachomatis* relies on host-cell derived nutrients and energy, this bacterial pathogen must avoid globally inhibiting host-cell function while building what is essentially a novel organelle. Through strategic deployment of effectors into the host cytosol and inclusion membrane, *C. trachomatis* actively remodels host-cell structures from within the inclusion. This enables the bacteria to obtain the required metabolites and regulate specific organelle functions. This work focuses on: understanding which host proteins and cellular structures are repositioned around the growing inclusion; identifying which bacterial effectors are responsible for these modifications; and elucidating the mechanisms by which *C. trachomatis* calibrates organelle function to divert specific resources to the replicating bacteria while maintaining host viability.

Previously, we identified several host proteins recruited to the inclusion membrane through interactions with specific *C. trachomatis* inclusion membrane-localized effectors (Incs) and characterized alterations to the host ubiquitin landscape induced by infection. Until recently, the host targets of only a few Incs had been identified. We utilized high-

throughput affinity purification-mass spectrometry to comprehensively define the Inc-human protein interactome, and discovered putative binding partners for 38/58 of the predicted *C. trachomatis* Incs. Using confocal immunofluorescence microscopy, we screened ~200 of the 335 identified high-confidence Inc-human protein-protein interactions for localization at the inclusion membrane, and we identified the recruitment of many host proteins involved in host processes consistent with *Chlamydia's* intracellular life cycle. Thus, *Chlamydia* effectors recruit distinct subsets of host proteins to the inclusion, and mediate precise changes to the landscape of the host cell.

In the first project, we characterized an interaction between the host dynactin complex, and the *C. trachomatis* Inc CT192, hereafter named Dre1 for Dynactin Recruiting Effector 1 (Chapter 2). In eukaryotes, dynactin is a ubiquitous and multifunctional protein complex that modulates the activity of the microtubule motor, dynein, at many different cellular structures. Using a combination of confocal immunofluorescence microscopy and biochemistry, we show that dynactin is recruited to the inclusion by Dre1 and that the Dre1:dynactin interaction modulates the positioning of specific host organelles, including the centrosome, mitotic spindle, and Golgi Apparatus around the inclusion. Deletion of Dre1 resulted in decreased *C. trachomatis* fitness in cell-based assays and in a mouse model of infection. By targeting particular functions of the host dynactin complex, Dre1 facilitates re-arrangement of specific organelles around the growing inclusion. Thus, *C. trachomatis* employs a single effector to evoke large-scale changes in host cell organelle organization.

In the second project, I describe my pilot work using cross-linking mass spectrometry and cryo-electron microscopy to physically map the interaction between Dre1 and the host dynactin complex (Chapter 3). We report preliminary evidence that Dre1 binds along the Arp1 filament of the dynactin complex. Typically, the Arp1 filament mediates interactions with dynein and various adaptors that enhance processivity or specify cargo-binding of this tripartite complex. Given that Dre1 binds at this same position, we believe that further structural resolution will reveal the mechanism by which Dre1 is able to target particular functions or regulatory states of this omnipresent and versatile protein complex.

In the third project, I describe my contributions to identifying a novel inhibitor of the type III secretion system, and show that *C. trachomatis*' ability to assemble secretion machinery is essential for virulence (Chapter 4). The type III secretion system is a highly conserved, needle-like apparatus that many diverse pathogens use to inject effector proteins into the host cytosol. First identified through its inhibition of the *Yersinia pestis* type III secretion system, 4EpDN is a compound that appears to have broad efficacy against evolutionarily distant injectisome type III secretion systems. This compound does not, however, target the *Salmonella* flagellar type III secretion system, indicating that 4EpDN specifically inhibits injectisome type III machinery. As an obligate intracellular pathogen, *C. trachomatis* is absolutely reliant on its injectisome type III secretion system to build the inclusion within the hostile environment of the host cytosol. We show that 4EpDN inhibited *C. trachomatis* progeny production and reinfection, but not initial inclusion formation. This suggests that 4EpDN prevents assembly of *de novo* type III secretion machinery over the course of the *Chlamydial* intracellular life cycle, but does

not inhibit secretion by the assembled type III injectisomes that were pre-packaged in the bacteria prior to exposure to 4EpDN. We then utilized *Chlamydia's* requirement for the type III secretion system to apply strong selective pressure to bacteria passaged in the presence of 4EpDN at MIC90 and isolate resistant mutants. We are currently sequencing mutants that escaped inhibition to determine the genes involved in resistance and to elucidate the mechanism by which 4EpDN targets injectisome type III secretion systems. As antibiotic-resistant bacteria are an emerging global health threat, new antimicrobials are urgently needed. Understanding how this compound targets the injectisome of multiple pathogens may help with the generation of novel therapeutics to treat recalcitrant infections.

Together, this thesis work illustrates the importance of *C. trachomatis* effectors in constructing and maintaining infection in host cells, as well as the importance of *Chlamydia's* ability to specifically modulate host functions that support bacterial growth without globally altering host fitness. The interdisciplinary nature of this work, which spans high-resolution microscopy, cell biology, chemistry, biochemistry, genetics, microbiology, and structural analysis, has revealed exciting insights into how *C. trachomatis* successfully establishes its intracellular replicative niche.

TABLE OF CONTENTS

LIST OF FIGURES AND TABLES

CHAPTER 2

CHAPTER 3

CHAPTER 4

CHAPTER ONE

INTRODUCTION

“The truth is we don’t know what we don’t know.
We don’t even know the questions we need to ask in order to find out,
But when we learn one tiny little thing, a dim light comes on in a dark hallway,
And suddenly a new question appears.
We spend decades, centuries, millennia,
trying to answer that one question so that another dim light will come on.
That’s science, but that’s also everything else, isn’t it?
Try. Experiment. Ask a ton of questions.”
- Yaa Gyasi

Most dangerous microorganisms that infect mammals are neutralized by a combination of innate and adaptive immune responses. Over time, certain pathogens have developed and refined strategies to replicate within the cells of host organisms as a mechanism to avoid immune surveillance. However, the intracellular environment is not free of threats to a developing pathogen. Intracellular pathogens often exhibit parasitic lifestyles, relying on host resources to survive as larger fractions of their genome become dedicated to modulating the hostile intracellular environment of the host cell.

Host cell immune surveillance mechanisms include the activity of toll-like receptors and other pattern recognition receptors (PRRs) that recognize pathogen-associated molecular pattern molecules (PAMPs) such as lipopolysaccharide and peptidoglycan. Detection of PAMPs leads to activation of varied signaling pathways that typically lead to cell death via apoptosis or engulfment of the threat via autophagy and subsequent fusion of the autophagosome with degradative compartments (i.e. the lysosome) (Mogensen, 2009). In order to escape detection by their host cell, intracellular pathogens have developed multiple strategies to subvert these innate immune responses.

Many intracellular pathogens harness or mimic the endocytic machinery of the host cell to facilitate invasion and are internalized through actin-mediated processes that ultimately lead to envelopment of the microbe within a membrane-bound compartment (Walpole & Grinstein, 2020). Some pathogens, for example the bacteria *Rickettsia* and *Listeria*, lyse this compartment and reside within the cytosol, where they have developed mechanisms to specifically activate anti-viral innate immune responses that have an adverse effect on

the anti-bacterial immune responses, thus leaving the host more susceptible to lethal infection (Demiroz et al., 2021). Other pathogens, including *Mycobacterium*, *Legionella*, *Salmonella*, *Coxiella*, *Toxoplasma*, *Anaplasma*, and *Chlamydia* reside within their membrane-bound compartments (Moore & Ouellette, 2014). This compartment shelters encapsulated pathogens from detection by PRRs, however, it also provides a physical barrier separating the microbes from nutrients available in the host cell. To maintain access to these nutrients and to promote their growth and development, pathogens evolved strategies to specifically modify this compartment.

As intracellular pathogens have co-evolved with their host cells, often over the course of hundreds of millions of years, many have lost the ability to grow outside of their host cells (Fields et al., 2011). These obligate intracellular bacteria require a viable host cell to obtain metabolites necessary for development and ultimately transmission to a new host cell, and therefore, must employ specificity in modulating and exploiting host cell functions. Examples of obligate intracellular pathogens include *Chlamydia*, *Rickettsia*, and *Coxiella* (McClure et al., 2017). Despite the absolute reliance on host cells for growth, this class of pathogens has evolved distinct strategies that allow for colonization and spread throughout diverse tissues and cell types (Fields et al., 2011). Though infections with obligate intracellular pathogens may not be initially detrimental to the host cell, chronic or recurrent infections can lead to immune responses that damage tissues and that cause systemic health issues (Moore & Ouellette, 2014).

Chlamydiae are Gram-negative, obligate intracellular pathogens that are symbionts of varied organisms ranging from humans to amoebae (Bachmann et al., 2014). The Chlamydiaceae family is the best-characterized group in the Chlamydiae phylum, and it comprises 11 species that are pathogenic to humans or animals (Elwell et al., 2016). Some species that infect animals can be transmitted to humans (Bennett et al., 2020). *Chlamydia trachomatis* and *Chlamydia pneumoniae* are the major species that infect humans and are responsible for a wide range of diseases (Bennett et al., 2020; Malhotra et al., 2013). *C. pneumoniae* causes respiratory infections that account for ~10% of community-acquired pneumonia. It is linked to a number of chronic diseases including asthma, atherosclerosis, and arthritis (Bachmann et al., 2014; Bennett et al., 2020). Strains of *C. trachomatis* are divided into three biovars, which are defined as strain variants that differ physiologically and/or biochemically from other strains of a given species. The trachoma biovar infects the conjunctiva and is the leading cause of non-congenital blindness in developing nations. The urogenital tract biovar is the most prevalent sexually transmitted bacterium. In women, nearly 80% of genital tract infections are asymptomatic; however, 15-40% ascend to the upper genital tract, where they can lead to serious sequelae, including pelvic inflammatory disease, infertility, and ectopic pregnancy (Malhotra et al., 2013). The lymphogranuloma venereum (LGV) biovar causes more aggressive infections that are capable of disseminating to regional lymph nodes and causing more systemic disease (de Vrieze & de Vries, 2014). Infection with *C. trachomatis* also facilitates the transmission of HIV, and has recently been associated with cervical and ovarian cancers (Malhotra et al., 2013; Smith et al., 2004; Zhu et al., 2016). Thus, *Chlamydia* spp. are important causes of human disease, and while

infections are treatable with antibiotics, no effective vaccine currently exists (Murthy et al., 2014).

In this work we focus on how *C. trachomatis*, an important public health threat, establishes a replicative niche within in the human cell. Despite its reduced genome size (Bachmann et al., 2014), *C. trachomatis* encodes a large number of effector proteins that are secreted into the host cytosol through the needle-like, type III secretion system. To understand how *C. trachomatis* utilizes this arsenal of effectors, we performed an affinity-purification mass spectrometry screen (AP-MS) to identify host targets of these effectors (Mirrashidi et al., 2015). We then determined which of these host targets were re-localized upon *C. trachomatis* infection. We demonstrate that certain host proteins exhibited large localization changes upon infection including proteins involved in vesicle trafficking and lipid acquisition (e.g. Syntaxin 18, Sorting Nexins 5 and 6, sphingomyelin synthetase, and dynactin), though most proteins were not grossly re-localized during infection. Furthermore, we identified a number of effectors targeted host proteins involved in ubiquitylation pathways. Ubiquitylation is a post-translational modification that allows mechanistically diverse, reversible, and quantitative regulation of protein abundance, localization, and/or activity (Rape, 2018). Cellular processes modulated by ubiquitylation include proliferation, migration, PRR signaling, membrane trafficking, autophagy, as well as many others. We performed preliminary Ubiquitin Remnant Profiling (URP) to identify host proteins differentially ubiquitylated by *C. trachomatis* infection and to characterize how this pathogen alters the ubiquitin landscape of the host cell. We saw that, in terms of both host target re-localization and ubiquitylation, *C. trachomatis* effectors exhibit specific

effects, rather than global alterations that would affect host-cell viability. This is consistent with the notion that *C. trachomatis* requires a largely functional host cell in which to proliferate.

Our AP-MS screen identified an interaction between the *C. trachomatis* effector CT192 (homolog of CTL0444; hereafter referred to as Dre1) and the host dynactin complex (Mirrashidi et al., 2015). The 11-subunit dynactin complex is an essential cofactor for the primary microtubule (MT)-based retrograde motor, dynein, which transports cellular cargo (Reck-Peterson et al., 2018). Dynactin also localizes at the Golgi and centrosomes, where it anchors and organizes MTs (Corthésy-Theulaz et al., 1992; Rios, 2014; Sanchez & Feldman, 2017). At the centrosome dynactin also plays a role in positioning the spindle during cell division (Okumura et al., 2018). Using isogenic *C. trachomatis* mutant strains, we show that dynactin is recruited to the membrane-bound compartment encapsulating the bacteria (referred to as the inclusion) in a Dre1-dependent manner (Chapter 2). Furthermore, Dre1 appears to target specific sub-populations of dynactin (Chapter 2). We demonstrate that the Dre1-dynactin interaction is required for centrosome and Golgi recruitment to the inclusion, positioning of the inclusion at spindle poles during host cell division, and virulence in a murine model of upper genital tract infection (Chapter 2). These results suggest that the interaction between Dre1 and dynactin is critical for the *C. trachomatis* intracellular life cycle, and serves to modulate the positioning of specific host organelles to facilitate development of the *C. trachomatis* inclusion.

To understand the mechanism by which Dre1 targets specific dynactin functions or regulatory states, we designed cross-linking mass spectrometry experiments and mapped the interaction surface between Dre1 and dynactin (Chapter 3). We show that the C-terminus of Dre1 mediates binding to the actin-like filament of dynactin made up of eight Arp1 monomers (Chapter 3). Dynactin, dynein, and associated adaptor proteins interface with one another along the length of this filament (Urnavicius et al., 2015). An attractive hypothesis is that Dre1 binds the Arp1 filament to monitor the composition or structure of various dynactin-containing complexes. Dre1 might bind Arp1 to stabilize dynactin in complex with particular adaptors, or it may preferentially bind dynactin not associated with adaptors. Dre1 might also replace an adaptor to form a tripartite complex with dynein. Given that no known adaptors co-purify with Dre1 (Chapter 2, Mirrashidi et al., 2015), we favor the latter two models. Future cryo electron microscopy (cryo EM) and *in vitro* processivity studies will be aimed at determining if the addition of Dre1 to dynactin-dynein complexes alters their structure, activity, or associated binding partners in any way.

Together, these finding highlight how a single *C. trachomatis* effector, Dre1, targets specific sub-populations of a ubiquitous and multifunctional host protein complex in order to restructure particular organelles around the growing inclusion during infection. Combined with future structural studies, this work provides a blueprint for how pathogen effectors employ selectivity in modulating host proteins and processes in order to integrate the *C. trachomatis* inclusion within existing host cell pathways and processes and preserve host viability.

Given that *C. trachomatis* replicates within a membrane bound compartment, secreted effectors play an outsize role in the ability of this pathogen to modulate the host cell and acquire nutrients. *Chlamydiae* devote ~10% of their genome to virulence effectors (Betts-Hampikian & Fields, 2010). These effectors are delivered through specialized secretion systems to the bacterial surface (type V), to the inclusion lumen (type II), or to the host cytosol by the type III secretions system (T3SS) (Fields, 2014). During *C. trachomatis* infection, the T3SS enables the direct injection of bacterial effectors into the host cytosol at various stages of infection. In this work we identified a cyclic peptomer that inhibits T3SS from a broad range of Gram-negative bacteria including *Yersinia*, *Salmonella*, and *Chlamydia*. We provide evidence that this compound prevents T3SS assembly (Chapter 4, Lam et al., 2021). We leveraged *C. trachomatis'* absolute requirement of the T3SS during infection to passage bacteria in the presence of this compound and isolate resistant mutants (Chapter 4). In future work, we will sequence these mutants to identify genes that mediate resistance, which will shed light on the compound's mechanism of action.

Overall, this thesis work demonstrates the importance of *C. trachomatis* effectors in establishing and maintaining infection in host cells, as well as the importance of employing selectivity in modulating host functions to support microbial growth while maintaining host fitness. Understanding how this medically important pathogen specifically targets host cell processes in order to survive the intracellular environment and to cause disease may shed light on the pathology of human infections and eventually, lead to the generation of desperately needed therapeutics.

REFERENCES

Bachmann, N. L., Polkinghorne, A., & Timms, P. (2014). Chlamydia genomics: Providing novel insights into chlamydial biology. *Trends in Microbiology*, *22*(8), 464–472. https://doi.org/10.1016/j.tim.2014.04.013

Bennett, J. E., Dolin, R., & Blaser, M. J. (Eds.). (2020). *Mandell, Douglas, and Bennett's principles and practice of infectious diseases* (Ninth edition). Elsevier.

Betts-Hampikian, H. J., & Fields, K. A. (2010). The Chlamydial Type III Secretion Mechanism: Revealing Cracks in a Tough Nut. *Frontiers in Microbiology*, *1*, 114. https://doi.org/10.3389/fmicb.2010.00114

Corthésy-Theulaz, I., Pauloin, A., & Pfeffer, S. R. (1992). Cytoplasmic dynein participates in the centrosomal localization of the Golgi complex. *Journal of Cell Biology*, *118*(6), 1333–1345. https://doi.org/10.1083/jcb.118.6.1333

de Vrieze, N. H. N., & de Vries, H. J. C. (2014). Lymphogranuloma venereum among men who have sex with men. An epidemiological and clinical review. *Expert Review of Anti-Infective Therapy*, *12*(6), 697–704. https://doi.org/10.1586/14787210.2014.901169

Demiroz, D., Platanitis, E., Bryant, M., Fischer, P., Prchal-Murphy, M., Lercher, A., Lassnig, C., Baccarini, M., Müller, M., Bergthaler, A., Sexl, V., Dolezal, M., & Decker, T. (2021). Listeria monocytogenes infection rewires host metabolism with regulatory input from type I interferons. *PLOS Pathogens*, *17*(7), e1009697. https://doi.org/10.1371/journal.ppat.1009697

Elwell, C., Mirrashidi, K., & Engel, J. (2016). Chlamydia cell biology and pathogenesis. *Nature Reviews Microbiology*, *14*(6), 385–400. https://doi.org/10.1038/nrmicro.2016.30

Fields, K. A. (2014). Protein Secretion and *Chlamydia* Pathogenesis. In M. Tan & P. M. Bavoil (Eds.), *Intracellular Pathogens I* (pp. 192–216). ASM Press. https://doi.org/10.1128/9781555817329.ch9

Fields, K. A., Heinzen, R. A., & Carabeo, R. (2011). The Obligate Intracellular Lifestyle. *Frontiers in Microbiology*, *2*. https://doi.org/10.3389/fmicb.2011.00099

Lam, H. N., Lau, T., Lentz, A., Sherry, J., Cabrera-Cortez, A., Hug, K., Lalljie, A., Engel, J., Lokey, R. S., & Auerbuch, V. (2021). Developing Cyclic Peptomers as Broad-Spectrum Type III Secretion System Inhibitors in Gram-Negative Bacteria. *Antimicrobial Agents and Chemotherapy*, *65*(7), e0169020. https://doi.org/10.1128/AAC.01690-20

Leon-Sicairos, N., Reyes-Cortes, R., Guadrón-Llanos, A. M., Madueña-Molina, J., Leon-Sicairos, C., & Canizalez-Román, A. (2015). Strategies of Intracellular Pathogens for Obtaining Iron from the Environment. *BioMed Research International*, *2015*, 1–17. https://doi.org/10.1155/2015/476534

Malhotra, M., Sood, S., Mukherjee, A., Muralidhar, S., & Bala, M. (2013). Genital Chlamydia trachomatis: An update. *The Indian Journal of Medical Research*, *138*(3), 303–316.

Mandell, G. L., Bennett, J. E., & Dolin, R. (Eds.). (2010). *Mandell, Douglas, and Bennett's principles and practice of infectious diseases* (7th ed). Churchill Livingstone/Elsevier.

McClure, E. E., Chávez, A. S. O., Shaw, D. K., Carlyon, J. A., Ganta, R. R., Noh, S. M., Wood, D. O., Bavoil, P. M., Brayton, K. A., Martinez, J. J., McBride, J. W., Valdivia, R. H., Munderloh, U. G., & Pedra, J. H. F. (2017). Engineering of obligate intracellular bacteria: Progress, challenges and paradigms. *Nature Reviews Microbiology*, *15*(9), 544–558. https://doi.org/10.1038/nrmicro.2017.59

Mirrashidi, K. M., Elwell, C. A., Verschueren, E., Johnson, J. R., Frando, A., Von Dollen, J., Rosenberg, O., Gulbahce, N., Jang, G., Johnson, T., Jäger, S., Gopalakrishnan, A. M., Sherry, J., Dunn, J. D., Olive, A., Penn, B., Shales, M., Cox, J. S., Starnbach, M. N., … Engel, J. (2015). Global Mapping of the Inc-Human Interactome Reveals that Retromer Restricts Chlamydia Infection. *Cell Host & Microbe*, *18*(1), 109–121. https://doi.org/10.1016/j.chom.2015.06.004

Mogensen, T. H. (2009). Pathogen Recognition and Inflammatory Signaling in Innate Immune Defenses. *Clinical Microbiology Reviews*, *22*(2), 240–273. https://doi.org/10.1128/CMR.00046-08

Moore, E. R., & Ouellette, S. P. (2014). Reconceptualizing the chlamydial inclusion as a pathogen-specified parasitic organelle: An expanded role for Inc proteins. *Frontiers in Cellular and Infection Microbiology*, *4*. https://doi.org/10.3389/fcimb.2014.00157

Murphy, K. M., & Weaver, C. (2017). *Janeway's immunobiology* (9th edition). GS, Garland Science, Taylor & Francis Group.

Murthy, A. K., Arulanandam, B. P., & Zhong, G. (2014). *Chlamydia* Vaccine: Progress and Challenges. In M. Tan & P. M. Bavoil (Eds.), *Intracellular Pathogens I* (pp. 311–333). ASM Press. https://doi.org/10.1128/9781555817329.ch14

Okumura, M., Natsume, T., Kanemaki, M. T., & Kiyomitsu, T. (2018). Dynein–Dynactin–NuMA clusters generate cortical spindle-pulling forces as a multi-arm ensemble. *ELife*, *7*, e36559. https://doi.org/10.7554/eLife.36559

Rape, M. (2018). Ubiquitylation at the crossroads of development and disease. *Nature Reviews Molecular Cell Biology*, *19*(1), 59–70. https://doi.org/10.1038/nrm.2017.83

Reck-Peterson, S. L., Redwine, W. B., Vale, R. D., & Carter, A. P. (2018). The cytoplasmic dynein transport machinery and its many cargoes. *Nature Reviews Molecular Cell Biology*, *19*(6), 382–398. https://doi.org/10.1038/s41580-018-0004-3

Rios, R. M. (2014). The centrosome–Golgi apparatus nexus. *Philosophical Transactions of the Royal Society B: Biological Sciences*, *369*(1650), 20130462. https://doi.org/10.1098/rstb.2013.0462

Sanchez, A. D., & Feldman, J. L. (2017). Microtubule-organizing centers: From the centrosome to non-centrosomal sites. *Current Opinion in Cell Biology*, *44*, 93–101. https://doi.org/10.1016/j.ceb.2016.09.003

Smith, J. S., Bosetti, C., Muñoz, N., Herrero, R., Bosch, F. X., Eluf-Neto, J., Meijer, C. J. L. M., van den Brule, A. J. C., Franceschi, S., & Peeling, R. W. (2004). *Chlamydia trachomatis* and invasive cervical cancer: A pooled analysis of the IARC multicentric case-control study: *C. Trachomatis* and Invasive Cervical Cancer. *International Journal of Cancer*, *111*(3), 431–439. https://doi.org/10.1002/ijc.20257

Tan, M., & Bavoil, P. M. (2012). *Intracellular pathogens I: Chlamydiales*. https://doi.org/10.1002/9781683670612

Urnavicius, L., Zhang, K., Diamant, A. G., Motz, C., Schlager, M. A., Yu, M., Patel, N. A., Robinson, C. V., & Carter, A. P. (2015). The structure of the dynactin complex and

its interaction with dynein. *Science (New York, N.Y.)*, *347*(6229), 1441–1446. https://doi.org/10.1126/science.aaa4080

Walpole, G. F. W., & Grinstein, S. (2020). Endocytosis and the internalization of pathogenic organisms: Focus on phosphoinositides. *F1000Research*, *9*, F1000 Faculty Rev-368. https://doi.org/10.12688/f1000research.22393.1

Zhu, H., Shen, Z., Luo, H., Zhang, W., & Zhu, X. (2016). Chlamydia Trachomatis Infection-Associated Risk of Cervical Cancer: A Meta-Analysis. *Medicine*, *95*(13), e3077. https://doi.org/10.1097/MD.0000000000003077

CHAPTER TWO

DRE1 INTERACTS WITH DYNACTIN TO REPOSITION HOST ORGANELLES DURING INFECTION

“Be more than men. Be steady to your purposes and firm as a rock.
This ice is not made of such stuff as your hearts may be;
it is mutable and cannot withstand you if you say that it shall not.”
- Mary Shelley

SUMMARY

Chlamydia trachomatis is an obligate intracellular pathogen that replicates within a specialized membrane-bound compartment, the inclusion. *Chlamydia* species express a unique class of effectors, Incs, which are translocated from the bacteria by a Type III secretion system and are inserted into the inclusion membrane where they modulate the host-bacterium interface. *C. trachomatis* repositions specific host organelles during infection to acquire nutrients and evade host cell surveillance, however the bacterial and host proteins controlling these processes are largely unknown. Here, we identify an interaction between the host dynactin complex and the *C. trachomatis* Inc CT192 (CTL0444), hereafter named Dre1 for Dynactin Recruiting Effector 1. We show that dynactin is recruited to the inclusion in a Dre1-dependent manner and that inactivation of Dre1 diminishes the recruitment of specific host organelles, including the centrosome, mitotic spindle, and Golgi to the inclusion. Deletion of Dre1 results in decreased *C. trachomatis* fitness in cell-based assays and in a mouse model of infection. By targeting particular functions of the versatile host dynactin complex, Dre1 facilitates re-arrangement of certain organelles around the growing inclusion. Our work highlights how *C. trachomatis* employs a single effector to evoke specific, large-scale changes in host cell organization that establish the intracellular replicative niche without globally inhibiting host cellular function.

INTRODUCTION

Obligate intracellular pathogens must establish a replicative niche within host cells, which often necessitates the rearrangement and repurposing of host cellular structures (Moore and Ouellette, 2014). In particular, intracellular, pathogens that reside within a membrane-bound compartment build what is essentially a novel organelle within a cell. As they require host-derived nutrients and energy, they must do so without globally inhibiting host cell trafficking and organelle function while at the same time evading the host cell's immune surveillance pathways. Here we elucidate how *Chlamydia trachomatis*, an obligate intracellular pathogen with a dramatically reduced genome, interacts with a single ubiquitous and versatile host protein complex to facilitate the rearrangement of specific host organelles around its growing replicative niche.

Chlamydia trachomatis is a gram-negative bacterial pathogen that is an important cause of disease in humans (Mandell et al., 2010). Specific *C. trachomatis* biovars can infect either the conjunctival epithelium that lines the inside of the eyelid, or the mucosal epithelial cells of the urogenital tract. Although infections can be treated with antibiotics, the majority of infections are asymptomatic and no effective vaccine exist, resulting in a high global prevalence of disease. The WHO estimates that over 131 million new *C. trachomatis* infections occur annually (Rey-Ladino et al., 2014; World Health Organization, 2016). Sequelae of untreated infection include blinding trachoma for ocular strains or complications from ascending urogenital infections such as pelvic inflammatory disease and infertility (Darville & Hiltke, 2010; Malhotra et al., 2013). Furthermore, *C. trachomatis* infections have recently been linked with the development of both cervical

and ovarian cancer (Smith et al., 2004; Zhu et al., 2016). Uncovering the mechanisms by which *C. trachomatis* establishes its intracellular niche may lead to a better understanding of how this pathogen causes disease and inform the development of targeted therapeutics.

All *Chlamydia* species undergo a biphasic developmental cycle in which the infectious Elementary Body (EB) binds and enters non-phagocytic host cells through receptor mediated endocytosis, and once taken up by the host, transitions to the replicative form, the Reticulate Body (RB) (Bastidas et al., 2013; Chiarelli et al., 2020; Elwell et al., 2016). Following internalization, *Chlamydia* remains within a membrane bound compartment (the inclusion) that it actively modifies to block fusion with the lysosome (Elwell et al., 2016; Moore & Ouellette, 2014). As EBs differentiate to RBs, the growing inclusion traffics along microtubules (MTs) in a dynein-dependent manner to the host centrosome (Grieshaber et al., 2003; Hackstadt et al., 1999). The centrosome is a non-membrane bound organelle attached to the nucleus. It serves as a microtubule organizing center (MTOC) by initiating the assembly of MT networks, and then anchoring and stabilizing these networks (Sanchez & Feldman, 2017). The MTOC, in turn, provides a template that specifies the position of other organelles within the host cell. The inclusion associates tightly with the centrosome throughout the remainder of the *C. trachomatis* replicative cycle. As a result, the centrosome is relocated away from the nucleus during inclusion expansion at late stages of growth (Brown et al., 2014; Grieshaber et al., 2003, 2006; Knowlton et al., 2011). Approximately 24-72 hours following initial infection, RBs differentiate back to EBs, the infectious forms. Mature EBs are released to infect

neighboring cells by either lysing the host cell or through an exocytosis-like mechanism called extrusion.

Chlamydia lacks many essential biosynthetic pathways and must therefore interact with various host compartments such as the cytoskeleton, Golgi Apparatus, mitochondria, lipid droplets, and endoplasmic reticulum (ER) to acquire host-produced metabolites including ATP, sphingolipids, and cholesterol (Dickinson et al., 2019; Elwell et al., 2016). As many of these host cell structures are arrayed around the centrosome, tight association with the centrosome would provide the physical opportunity for the inclusion to interact with host compartments and obtain the nutrients required to facilitate intracellular growth. Indeed, *Chlamydia* selectively repositions actin, microtubules, the mitotic spindle, Golgi, ER, and lipid droplets around the developing inclusion during infection, though a detailed understanding of how bacterial and host proteins facilitate this massive host cell reorganization remains elusive (Andersen et al., 2021; C. Elwell et al., 2016).

Chlamydia employs a needle-like Type Three Secretion System (T3SS) to secrete approximately 100 effector proteins into the host cytoplasm (Dehoux et al., 2011; Mueller et al., 2014). A large subset of these translocated effectors, known as Incs, are transcribed and inserted into the inclusion membrane (IM) at distinct times throughout the *Chlamydia* life cycle (Lutter et al., 2012; Moore & Ouellette, 2014; Weber et al., 2015). Incs are defined by their conserved topology; they are composed of two or more short membrane-spanning domains separated by a short loop region (Bannantine et al., 2000). Once inserted into the IM, Incs extend their N- and C-terminal domains into the host

cytoplasm (Rockey et al., 2002). Given that Incs are ideally positioned to mediate interactions with the host, we previously utilized an affinity-purification mass spectrometry (AP-MS) based strategy to systematically identify host binding partners of the Incs (Mirrashidi et al., 2015). This study identified a predicted interaction between the *C. trachomatis* Serovar D Inc, CT192 (homolog of CTL0444; hereafter referred to as Dre1), an early expressed Inc of unknown function (Almeida et al., 2012), and the host dynactin complex.

Dynactin is critical for most functions of cytoplasmic dynein-1, the primary eukaryotic minus-end directed MT motor. Dynactin serves to link dynein to specific cargo and to enhance processivity of dynein along MTs, facilitating trafficking of various cargo throughout the cell (Holleran et al., 2001; Johansson et al., 2007; Kardon et al., 2009; King & Schroer, 2000; McKenney et al., 2014; Muresan et al., 2001; Reck-Peterson et al., 2018). Together, dynein and dynactin generate the force required to regulate the shape and positioning of various organelles and cellular structures. In addition, dynactin directly binds microtubules and functions to anchor and organize MTs arrayed at the centrosome and Golgi apparatus (GA) (Corthésy-Theulaz et al., 1992; Lele et al., 2018; Reck-Peterson et al., 2018; Torisawa & Kimura, 2020). Along with many viruses, *C. trachomatis* utilizes dynein to traffic toward the center of the host cell (Grieshaber et al., 2003). In this work, we show that while Dre1 is not required for trafficking of the inclusion along MTs, Dre1 instead recruits dynactin to the inclusion to control the positioning of dynactin-positive organelles including the centrosome, mitotic spindle, and GA during infection. By binding a ubiquitous and multifunctional host protein complex, a single *C.*

trachomatis Inc, Dre1 (for Dynactin Recruiting Effector 1) specifically restructures the host cell interior to facilitate *C. trachomatis* growth without globally inhibiting host cellular functions.

RESULTS

Dynactin interacts specifically with Dre1 during *C. trachomatis* infection.

Our previous AP-MS screen, referred to here as the "Transfection Interactome", predicted a high-confidence interaction between Dre1 transiently expressed in HEK293T cells (Figure 2.1A, B) and all 11 subunits of the mega-dalton sized host dynactin complex (Mirrashidi et al., 2015). Interactions were scored using MiST (Jager et al., 2012) and CompPASS (Sowa et al., 2009) algorithms, which prioritize interactions based on their reproducibility, abundance, and specificity. Three dynactin subunits that co-purified with Dre1 (CapZa, CapZb, and beta-actin) were not in the top 5% of MiST scores, likely because their specificity scores were penalized due to their interactions with actin filaments that are regulated by other Incs (Andersen et. al., 2021, Elwell et. al., 2016).

Our previously published Transfection Interactome was performed with Inc proteins from *C. trachomatis* Serovar D, which are highly conserved in Serovar L2 (Dehoux et al., 2011; Lutter et al., 2012). Since *Chlamydia* genetics has been primarily developed for L2, we performed all subsequent studies with L2. To confirm that dynactin interacts with Dre1 in the context of *C. trachomatis* L2 infection and to potentially uncover additional Dre1-interacting partners that may have been missed in our transfection interactome, we infected HeLa cells for 40 hours with L2 transformed with a plasmid constitutively expressing Dre1 fused to a FLAG tag (L2+pDre1$_{FLAG}$), and performed affinity purification using anti-FLAG magnetic beads (Figure 2.1A). Cells infected with L2+pBOMB$_{FLAG}$ vector served as a control. Entire eluates were then subjected to MS without gel purification. All APs were performed in triplicate, and expression of Dre1 in the eluates was confirmed by

immunoblotting with an anti-FLAG antibody and by silver stain (Figure S2.1A). To generate a set of high-confidence Dre1 interacting partners, we measured enrichment of host peptides in Dre1 eluates compared to control eluates and then scored the reproducibility and abundance of these peptides using the SAINT algorithm (Table 1; Teo et. al., 2014). Next, we compared this data set to the high-confidence interactions predicted for Dre1 in the Transfection Interactome and selected Dre1-host PPIs in common to both data sets. This strategy generated a list of high confidence interactions specific to Dre1 that were also found during infection "Dre1 Infection Interactome" (Figure 2.1A and 2.1B).

Similar to the transfection interactome, all dynactin subunits except beta-actin were represented within the top 10% of scored interactions for Dre1 during infection (Figure 2.1B), suggesting that they were among the most reproducible and abundant interacting partners of Dre1 during infection. $p150^{glued}$, a dynactin subunit that scored highly in the Transfection Interactome, did not score as highly in the Dre1 Infection Interactome due to non-specific post-lysis cleavage, likely by the Chlamydial protease CPAF (Tan & Sütterlin, 2014). Notably, in both our transfection and infection interactomes, Dre1 did not co-purify with dynein or any of the known adaptors that regulate dynein or dynactin activity.

We further confirmed the specificity of the interaction between Dre1 and dynactin during infection by infecting HeLa cells with *C. trachomatis* strains expressing either plasmid-encoded $Dre1_{FLAG}$ or $IncG_{FLAG}$ (an unrelated Inc that should not bind dynactin) and

performing FLAG APs. Endogenous dynactin (p27 and Arp1a) co-purified with Dre1 but not with IncG (Figure S2.1B). Together, these data demonstrate that Dynactin interacts reproducibly and specifically with Dre1 and that this interaction occurs during *C. trachomatis* infection.

Dre1 is required for the recruitment of dynactin to the inclusion during infection.

Dynactin localizes at multiple sites in the cell, including MTs, the mitotic spindle, centrosome, nuclear envelope, Golgi apparatus, kinetochores, and the cell cortex (Tirumala & Ananthanarayanan, 2020). In HeLa cells infected with L2+pDre1$_{FLAG}$, endogenous p150^{glued} (a dynactin subunit) and Dre1 colocalize at the inclusion membrane (Figure S2.1D). Likewise, transfected GFP-Arp1a (another dynactin subunit) is recruited to the inclusion membrane at 24 hours post infection (hpi; Figure 2.1C). To determine if Dre1 is required to recruit dynactin to the inclusion, we utilized a chemically mutagenized strain of *C. trachomatis* L2 that contains a single nucleotide variant (SNV) in Dre1 that introduces a stop codon at amino acid 20 (Table 2; hereafter we refer to this mutant as L2Δ*dre1*). Even if the 20 amino acid peptide is expressed and is stable, it is not predicted to bind dynactin (see Figure 2.2). Indeed, in HeLa cells infected with L2Δ*dre1*, GFP-Arp1a is not recruited to the inclusion. To link loss of Dre1 with loss of dynactin recruitment, we complemented L2Δ*dre1* with a plasmid constitutively expressing Dre1 (L2Δ*dre1*+pDre1$_{FLAG}$). Recruitment of the transfected GFP-Arp1a was restored in the complemented mutant (Figure 2.1C). Thus, Dre1 is necessary for recruitment of dynactin to the inclusion. Interestingly we did not observe an obvious defect in trafficking of

L2Δ*dre1* inclusions to the MTOC (Figure 2.1C), nor did we see a defect in number of inclusions compared to L2 infection (Figure S2.6A).

Dynactin-binding domain targets Dre1 to the Centrosomal MTOC.

To define the region in Dre1 necessary and sufficient to interact with dynactin, we transfected HEK293T cells with deletion mutants of Dre1. All constructs containing a fragment of the Dre1 C-terminal cytoplasmic domain ($Dre1_{181-231}$) co-AP with endogenous dynactin ($p150^{glued}$, p27), indicating that this region is required for the interaction with dynactin (labeled Dynactin Binding Domain, DBD, Figure 2.2 A, B). The construct encompassing the Dre1 C-terminal ~100 amino acids ($Dre1_{134-231}$) was sufficient to interact with dynactin. Bioinformatic analysis of $Dre1_{134-231}$ failed to reveal any known motifs, or any sequence homology to other proteins.

Dynactin localizes to multiple compartments and structures in cells where it organizes MTs, facilitates vesicle trafficking, and positions organelles, suggesting that there may be functionally distinct sub-populations of dynactin (Schroer & Verma, 2021; Tirumala & Ananthanarayanan, 2020). Since *C. trachomatis* inclusions associate with centrosomes and the MTOC (Grieshaber et al., 2003, 2006; Hackstadt et al., 1999), we were particularly interested in the population of dynactin that localizes at the centrosome, where it anchors MTs and organizes MT arrays during interphase as well as mitosis (Askham et al., 2002; Quintyne et al., 1999; Quintyne & Schroer, 2002). Indeed, live-cell microscopy of HeLa cells showed that the transiently expressed C-terminal fragment of Dre1 ($Dre1_{81-231}$) fused to superfolder GFP (sfGFP) localizes specifically at the MTOC

(Figure 2.2C) and centrosome (Figure 2.2D), but not along MTs. Dre1 localization requires its dynactin-binding domain, as $Dre1_{81-180}$ fails to localize to the MTOC or centrosome (Fig 2.2C). Furthermore, Dre1 localization does not depend on an intact MT network, as Dre1 and dynactin continue to localize at the centrosome in HeLa cells that have been cold-treated with Nocodazole to disrupt microtubules (Figure S2.2A). Taken together, these data demonstrate that Dre1 specifically interacts with dynactin at centrosomes, and they suggest that the Dre1:dynactin interaction might be targeting dynactin sub-populations that are involved in organizing MTs nucleated by organelles rather than sub-populations actively involved in MT transport.

Dre1 repositions centrosomes and primary cilia during infection.

In addition to its role in MT organization at the centrosome, dynactin is also involved in centrosome positioning at the juxta-nuclear region within a cell (Burakov et al., 2003; Quintyne et al., 1999). During *C. trachomatis* infection, centrosomes are recruited away from their canonical juxta-nuclear position and instead, maintain a tight association with the inclusion membrane (Brown et al., 2014). This process is dependent on de novo bacterial protein synthesis, suggesting that a *C. trachomatis* effector(s) is involved (Grieshaber et al., 2003). We therefore tested whether Dre1 is necessary for *C. trachomatis*-mediated recruitment of centrosomes to the inclusion.

We performed immunofluorescence (IF) microscopy in HeLa cells infected with L2, L2Δ*dre1*, or L2Δ*dre1*+$pDre1_{FLAG}$ for 36 hours, and measured the distance between the centrosomes and the nearest nuclear face in three dimensions (Figure 2.3A, B).

Centrosomes were visualized using antibodies to endogenous γ-Tubulin, which stains the pericentriolar material (PCM), or to centrin, which stains centrioles. Compared to uninfected cells, the average distance between the centrosome and the nucleus in was 0.76μm, that distance increased to 7.34μm or 8.66μm in cells infected with L2 or L2Δ*dre1*+pDre1$_{FLAG}$, respectively. Importantly, in HeLa cells infected with L2Δ*dre1*, the distance between the centrosome and the nucleus was significantly less (2.99μm). Thus, Dre1 contributes to centrosome repositioning during infection, though other *C. trachomatis* effectors may be involved.

The primary cilium is a MT-based organelle involved in sensing and motility that originates from the centrosome. As Dre1 mediates the position of the centrosome during infection, we tested whether Dre1 is involved in positioning of cilia during *C. trachomatis* infection. For these experiments, we utilized A2EN cells, an immortalized human endocervical epithelial cell line that can be grown as a pseudo-polarized monolayer. We fixed and stained pseudo-polarized and infected A2EN cells for Arl13b (which is highly enriched on the ciliary membrane) and IncE (to delineate the inclusion membrane) at 24hpi. In L2-or L2Δdre1+pDre1FLAG-infected A2EN cells, one end of the cilium localizes on the inclusion membrane while in cells infected with L2Δ*dre1*, the base of the cilium appears to be anchored near the nucleus (Figure S2.3B). Together these results demonstrate that Dre1 repositions the centrosome and primary cilium, a structure templated by the centrosome, at the inclusion membrane.

Dre1 expression increases centrosome spread during interphase and induces abnormal spindle formation during mitosis.

In interphase, the centrosome is a single-copy organelle that serves as the primary MTOC in eukaryotic cells. The centrosome is duplicated concurrently with host DNA during S-phase. During M-phase duplicated centrosomes separate from one another and form the two spindle poles that organize MT structures and mediate equal partitioning of host DNA to daughter cells (Bettencourt-Dias & Glover, 2007; Conduit et al., 2015). Migration of duplicated centrosomes depends on dynein and dynactin function (Robinson et al., 1999). Formation of a bipolar spindle is important to avoid chromosome segregation errors and genomic instability. Many cancer cells have supernumerary centrosomes, and in order to successfully produce progeny, these cells cluster excess centrosomes during interphase and mitosis to form pseudo-bipolar spindles via interactions between the centrosome and MT minus ends (Milunović-Jevtić et al., 2016; Pannu et al., 2014).

C. trachomatis infection induces centrosome overduplication, in a process dependent on both the *Chlamydia* protease, CPAF, and on progression of the host centrosome duplication pathway (Brown et al., 2014; Grieshaber et al., 2006; K. A. Johnson et al., 2009). In addition, *C. trachomatis* prevents clustering of these supernumerary centrosomes, which leads to abnormal spindle formation (Brown et al., 2014). To determine whether Dre1 plays a role in centrosome overduplication, we compared the number of centrosomes in uninfected and infected HeLa cells at 36hpi. While uninfected cells contained on average 2.08 centrosomes per cell, L2-, L2Δ*dre1*- and L2Δ*dre1*+pDre1$_{FLAG}$ -infected cells all exhibited a similar increase in the number of

centrosomes per cell (2.76, 2.64, 2.68, respectively, $p < 0.05$ compared to uninfected cells but $p > 0.05$ when all the *C. trachomatis* strains were compared to each other; Fig S3A). This data indicates that Dre1 is not required for *C. trachomatis*-mediated centrosome overduplication and is consistent with published results showing that while dynactin plays a role in centrosome homeostasis and function, dysregulation of dynactin does not result in centrosome copy number defects (Chen et al., 2015).

We next determined whether Dre1 prevents clustering of supernumerary centrosomes by measuring centrosome spread and spindle polarity in HeLa cells infected with the isogenic Dre1 strains at 36hpi. Cells were stained with antibodies to γ-Tubulin at 36hpi, and centrosome clustering was measured by determining the area of the convex hull that contains all centrosomes in a cell (Figure 2.3C). In L2- and L2Δ*dre1*+pDre1$_{FLAG}$ -infected cells, centrosomes occupy an area of 52.9μm^2 and 52.5μm^2, respectively. In contrast, in L2Δ*dre1*- infected cells, centrosomes occupy an area of 15.7μm^2 (Figure 2.3D). Thus, the Dre1:dynactin interaction at centrosomes overrides the host cell's usual clustering mechanisms and enables *C. trachomatis* to dictate centrosome positioning during interphase.

Inhibition of centrosome clustering during interphase leads to the development of abnormal spindles during mitosis, which are associated with mitotic failure and/or genomic instability. In addition, dynactin dysregulation induces formation of multipolar spindles (Drosopoulos et al., 2014). We therefore tested whether Dre1:dynactin interaction contributes to the formation of aberrant spindles during infection. We used a

brief cold-shock to synchronize HeLa cells (Rieder & Cole, 2002), and then infected the synchronized cells with L2, L2Δ*dre1*, and L2Δ*dre1*+pDre1$_{FLAG}$ for 24 hours. We stained cells with antibodies to γ-tubulin and p150^{glued} to visualize spindles by IF. Uninfected mitotic cells nearly always formed bipolar spindles, while 47.4% and 52% of mitotic L2-infected or L2Δ*dre1*+pDre1-infected cells exhibited aberrant spindles, respectively (Figure 2.3E, 2.4A). Similar to uninfected cells, aberrant spindles were rarely observed in L2Δ*dre1*-infected mitotic cells. These results are consistent with published work from that suggests that there are at least two effector pathways that work together to control number and positioning of centrosomes during infection. Our data support a model where Dre1 is involved in positioning of centrosomes during interphase and mitosis, but not in the dysregulation of centrosome copy number.

Dre1 is required for inclusion localization at spindle poles during host cell division. Dynactin is recruited to the MT minus ends that congregate at spindle poles during mitosis (Hueschen et al., 2017). Given our data that demonstrates that Dre1 mediates association between the inclusion and centrosomes during interphase (Figure 2.3A,B), we next tested whether Dre1 maintains this association at spindle poles during mitosis. The *C. trachomatis* inclusion has been shown to localize at the center of the spindle where host chromosomes align for segregation; this localization is dependent on *C. trachomatis* translation (Greene, 2003; Sun et al., 2011) and may be a mechanism by which infection induces mitotic failure. Interaction with dynactin at the spindle pole might be the first step by which the inclusion positions itself within the host spindle to interfere with host mitosis.

We determined whether inclusions localize at spindle poles during infection by infecting cold-synchronized HeLa cells for 24 hours, and staining fixed cells for DNA, IncE (to delineate the inclusion membrane), and $p150^{glued}$ (to reveal the spindle architecture), and DAPI (to visualize chromosomes; Figure 2.4A). Indeed, L2 inclusions were localized at the spindle poles. In contrast, L2Δ*dre1* inclusions were displaced from the spindle pole, and were often found displaced from the spindle and metaphase plate. Localization of the inclusion at the spindle pole is restored in the complemented mutant. Interestingly, Dre1-directed localization of the inclusion at the spindle pole often leads to displacement of host chromosomes from the metaphase plate (Figure 2.4A).

Dre1 contributes to infection-induced multinucleation.

C. trachomatis infection induces cytokinesis failure and multinucleation (Alzhanov et al., 2009; Brown et al., 2012; Sun et al., 2016). We therefore tested whether *C. trachomatis* induced host cell multinucleation was Dre1-dependent. Uninfected HeLa cells had a multinucleation rate of 1.6% (Figure S2.4A), while 22.3% of L2 infected cells were multinucleated by 48hpi (Figure 2.4B). In contrast, only 8.3% of cells infected with L2Δ*dre1* were multinucleated, while L2Δ*dre1*+$pDre1_{FLAG}$-infected cells exhibited multinucleation rates similar to L2-infected cells (18.8%). Our results demonstrate that without Dre1, *C. trachomatis*-infected cells do not have mis-positioned centrosomes, aberrant spindles arising from un-clustered centrosomes, nor do they have an inclusion is positioned at the spindle pole. Thus, Dre1 contributes to infection-induced multinucleation.

Dre1 mediates GA recruitment to the inclusion membrane.

Our work demonstrates that Dre1 binds dynactin and modulates the positioning of a MTOC (the centrosome) with respect to the inclusion membrane. In eukaryotic cells, the Golgi apparatus (GA) also functions as an MTOC, and dynein/dynactin regulates its structure as well as the perinuclear localization (Jaarsma & Hoogenraad, 2015; Rios, 2014; Yadav & Linstedt, 2011). Disruption of dynactin causes GA fragmentation and dispersal (Palmer et al., 2009; Yadav & Linstedt, 2011). Dynactin can bind to MTs anchored at the GA, as well as to βIII spectrin on GA membranes through its Arp1 subunit (Holleran et al., 2001; Yadav & Linstedt, 2011). *C. trachomatis* infection fragments the GA into mini-stacks that are recruited around the inclusion, which enhances progeny production (Heuer et al., 2009). To test the hypothesis that Dre1 mediates recruitment of the GA to the inclusion through its interaction with dynactin, HeLa cells were infected for 24 hrs with L2, L2Δ*dre1*, and L2Δ*dre1*+pDre1, fixed, and stained with anti-GM130 (a *cis*-GA marker) (Figure 2.5A). 52.8% of the inclusion surface area is within 1μm of the GA in L2-infected cells, whereas only 23.3% of the IM in L2Δ*dre1*-infected cells was within 1μm of the GA (Figure 2.5B). GA recruitment was restored to L2 levels (55.5%) in the complemented mutant strain. These data demonstrate that Dre1 contributes to GA recruitment at the inclusion membrane.

Dre1 is required for efficient inclusion fusion at the centrosomal MTOC.

In cells infected with multiple L2 bacteria, each bacterium is typically enclosed in a separate inclusion, which then traffics along MTs to the MTOC/juxta-nuclear region. Over a period of ~ 24 hrs, multiple MTOC-localized inclusions undergo homotypic fusion

(Richards et al., 2013). While many details of the homotypic fusion process remain to be elucidated, it is known that the inclusion membrane protein IncA, which encodes 2 SNARE-like domains, is absolutely required for homotypic fusion (Cingolani et al., 2019; Weber et al., 2016). These fusion events are critical for pathogenicity (Geisler et al., 2001) and may be a mechanism for genetic exchange between RBs or a strategy to avoid competing for the same resources in the host cell. Given that inclusion fusion requires association with the centrosomal MTOC (Richards et al., 2013), we tested the hypothesis that Dre1-mediated interaction between multiple inclusions and centrosomal dynactin may facilitate inclusion fusion. This mechanism is analogous to the mechanism by which Rab GTPases tether vesicles to their target organelles prior to fusion.

In cells infected with L2Δ*dre1* at a high MOI, we observed a significant delay in inclusion fusion compared to L2 (Figure 2.6A). By 24hpi, the average number of inclusions per infected cell was 1.07, indicating that the vast majority of cells had undergone fusion, whereas cells infected with L2Δ*dre1* had an average of 1.77 inclusions per cell (Figure 2.6B). The complemented mutant had 1.27 inclusions per infected cell; demonstrating that fusion was restored to nearly wild type levels. By 48hpi, L2Δ*dre1* inclusions are nearly fully fused; thus, Dre1 contributes to efficient inclusion fusion but is not absolutely required. Furthermore, L2-infected cells containing multiple inclusions exhibited Dre1-dependent GFP-Arp1a localization at the boundary membranes between unfused inclusions (Figure 2.6A). Importantly, loss of Dre1 does not affect IncA expression or localization (Figure 2.1C).

We observed that the rare L2Δ*dre1* inclusions that remained unfused at 48hpi were located on opposite sides of the nucleus from one another. We hypothesized that these non-fused inclusion events arose as a consequence of trafficking along MTs to minus ends that are not anchored at the primary MTOC. To test this notion, we performed coinfections using a GFP-expressing L2, which should localize at the centrosome, and L2Δ*dre1* (which was not fluorescent). HeLa cells were infected with a 1:1 mix of $L2_{GFP}$ and L2Δ*dre1* for 48 hours. Cells were fixed and stained using antibodies to γ-Tubulin and IncA, and stained with Wheat Germ Agglutinin (WGA). Figure 2.6C shows that in the exceedingly rare cases that there are two $L2_{GFP}$ inclusions within the same cell, they are both found adjacent to the centrosome 100% of the time. In a cell containing one $L2_{GFP}$ inclusion and one L2Δ*dre1* inclusion, 90% of inclusions are on opposite sides of the nucleus. Furthermore, in cells harboring two L2Δ*dre1* inclusions, these inclusions are also found on opposite sides of the nucleus at similar rates as cells harboring both an $L2_{GFP}$ inclusion and an L2Δdre1 inclusion. We thus conclude that the relative defect in L2Δ*dre1* inclusion fusion is at least in part a consequence of the failure of the inclusions to be juxtaposed at the primary MTOC.

Dre1 is required for virulence in cell culture and a mouse model of upper genital tract infection.

Given that L2Δ*dre1* was initially identified by its small plaque phenotype (Kokes et al., 2015), and that loss of Dre1 expression during infection contributes to defects in repositioning host organelles around the inclusion, we tested the contribution of Dre1 to virulence in cell-based and a murine model of upper genital tract infection. First, we

quantified whether Dre1 is required for *C. trachomatis* progeny production in HeLa cells or in pseudo-polarized A2EN cells. L2 infections harvested at 48hpi in HeLa cells, when L2Δ*dre1* no longer exhibits a fusion defect, yielded an 8-fold greater amount of EBs compared L2Δ*dre1* infections (Figure 2.7B). Likewise, L2 EBs harvested at 48hpi in A2EN cells produces 6-fold more EBs than L2Δdre1 (Figure 2.7A). In both HeLa and A2EN cells L2Δ*dre1*+pDre1$_{FLAG}$ produces comparable numbers of EBs as L2 infection (Figure 2.7A, B). Thus, Dre1 is required for efficient production of infectious progeny in two different cell lines, and this virulence defect is unlikely due to the delay in inclusion fusion.

Finally, we tested whether Dre1 contributes to infection in a well-established mouse model of *C. trachomatis*-induced human genital tract disease (Sixt et al., 2017). Female C57BL/6 mice were pre-treated with progesterone for 2 weeks to synchronize their estrus cycles and were then transcervically infected with either L2 or L2Δ*dre1*. This mode of inoculation mimics ascending infection. Mice were sacrificed on days 3 and 5 post infection, and bacterial burden in isolated genital tracts was measured in 5 mice per strain using qRT-PCR against *Chlamydia* 16s rRNA. At 5 days post infection, L2Δ*dre1* was mostly cleared from the mice, while there were 10-fold higher levels of bacteria in the mice infected with L2 (Figure 2.7C). This result is consistent with the progeny defect observed *in cellulo.*

DISCUSSION

In order to evade host-cell innate immune surveillance, internalized *Chlamydia* develop within a membrane-bound compartment. Given that *C. trachomatis* relies on host cell-derived nutrients and energy, this bacterial pathogen must avoid globally inhibiting host cell function while building what is essentially a novel organelle. Through strategic deployment of effectors into the host cytosol and inclusion membrane, *C. trachomatis* actively remodels host cell structures from within the inclusion. In this work, we identified and characterized an interaction between the Inc Dre1 (CT192) and the host dynactin complex during infection (Figure 2.1). We found that the dynactin-binding domain (DBD) of Dre1 specifically targets this effector to the centrosomal MTOC (Figure 2.2) and that Dre1 is required for infection-induced centrosome repositioning (Figure 2.3), as well as the repositioning of organelles templated by the centrosome including the primary cilium (Figure S2.3). Furthermore, we demonstrate that Dre1 prevents clustering (though not the generation) of supernumerary centrosomes in infected cells (Figures 2.3, S2.3), suggesting that, Dre1 overrides the host cell's intrinsic mechanisms for determining centrosome positioning during infection through its interaction with dynactin. We show that Dre1 interacts selectively with dynactin stably associated with specific organelles in order to modulate their recruitment to the growing inclusion (Figures 2.3-2.5). Importantly, we determined that the Dre1:dynactin interaction is critical to the intracellular survival and pathogenesis of *C. trachomatis* infections (Figure 2.7). Thus, this single Inc selectively evokes large-scale changes in host cell organelle organization. Given that *Chlamydia* species encode anywhere from 25-100 Incs as well as dozens of additional secreted

effectors, it is not surprising that this pathogen is so effective at causing diverse and often devastating diseases.

Our work underscores the nuances of dynactin regulation and may prove useful in further dissecting its diverse cellular functions. Dynactin is an adaptor for the minus-end directed MT motor dynein; many intracellular pathogens interact with dynein (Henry et al., 2006) but our work identifies *C. trachomatis* as one of the few pathogens to interact directly with dynactin. Although *C. trachomatis* is known to traffic along MTs in a dynein-dependent manner to reach the host MTOC, we show that Dre1 is not required for trafficking from the cell periphery to the juxtanuclear position. This observation could be explained if another effector can fulfill this role. Indeed, the Inc CT850 has been shown to interact with dynein (Mital et al., 2015). Furthermore, disruption of dynactin by overexpression of its dynamitin (p50) subunit does not affect trafficking of the inclusion to the centrosome (Grieshaber et al., 2003). Dre1 could function to stabilize the dynactin complex in the face of perturbations, such as dynamitin overexpression, to employ redundancy in ensuring that the inclusion localizes at the centrosomal MTOC. However, given that Dre1 is one of the few pathogen effectors that specifically target dynactin rather than dynein, and that Dre1 does not AP with any known adaptor proteins that enhance dynein processivity (Table 1), we speculate that the primary role of the Dre1:dynactin interaction might be to target the MT-binding and MT-organizing functions of dynactin (which are not impeded by dynamitin overexpression), rather than targeting actively trafficking dynactin/dynein complexes (Eckley et al., 1999; Jacquot et al., 2010; Melkonian et al., 2007; Wittmann & Hyman, 1998).

An attractive model for the role of the Dre1:dynactin interaction is that Dre1 targets subpopulations of dynactin that function to anchor MTs at organelles, which would then allow *C. trachomatis* to recruit these organelles to the inclusion, thereby modulating their position, structure, or function. Indeed, our work demonstrates that Dre1 specifically localizes to the centrosomal MTOC (Figure 2.2) and that Dre1 is necessary for *C. trachomatis* to specifically disrupt positioning of MTOC-associated structures, including the centrosome, mitotic spindle, and primary cilium (Figures 2.3-2.5). In eukaryotic cells the GA can serve as a MTOC, and dynactin plays a role in anchoring MTs at this organelle (Yadav & Linstedt, 2011). During *C. trachomatis* infection the GA is recruited around the inclusion, which facilitates lipid acquisition by *C. trachomatis* and enhances progeny production (Heuer et al 2009). We demonstrate that Dre1 contributes to GA recruitment to the inclusion, although it is not exclusively required. Indeed, several other *C. trachomatis* effectors, including InaC/CT813 and ChlaDub1, have also been shown to mediate GA fragmentation and recruitment to the inclusion (Kokes et al., 2015; Pruneda et al., 2018; Wesolowski et al., 2017). Thus, multiple host organelles with dynactin-mediated MT organizing capacity are repositioned during infection by Dre1. Furthermore, Dre1 appears dispensable for positioning of organelles that lack stable pools of dynactin, such as mitochondria (Figure S2.5).

Our finding that Dre1 recruits of centrosomes away from the nucleus to the inclusion and prevents clustering of supernumerary centrosomes was striking (Figure 2.3). Interestingly, the degree of centrosome-inclusion association during infection amongst different species of *Chlamydia* correlates with conservation of Dre1. Only species with

Dre1 homologues have been shown to reposition centrosomes, and the extent of repositioning is highest in the species where Dre1 is most conserved (Brown et al., 2014; Mital & Hackstadt, 2011; Stephens et al., 1998). Our observation that Dre1 is not required for centrosome overduplication (Figure S2.3) is consistent with published work that links this process to the *Chlamydia* secreted protease, CPAF (Brown et al., 2014; K. A. Johnson et al., 2009; Knowlton et al., 2011). However, our work does suggest that Dre1 is required to cluster supernumerary centrosomes during interphase and mitosis (Figures 2.3, 2.4). In non-cancerous cells, the presence of supernumerary centrosomes activates checkpoints that induce cell death, given that centrosome overduplication leads to the formation of aberrant mitotic spindles, chromosome segregation errors, and aneuploidy. Centrosome overduplication is frequently observed in aggressive cancers, though cancer cells cluster extra centrosomes to achieve a seemingly normal bipolar division which allows for proliferation.

Our results suggest a mechanism whereby *C. trachomatis* induces centrosome overduplication, and through the activity of Dre1, overrides the host's centrosome positioning pathways (Figure 2.3) which results in construction of abnormal spindles (Figures 2.3, 2.4). Abnormal spindles interfere with cytokinesis and induce multinucleation, which is a hallmark of *C. trachomatis* infected cells. We demonstrate that loss of Dre1 decreases levels of infection-induced multinucleation (Figure 2.4), though it does not completely return multinucleation to levels seen in uninfected cells (Figure S2.4), a finding consistent with work showing that CPAF, and potentially other effectors, contribute to multinucleation during *C. trachomatis* infection (Alzhanov et al., 2009; Brown

et al., 2014). We speculate that cytokinesis failure might be a mechanism by which C. trachomatis avoids giving up resources and “real estate” to a daughter cell, which is consistent with work showing that multinucleated cells have an increased GA content. Taken together, our data suggest that the Dre1:dynactin interaction positions the inclusion close to organelles that provide essential nutrients (such as the GA) and circumvents the threat of losing half of the cell’s resources to a daughter during mitosis. Thus, Dre1 is important for maintaining the unique intracellular niche for the inclusion.

The ability of Dre1 to induce centrosome and mitotic abnormalities could be the key to explaining the role of *C. trachomatis* as a co-factor, along with human papilloma virus (HPV), in the development of cervical cancer (Smith et al., 2004; Zhu et al., 2016), the fourth leading cause of cancer deaths among women (Arbyn et al., 2020; Jemal et al., 2011). As centrosome de-clustering agents have been identified as promising targeted cancer therapeutics (Liu & Pelletier, 2019), Dre1 may be an attractive candidate for future studies. We note that since our experiments thus far have been performed in transformed cell lines, it will be important to test the downstream consequences of Dre-mediated centrosome and mitotic abnormalities in primary cells, or in an animal model. It will be of even greater interest to define the effects of infection with L2 compared to L2Δ*dre1* in models of HPV infection.

A unique aspect of *C. trachomatis* infection is that in cells infected with multiple bacteria, individual inclusions traffic to the MTOC and undergo homotypic fusion. These fusion events are critical for pathogenicity; rare, clinical isolates that are non-fusogenic are

associated with less severe genital tract infection compared to WT infections (Geisler et al., 2001). IncA, which possesses two SNARE-like domains, is absolutely required for inclusion fusion, but the role of other effectors and host cell components, is incompletely understood (Cingolani et al., 2019; Weber et al., 2016). Our data demonstrate that Dre1 contributes to efficient fusion of inclusions within the same cell and that dynactin may be recruited to the site of membrane fusion (Figure 2.6). We hypothesize that this is another example of Dre1 binding dynactin to position organelles – this time the organelle in question is the inclusion itself. Dre1 does not affect IncA expression or localization, nor does it affect inclusion trafficking to the centrosome. Rather, our work suggests that Dre1, by binding dynactin at the centrosome, which is a single-copy organelle during interphase, is critical to juxtaposing inclusions to allow the *C. trachomatis*- encoded fusion machinery to engage. This idea is further supported by our observations that inclusions in L2:L2Δ*dre1* co-infected cells fail to fuse if they are localized on opposite sides of the nucleus. Without Dre1, inclusions may not efficiently discriminate between local MT minus ends and the centrosomal MTOC of the host cell.

We performed the majority of our experiments in HeLa cells, where the MTOC forms at the centrosome, however, *C. trachomatis* typically infects polarized epithelial cells where there are multiple non-centrosomal MTOCs during interphase. Determining how Dre1 perturbs cells where the function of centrosome and the MTOC are separated and may provide insight into the relationship between various classes of MTOC. We observed a more severe replication defect in L2Δ*dre1*-infected pseudo-polarized A2EN cells

compared to HeLa cells (Figure 2.7) and we speculate that distinguishing between these two structures may be important for *C. trachomatis* intracellular growth.

An important question for the future is how Dre1 interacts with dynactin at a molecular level. One possible model is that Dre1 functions as a mimic for one or more adaptor proteins associated with the dynactin-dynein complex. Most identified adaptors that specify cargo-binding or modulate processivity of the dynactin-dynein complex contain long coiled-coil domains (Reck-Peterson et al., 2018). While we have not yet addressed this question, we note that bioinformatic analysis of Dre1 failed to reveal any sequence or structural homology to known proteins, including known adaptors. Second, we delineated the C-terminal 100 residues of Dre1 as being necessary and sufficient to bind dynactin and demonstrated that this domain targets ectopically expressed Dre1 to the centrosomal MTOC (Figure 2.2). Thus, rather than functioning as a cargo mimic, Dre1 may target specific subpopulations of dynactin that are associated with MT minus ends. Future structural analyses to determine if Dre1 can distinguish and selectively interact with dynactin in complex with particular adaptors and to determine whether association with Dre1 alters the regulatory state or activity of dynactin will be required to address these important biological questions.

In summary, we have identified a *C. trachomatis* effector that binds host dynactin, not to facilitate intracellular transport of the pathogen, but rather to reposition organelles including the centrosome and GA around the growing inclusion. We hypothesize that Dre1 binds dynactin complexes stably associated with organelles that nucleate and

organize MTs, and that Dre1 might be targeting dynactin subpopulations that are specifically involved in mediating organelle positioning within the cell. This selectivity would allow *C. trachomatis* to override host mechanisms for organelle positioning and create a replicative niche without globally altering trafficking or organelle function. Our work further highlights how a single pathogen effector can facilitate large scale changes in host cell architecture by interacting with a single, ubiquitous host protein complex. Future elucidation of the molecular basis of Dre1:dynactin interaction may provide insight into the regulation and activities of this essential host protein complex and will have broad implications throughout biology.

MATERIALS AND METHODS

Cell Culture and Bacterial Propagation.

HeLa 229, Vero, and A2EN cells were obtained from American Type Culture Collection (ATCC). HeLa cells were cultured and maintained in Eagle's Minimum Essential Medium (MEM; UCSF Cell Culture Facility) supplemented with 10% (v/v) fetal bovine serum (FBS) from Gemini at 37ºC in 5% $C0_2$. HEK293T cells (a generous gift from NJ Krogan, UCSF) and Vero cells were cultured and maintained in Dulbecco's modified Eagle's Medium (DMEM, UCSF Cell Culture Facility) supplemented with 10% (v/v) FBS at 37ºC in 5% $C0_2$. A2EN cells were cultured and maintained in Keratinocyte Media (Gibco) supplemented with 50µg/mL Bovine Pituitary Extract (Gibco), 0.5ng/mL Human Recombinant EGF (Gibco), and 10% (v/v) FBS at 37ºC in 5% $C0_2$. Cells were routinely tested for mycoplasma (Molecular Probes, M-7006). *C. trachomatis* serovar L2 (434/Bu) and derivative strains used in these studies are listed in Table S3. *C. trachomatis* was routinely propagated in either HeLa 229 epithelial cell monolayers or Vero cell monolayers as previously described (Elwell et al., 2011). HeLa cells were used for all experiments unless otherwise specified. Stellar™ chemically competent cells (Takara) were used to produce constructs for ectopic expression in mammalian cells, while *dam*$^-$/*dcm*$^-$ chemically competent *Escherichia coli* (NEB) were used to produce unmethylated constructs for transformation into *C. trachomatis*.

Plasmid construction.

The Dre1 gene and various deletion derivatives used for ectopic expression in mammalian cells were PCR amplified from genomic *C. trachomatis* L2 (434/Bu) DNA and

subcloned into the EcoRI and NotI sites in pcDNA4.0/2xStrepII (Jager et. al. 2011) using the primers indicated (Table S2). Dre1 constructs were verified by forward and reverse sequencing. Superfolder (sf) GFP was amplified from a construct kindly provided by Dr. Ron Vale (HHMI, UCSF) and cloned into each Dre1 truncation strain as a C-terminal fusion. Centrin-2 and Mito-7 tagged with mCherry or mEmerald, respectively, were obtained from the Center for Advanced Light Microscopy (Nikon Imaging Center, UCSF). GFP-hARP1a was obtained from the Dumont lab (UCSF). To express epitope-tagged Dre1 during *C. trachomatis* infection, Dre1 was amplified from genomic *C. trachomatis* L2 (434/Bu) DNA and subcloned into the NotI and SalI sites in the *E. coli*/*Chlamydia* pBOMB4 shuttle vector generously provided by Drs. Ted Hackstadt and Mary Weber (Bauler & Hackstadt, 2014). The p2TK2-mCherry *E. coli*/*Chlamydia* shuttle vector encoding pTet-IncG-FLAG was previously generated in collaboration with the Derré lab (Mirrashidi et al., 2015).

Generation of *C. trachomatis* strains.

Rifampin-resistant *C. trachomatis* L2 (434/Bu) was mutagenized using EMS to generate a library of nearly 1000 mutants (Nguyen & Valdivia, 2012). Pooled sequencing identified a mutant strain with a SNV that introduces an early stop codon at amino acid 20 of Dre1 (R20*). This mutant was plaque purified (CTL2-M0463, hereafter referred to as L2Δ*dre1*), and subjected to whole genome sequencing as previously described (Kokes et al., 2015). Its DNA sequence was compared to that of the L2 Rif^R parental strain to identify other SNVs in L2Δ*dre1* (Table S2). Importantly, L2Δ*dre1* contains no other nonsense mutations, and was re-sequenced periodically to confirm that stocks retained the R20*

mutation. Plasmid DNA was isolated from *dam*$^{-}$/*dcm*$^{-}$ *E. coli* or *C. trachomatis* was transformed into *C. trachomatis* L2 Rif^{R} or *C. trachomatis* L2Δ*dre1* as previously described with slight modifications (C. M. Johnson & Fisher, 2013; Wang et al., 2011). Briefly, 10µg of plasmid was mixed with 1 x 10^{7} IFUs of C. trachomatis L2 and 1X Transformation Buffer (10 mM Tris pH 7.4 in 50mM $CaCl_2$) in 200 µl and incubated at room temperature for 30 minutes. The entire transformation mix was added to Vero cells seeded in 6-well plates (33.3µl/well). At 12 hpi, 5 mg/mL Ampicillin (Sigma) was added to select for transformed *Chlamydia*. After 3 initial passages, Ampicillin was increased to 50 mg/mL until transformed *Chlamydia* was expanded. Clonal populations of transformants were isolated under selection by plaque assay in Vero cells. *C. trachomatis* L2 Rif^{R} (parental strain) and L2Δ*dre1* were each transformed with empty vector. L2Δ*dre1* was transformed with pBOMB4-Dre1-FLAG for complementation. The *C. trachomatis* L2 Rif^{R} parental strain was transformed with pBOMB4-Dre1-FLAG to generate an overexpression strain (see Table S2 for a list of constructed *C. trachomatis* strains).

FLAG immunoprecipitations.

To generate the Dre1 infection interactome, 8 x 6-well plates of 80% confluent HeLa cells were infected with either wild-type *C. trachomatis* expressing plasmid-encoded Dre1$_{FLAG}$ or empty vector at a MOI of 5 for 36 hours. For all other FLAG immunoprecipitations, 3 x 6-well plates of 80% confluent HeLa cells were infected with the indicated *C. trachomatis* strains expressing a FLAG-tagged Inc for 36 hours. 10µM MG132 was added 4 hours prior to lysis, and cells were lysed on the plates for 30 minutes at 4ºC in Lysis Buffer (50mM Tris-HCl pH 7.5, 150mM NaCl, 1mM EDTA, 0.5% NP-40, PhosStop, Roche

Complete Protease Inhibitor). Lysates were clarified by centrifugation at 13,000rpm, 4ºC for 15 minutes. Supernatants were then incubated 30µl anti-FLAG magnetic beads (Millipore Sigma) rotating overnight at 4ºC. Beads were washed three times in Wash Buffer (50mM Tris-HCl pH 7.5, 150mM NaCl, 1mM EDTA, 0.05% NP-40) and then once in Final Wash Buffer (50mM Tris-HCl pH 7.5, 150mM NaCl, 1mM EDTA). Samples were eluted in 45µl of Elution Buffer (100µg/mL FLAG peptide in Final Wash Buffer; Millipore Sigma) for 25 minutes at room temperature with continuous gentle agitation. All purifications were performed in triplicate and assayed by anti-FLAG immunoblot using enhanced chemiluminescence (Amersham Biosciences) or by silver stain (Pierce). For FLAG immunoprecipitations not analyzed by MS, eluates were analyzed by immunoblot analysis with the following antibodies: anti-FLAG, anti-MOMP, anti-GAPDH, and anti-p27.

Sample preparation and mass spectrometry.

Eluates were digested with trypsin for LC-MS/MS analysis. Samples were denatured and reduced in 2M urea, 2mM DTT, 10mM NH_4HCO_3 for 30 min at 60° C, then alkylated with 2mM iodoacetamide at room temperature for 45 minutes. Trypsin (Promega) was added at a 1:100 enzyme: substrate ratio and digested at 37° C overnight. Following digestion, samples were then concentrated using C18 ZipTips (Millipore Sigma) according to manufacturer's instructions. Desalted samples were evaporated to dryness, and resuspended in 0.1% formic acid for MS analysis. Digested peptide mixtures were analyzed by LC-MS/MS on an Orbitrap Fusion Tribrid mass spectrometer (Thermo Fisher Scientific) equipped with an Easy-nLC 1200 HPLC (Thermo Fisher Scientific). Peptides were directly injected onto an analytical column (360 µm O.D. x 75 µm I.D.) with an

integrated emitter (New Objective) that was packed with 25cm of ReproSil Pur C18 AQ 1.9 µm particles (Dr. Maisch). The HPLC system delivered a gradient from 4% to 30% ACN in 0.1% formic acid over 43 min, followed by an increase to 80% ACN over 5min, and lastly a hold at 80% ACN for 20min. Peptides were introduced into the mass spectrometer by electrospray ionization in positive mode (1980V) with a transfer tube at 300° C. MS1 scans were performed with orbitrap detection in profile mode at a resolution of 120K, a scan range of 400-1600 m/z, a maximum in injection time of 100ms, and AGC target of 200K ions, 1 microscan, an S-Lens RV of 60. Peptides with peptide isotopic distribution patterns (MIPS = on) of charge state 2-7 were selected for data-dependent MS2 fragmentation, with a dynamic exclusion time of 20s, a single selection being allowed, a +/- 10ppm mass tolerance, and a minimum signal of 5K. Peptides selected for MS2 were fragmented by beam-type collisional activation (HCD), with a 1.6 m/z isolation window, a first mass of 100 m/z, a collision energy of 30, detection in the ion trap at a rapid scan rate in centroid mode, a 35 ms maximum injection time, and AGC target of 10K, inject ions for all available parallelizable time was activated.

Proteomics data analysis.

The mass spectrometry proteomics data have been deposited to the ProteomeXchange Consortium via the PRIDE partner repository (Perez-Riverol et al., 2019). All raw data was searched against both the Dre1 protein sequence and the canonical isoforms of the uniport human proteome (downloaded June 21, 2021) using MaxQuant (version 1.6.12.0) (Cox & Mann, 2008). Default search parameters were used to with the exception that match between runs was activated with a matching time window of 0.7 min. The default

parameters included trypsin specificity, a maximum of two missed cleavages, a 1% false-discovery rate at the peptide and protein level, a variable modification of oxididation on methionine, a variable modification of acetylation on the protein N-terminus. Finally, protein-protein interaction scoring of the identified proteins was performed with SAINTexpress, and high confidence protein-protein interactions were defined as those with a false discovery rate (BFDR) of less than 10% percent (Teo et al., 2014). We also included previously published high-confidence PPIs for Dre1 with a BFDR < 20% (Mirrashidi et al., 2015).

Strep affinity purifications.

For Strep affinity purifications, approximately 6 x 10^6 HEK293T cells were seeded in each of three 10 cm^2 plates, and were transfected using Avalanche-Omni Transfection Reagent (EZ Biosystems), following manufacturer's instructions. At 48 h after transfection cells were detached with 10 mM EDTA/D-PBS, washed with PBS, and lysed with 1mL of ice-cold Lysis Buffer at 4ºC for 30 minutes while rotating. Lysates were incubated with 30 uL of Strep-Tactin Sepharose beads (IBA) in 1 mL of Final Wash Buffer and incubated overnight, rotating at 4°C. Beads were washed three times in 1 mL of Wash Buffer and once in 1 mL of Final Wash Buffer. Samples were eluted in 45 µl of 10 mM $_D$-desthiobiotin (IBA) in Final Wash Buffer for 25 minutes at room temperature with continuous gentle agitation. Eluates were immunoblotted with anti-$p150^{glued}$, anti-Strep, and anti-GAPDH antibodies.

Fluorescence imaging.

HeLa cells were grown on glass coverslips in 24-well plates and infected with the indicated *C. trachomatis* strains (MOI ~ 1). Bacteria suspended in MEM supplemented with 10% FBS were centrifuged onto cell monolayers at 3500 RPM for 30 minutes at 4°C. *C. trachomatis*-infected HeLa cells were incubated at 37°C in 5% CO_2 for 1 hour, infection media aspirated, and fresh media added. Cells were then incubated at 37°C in 5% CO_2 for 24, 36, or 48 hours as indicated in the figure legends. For expression of tagged constructs, HeLa cells were transfected with the indicated constructs using Effectene (QIAGEN) for 24 hours prior to infection, according to manufacturer's instructions. Experiments requiring inclusion quantitation were performed at a low MOI (~0.2) to minimize cells with multiple inclusions. Experiments assaying efficiency of inclusion fusion were performed at a high MOI (~10) to maximize cells with multiple inclusions. When imaging centrosomes or cytoskeletal elements (including dynactin), cells were fixed in 100% ice-cold methanol for 6 minutes. For imaging the GA or transfected fluorescent fusion proteins, cells were fixed in 4% PFA in PBS for 15 minutes at room temperature and then permeabilized in pre-warmed 1X PBS containing 0.1% Triton X-100 for 5 minutes at room temperature. Cells were blocked in 1X PBS containing 1% BSA or 2% BSA (anti-Centrin-2) for 1.5 hrs, and stained with the indicated primary and fluorophore-conjugated secondary antibodies in blocking buffer for 1 hr each. Centrosomes were detected with anti-centrin to observe centrioles and anti-γ-Tubulin to observe pericentriolar material. MTs and mitotic spindles were stained with anti-β-tubulin or anti-$p150^{glued}$. Of note, we were unable to find a Dre1 antibody that detected endogenous levels by immunofluorescence microscopy. Coverslips were mounted in Vectashield

mounting media containing DAPI (Vector Laboratories) to identify bacteria and host cell nuclei. When quantitating number of nuclei or inclusions per cell, cells were stained with wheat-germ agglutinin 647 to delineate the plasma membrane. To assay Dre1 localization upon Nocodazole treatment, HeLa cells were grown on glass coverslips in 24-well plates, transfected with Dre1-sfGFP truncations for 24 hours and then treated with 100ng/mL Nocodazole or equivalent concentration DMSO for 3 hours, and then cold-shocked for 30min on ice. Cells were then immediately fixed in 4% PFA in PBS for 15 minutes at room temperature, permeabilized in pre-warmed 1X PBS containing 0.1% Triton X-100 for 5 minutes at room temperature and then stained with the indicated antibodies.

For co-localization of transfected Dre1-sfGFP truncation constructs and either (i) the MTOC (stained with the dye SiR-Tubulin 647; Cytoskeleton, Inc) or (ii) the centrosome (co-transfected with mCherry-Centrin2), HeLa cells were seeded on 24-well glass-bottom plates (MatTek, P24G-1.0-13-F) and transfected using Effectene (QIAGEN). At 24 hours post-transfection, cells were incubated with 100 nM SiR-Tubulin 647 dye in MEM for two hours at 37°C in 5% CO_2. Cells were then stained with 20nM PureBlu Hoescht (BioRad, 135-1304) in MEM for 15 minutes at 37°C in 5% CO_2. Cells were then washed with PBS, and incubated in phenol-free DMEM (UCSF Cell Culture Facility) at 37°C and 5% CO_2 and imaged with a spinning disc confocal microscope (as described below).

Microscopy.

Single Z slices or 0.3 µm-thick Z-stack images were acquired using Yokogawa CSU-X1 spinning disk confocal mounted on a Nikon Eclipse Ti inverted microscope equipped with

an Andora Clara digital camera and CFI APO TIRF 60x or 100x oil or PLAN APO 40x objective. Images were acquired by NIS- Elements software 4.10 (Nikon). For each set of experiments, the exposure time for each filter set for all images was identical. Images were processed with Nikon Elements, or Fiji Software.

A2EN pseudo-polarization.

Glass coverslips were placed in 24-well plates and submerged in 500µl of Type 1 collagen diluted to 30µg/mL in 20mM Acetic Acid in ddH_2O for 5 minutes at room temperature. Following aspiration, coverslips were washed with Keratinocyte media to remove residual acetic acid. Approximately 3.5 x 10^5 A2EN cells were seeded per well on collagen-coated coverslips. Cells were grown for 48 hours at 37˚ in 5% CO2. The media was aspirated to remove non-adherent cells and fresh media placed for 24 hours. Cells were infected with *C. trachomatis* by centrifuging bacteria diluted into 200µl of media per well onto cells at 500g for 5 minutes at room temperature. Infections were aspirated and cells were refed with warm media and incubated for 24 or 48 hours before fixation in either ice-cold MeOH or 4% PFA (see above for further detail).

Quantitation of inclusion formation.

HeLa cells, infected with the indicated *C. trachomatis* strain for 24 hours, were fixed with ice cold methanol or 4% PFA and visualized by confocal microscopy with anti-MOMP and fluorescent secondary antibodies. Images were acquired using a 40X objective and Nikon Elements pre-assigned image acquisition mode for 6 x 6 fields, creating a minimum of 30 usable fields per coverslip x 3 technical replicates, for a total of ~90 fields per condition

in which to enumerate inclusions. Data are mean ± SD of 3 independent biological replicates. To quantify production of infectious progeny, infected HeLa or A2EN cells were osmotically lysed in ddH_2O at 24, 36, or 48 hours post infection (hpi). 5-fold serial dilutions of harvested bacteria were used to infect fresh HeLa monolayers. At 24 hpi, inclusion formation was quantified as above.

Antibodies and reagents.

Primary antibodies were obtained from the following sources: mouse anti-p150^{glued} (BD Biosciences, 610473), mouse anti-FLAG (Millipore, F3165), rabbit anti-FLAG (Millipore, F7425), mouse anti-GAPDH (Millipore, MAB374), mouse anti-GM130 (BD Biosciences, 610823), mouse anti-centrin (Millipore, 04-1624), mouse anti-dynein, 74 kDa intermediate chains (Millipore, MAB1618), rabbit anti-p27 (DCTN6, Proteintech, 16947-1-AP), rabbit anti-γ-tubulin (Sigma, T3559), rabbit anti-Arl13b (Proteintech, 17711-1-AP), goat anti-MOMP L2 (Fitzgerald, 20C-CR2104GP), rabbit anti-Strep TagII HRP (Novagen, 71591–3), mouse anti- β-tubulin (Sigma, T4026). Mouse anti-IncA and rabbit anti-IncE antibodies were kindly provided by Dan Rockey (Oregon State University) and Ted Hackstadt (Rocky Mountain Laboratories), respectively. Secondary antibodies for immunofluorescence were derived from donkey and purchased from Life Technologies: anti-goat Alexafluor 647, anti-mouse Alexafluor 647, anti-rabbit Alexafluor 647, anti-mouse Alexafluor 568, anti-rabbit Alexafluor 568, anti-goat Alexafluor 488, anti-mouse Alexafluor 488, anti-rabbit Alexafluor 488. Nocodazole was purchased from Sigma (M1404). SiR-tubulin 647 was purchased from Cytoskeleton, Inc. Wheat-germ agglutinin 647 was purchased from Life Technologies (W32466). Heparin sodium salt was purchased from Sigma (H3393). (S)-

MG132 was purchased from Cayman Chemicals (10012628). Type 1 Collagen (ThermoFisher, A1048301).

Quantitation of centrosome recruitment and centrosome spread during interphase.

In images of acquired for HeLa cells infected for 36 hours, the centrosome to nucleus distance was calculated using Fiji to create 3D reconstructions of Z-stacks. A line was drawn from the centrosome (stained with anti-γ-Tubulin) to the nearest nuclear face (stained with DAPI) to calculate the centrosome-nucleus distance. Centrosome spread in infected HeLa cells was calculated at 36 hpi by using Fiji to generate maximum intensity projections of 3D image stacks of non-mitotic cells (defined as having uncoiled DNA and lacking spindles). The spread of centrosomes in these projections was calculated using the Fiji to draw a polygon encapsulating all centrosomes and then measuring the area of the convex hull corresponding to the polygon. Centrosome spread was calculated in > 40 cells per condition over three independent biological replicates, the average of the three replicates ± SD is overlaid on the individual measurements of centrosome spread.

Quantitation of aberrant spindles and multinucleation.

HeLa cells infected for 24 hours with the indicated *C. trachomatis* strains were fixed with 100% ice-cold MeOH and stained with antibodies to $p150^{glued}$ and γ-Tubulin to visualize mitotic spindles. The percent of mitotic cells containing aberrant spindles (defined as spindles with > 2 spindle poles) was calculated. For each condition > 45 mitotic cells across 3 independent biological replicates were counted and the average of the three replicates ± SD are represented. Multinucleation rates in infected cells were calculated at

36hpi by staining cells with WGA 647 to delineate the plasma membrane, and the fraction of infected cells containing > 1 nucleus (stained with DAPI) was determined. For each condition > 300 infected cells across 3 independent biological replicates were counted and the average of the three replicates ± SD are represented.

Quantitation of Golgi Apparatus (GA) recruitment.

To calculate GA recruitment to the inclusion membrane, HeLa cells were infected for 24 hours with the indicated *C. trachomatis* strains, fixed with 4% PFA, and stained with antibodies to GM130 (a *cis*-GA marker) and IncE. Fiji was used to generate maximum intensity projections from Z-stacks captured for each condition. Inclusion membrane signal in these 2D projections was traced to form a polygon, which was subsequently fitted to a circle that approximates the inclusion. A second, concentric circle was drawn with a radius 1 μm longer than the inclusion membrane circle to specify the region within the cell that is within 1 μm of the inclusion. The arc length of inclusion membrane corresponding to regions where GA signal falls between the outer and inner circles was transformed to an angle measurement using the angle tool in Fiji, and this value was divided by 360° (see Figure 4.5B). For each condition > 100 infected cells across 3 independent biological replicates were counted and the average of the three replicates ± SD are represented.

Murine Infection Model.

All experiments with mice were approved by the Institutional Animal Care and Use Committee of Duke University. Duke University maintains an animal care and use

program that is fully accredited by the Association for the Assessment of Accreditation of Laboratory Animal Care, International (AAALAC). Female C57BL/6J mice (Jackson Laboratory) were treated with 2.5 mg medroxyprogesterone (TEVA Pharmaceuticals) subcutaneously to synchronize their estrous cycles. Seven days later, 20 mice were infected transcervically with 1 x 10^7 EBs per mouse using an NSET Embryo Transfer device (ParaTechs). Mice were sacrificed at 3- and 5-days post infection, and the upper genital tracts were excised and trimmed of adipose tissue and immediately homogenized in 1 mL PBS (Gibco). DNA was extracted using a DNeasy kit (Qiagen) from 80 µL of homogenate following procedures recommended by the manufacturers.

RT-qPCR.

Quantitative PCR was performed on an a StepOne Plus Real Time PCR Systems (Applied Biosystems) using Power UP SYBR Green (ThermoFisher Scientific). Quantification of *C .trachomatis* 16S rRNA and mouse GAPDH were performed in triplicate and based on standard curves from dilutions of purified *C. trachomatis* and mouse DNA. Mouse PCR targets and primers used were: GAPDH (5'-ACTGAGCAAGAGAGGCCCTA-3', 5'-TATGGGGGTCTGGGATGGAA-3'), and *C. trachomatis* PCR targets and primers used were: 16S rRNA (5'-GGAGGCTGCAGTCGAGAATCT-3', 5'-TTACAACCCTAGAGCCTTCATCACA-3') (Sixt et al., 2017).

Statistical analysis.

For each experiment 3 or more independent biological replicates were performed and the results are plotted individually or combined and represented as mean ± SD, as described in figure legends. For experiments with naturally high variability due to the asynchronous nature of *C. trachomatis* infections, Superplots were used to represent the data (Figures 2.3B, 2.7A, 2.7B, and 2.7C; Lord et al., 2020). Briefly, all individual data points from all replicates are represented as small circles and color coded according to replicate number. Average values of each replicate were also color coded, and represented with triangles. The black bars represent the average of all replicates ± SD. All statistical analyses were performed using GraphPad Prism 9.0. All assays were analyzed using a one-way ANOVA with a two-tailed Welch's t-test. *Chlamydia* growth in the murine infection model used a two-tailed Mann–Whitney U-test.

ACKNOWLEDGEMENTS

We thank the members of the Engel lab for many conversations and support throughout the project. We thank Drs. Deborah Dean, Ted Hackstadt, Mary Weber, Dan Rockey, Isabel Derre, Sophie Dumont, Ron Vale, Robert Bastidas, and Raphael Valdivia for reagents; Dr. Anita Sil for the use of her confocal microscope; members of the Engel, and Dumont labs for advice, and Drs. Sophie Dumont, Alex Long, and Rick McKenney for consulting on the project at various stages. We acknowledge grant support from the NIH (J.S. F31AI133951, J.E. AI073770, AI105561) and the NSF (J.S. GRFP Fellowship).

REFERENCES

Almeida, F., Borges, V., Ferreira, R., Borrego, M. J., Gomes, J. P., & Mota, L. J. (2012). Polymorphisms in inc proteins and differential expression of inc genes among Chlamydia trachomatis strains correlate with invasiveness and tropism of lymphogranuloma venereum isolates. Journal of Bacteriology, 194(23), 6574–6585. https://doi.org/10.1128/JB.01428-12

Alzhanov, D. T., Weeks, S. K., Burnett, J. R., & Rockey, D. D. (2009). Cytokinesis is blocked in mammalian cells transfected with Chlamydia trachomatis gene CT223. BMC Microbiology, 9(1), 2. https://doi.org/10.1186/1471-2180-9-2

Andersen, S. E., Bulman, L. M., Steiert, B., Faris, R., & Weber, M. M. (2021). Got mutants? How advances in chlamydial genetics have furthered the study of effector proteins. Pathogens and Disease, 79(2), ftaa078. https://doi.org/10.1093/femspd/ftaa078

Arbyn, M., Weiderpass, E., Bruni, L., de Sanjosé, S., Saraiya, M., Ferlay, J., & Bray, F. (2020). Estimates of incidence and mortality of cervical cancer in 2018: A worldwide analysis. The Lancet. Global Health, 8(2), e191–e203. https://doi.org/10.1016/S2214-109X(19)30482-6

Askham, J. M., Vaughan, K. T., Goodson, H. V., & Morrison, E. E. (2002). Evidence that an interaction between EB1 and p150(Glued) is required for the formation and maintenance of a radial microtubule array anchored at the centrosome. Molecular Biology of the Cell, 13(10), 3627–3645. https://doi.org/10.1091/mbc.e02-01-0061

Bannantine, J. P., Griffiths, R. S., Viratyosin, W., Brown, W. J., & Rockey, D. D. (2000). A secondary structure motif predictive of protein localization to the chlamydial

inclusion membrane. Cellular Microbiology, 2(1), 35–47. https://doi.org/10.1046/j.1462-5822.2000.00029.x

Bastidas, R. J., Elwell, C. A., Engel, J. N., & Valdivia, R. H. (2013). Chlamydial Intracellular Survival Strategies. Cold Spring Harbor Perspectives in Medicine, 3(5), a010256–a010256. https://doi.org/10.1101/cshperspect.a010256

Bauler, L. D., & Hackstadt, T. (2014). Expression and Targeting of Secreted Proteins from Chlamydia trachomatis. Journal of Bacteriology, 196(7), 1325–1334. https://doi.org/10.1128/JB.01290-13

Bennett, J. E., Dolin, R., & Blaser, M. J. (Eds.). (2015). Mandell, Douglas, and Bennett's principles and practice of infectious diseases (Eighth edition). Elsevier/Saunders.

Bettencourt-Dias, M., & Glover, D. M. (2007). Centrosome biogenesis and function: Centrosomics brings new understanding. Nature Reviews Molecular Cell Biology, 8(6), 451–463. https://doi.org/10.1038/nrm2180

Brown, H. M., Knowlton, A. E., & Grieshaber, S. S. (2012). Chlamydial infection induces host cytokinesis failure at abscission. Cellular Microbiology, 14(10), 1554–1567. https://doi.org/10.1111/j.1462-5822.2012.01820.x

Brown, H. M., Knowlton, A. E., Snavely, E., Nguyen, B. D., Richards, T. S., & Grieshaber, S. S. (2014). Multinucleation during C. trachomatis Infections Is Caused by the Contribution of Two Effector Pathways. PLoS ONE, 9(6), e100763. https://doi.org/10.1371/journal.pone.0100763

Burakov, A., Nadezhdina, E., Slepchenko, B., & Rodionov, V. (2003). Centrosome positioning in interphase cells. The Journal of Cell Biology, 162(6), 963–969. https://doi.org/10.1083/jcb.200305082

Chen, T.-Y., Syu, J.-S., Han, T.-Y., Cheng, H.-L., Lu, F.-I., & Wang, C.-Y. (2015). Cell Cycle-Dependent Localization of Dynactin Subunit p150 glued at Centrosome. Journal of Cellular Biochemistry, 116(9), 2049–2060. https://doi.org/10.1002/jcb.25160

Chiarelli, T. J., Grieshaber, N. A., & Grieshaber, S. S. (2020). Live-Cell Forward Genetic Approach to Identify and Isolate Developmental Mutants in Chlamydia trachomatis. Journal of Visualized Experiments: JoVE, 160. https://doi.org/10.3791/61365

Cingolani, G., McCauley, M., Lobley, A., Bryer, A. J., Wesolowski, J., Greco, D. L., Lokareddy, R. K., Ronzone, E., Perilla, J. R., & Paumet, F. (2019). Structural basis for the homotypic fusion of chlamydial inclusions by the SNARE-like protein IncA. Nature Communications, 10(1), 2747. https://doi.org/10.1038/s41467-019-10806-9

Conduit, P. T., Wainman, A., & Raff, J. W. (2015). Centrosome function and assembly in animal cells. Nature Reviews Molecular Cell Biology, 16(10), 611–624. https://doi.org/10.1038/nrm4062

Cox, J., & Mann, M. (2008). MaxQuant enables high peptide identification rates, individualized p.p.b.-range mass accuracies and proteome-wide protein quantification. Nature Biotechnology, 26(12), 1367–1372. https://doi.org/10.1038/nbt.1511

Darville, T., & Hiltke, T. J. (2010). Pathogenesis of Genital Tract Disease Due to Chlamydia trachomatis. The Journal of Infectious Diseases, 201(S2), 114–125. https://doi.org/10.1086/652397

Dehoux, P., Flores, R., Dauga, C., Zhong, G., & Subtil, A. (2011). Multi-genome identification and characterization of chlamydiae-specific type III secretion substrates: The Inc proteins. BMC Genomics, 12, 109. https://doi.org/10.1186/1471-2164-12-109

Dickinson, M. S., Anderson, L. N., Webb-Robertson, B.-J. M., Hansen, J. R., Smith, R. D., Wright, A. T., & Hybiske, K. (2019). Proximity-dependent proteomics of the Chlamydia trachomatis inclusion membrane reveals functional interactions with endoplasmic reticulum exit sites. PLOS Pathogens, 15(4), e1007698. https://doi.org/10.1371/journal.ppat.1007698

Drosopoulos, K., Tang, C., Chao, W. C. H., & Linardopoulos, S. (2014). APC/C is an essential regulator of centrosome clustering. Nature Communications, 5(1), 3686. https://doi.org/10.1038/ncomms4686

Eckley, D. M., Gill, S. R., Melkonian, K. A., Bingham, J. B., Goodson, H. V., Heuser, J. E., & Schroer, T. A. (1999). Analysis of Dynactin Subcomplexes Reveals a Novel Actin-Related Protein Associated with the Arp1 Minifilament Pointed End. Journal of Cell Biology, 147(2), 307–320. https://doi.org/10.1083/jcb.147.2.307

Elwell, C. A., Jiang, S., Kim, J. H., Lee, A., Wittmann, T., Hanada, K., Melancon, P., & Engel, J. N. (2011). Chlamydia trachomatis Co-opts GBF1 and CERT to Acquire Host Sphingomyelin for Distinct Roles during Intracellular Development. PLoS Pathogens, 7(9), e1002198. https://doi.org/10.1371/journal.ppat.1002198

Elwell, C., Mirrashidi, K., & Engel, J. (2016). Chlamydia cell biology and pathogenesis. Nature Reviews Microbiology, 14(6), 385–400. https://doi.org/10.1038/nrmicro.2016.30

Geisler, W. M., Suchland, R. J., Rockey, D. D., & Stamm, W. E. (2001). Epidemiology and Clinical Manifestations of Unique Chlamydia trachomatis Isolates That Occupy Nonfusogenic Inclusions. The Journal of Infectious Diseases, 184(7), 879–884. https://doi.org/10.1086/323340

Greene, W. (2003). Inhibition of host cell cytokinesis by Chlamydia trachomatis infection. Journal of Infection, 47(1), 45–51. https://doi.org/10.1016/S0163-4453(03)00039-2

Grieshaber, S. S., Grieshaber, N. A., & Hackstadt, T. (2003). Chlamydia trachomatis uses host cell dynein to traffic to the microtubule-organizing center in a p50 dynamitin-independent process. Journal of Cell Science, 116(Pt 18), 3793–3802. https://doi.org/10.1242/jcs.00695

Grieshaber, S. S., Grieshaber, N. A., Miller, N., & Hackstadt, T. (2006). Chlamydia trachomatis causes centrosomal defects resulting in chromosomal segregation abnormalities. Traffic (Copenhagen, Denmark), 7(8), 940–949. https://doi.org/10.1111/j.1600-0854.2006.00439.x

Hackstadt, T., Fischer, E. R., Scidmore, M. A., Rockey, D. D., & Heinzen, R. A. (1997). Origins and functions of the chlamydial inclusion. Trends in Microbiology, 5(7), 288–293. https://doi.org/10.1016/S0966-842X(97)01061-5

Hackstadt, T., Scidmore-Carlson, M. A., Shaw, E. I., & Fischer, E. R. (1999). The Chlamydia trachomatis IncA protein is required for homotypic vesicle fusion. Cellular Microbiology, 1(2), 119–130. https://doi.org/10.1046/j.1462-5822.1999.00012.x

Henry, T., Gorvel, J.-P., & Meresse, S. (2006). Molecular motors hijacking by intracellular pathogens. Cellular Microbiology, 8(1), 23–32. https://doi.org/10.1111/j.1462-5822.2005.00649.x

Heuer, D., Rejman Lipinski, A., Machuy, N., Karlas, A., Wehrens, A., Siedler, F., Brinkmann, V., & Meyer, T. F. (2009). Chlamydia causes fragmentation of the Golgi compartment to ensure reproduction. Nature, 457(7230), 731–735. https://doi.org/10.1038/nature07578

Holleran, E. A., Ligon, L. A., Tokito, M., Stankewich, M. C., Morrow, J. S., & Holzbaur, E. L. F. (2001). BIII Spectrin Binds to the Arp1 Subunit of Dynactin. Journal of Biological Chemistry, 276(39), 36598–36605. https://doi.org/10.1074/jbc.M104838200

Hueschen, C. L., Kenny, S. J., Xu, K., & Dumont, S. (2017). NuMA recruits dynein activity to microtubule minus-ends at mitosis. ELife, 6, e29328. https://doi.org/10.7554/eLife.29328

Jaarsma, D., & Hoogenraad, C. C. (2015). Cytoplasmic dynein and its regulatory proteins in Golgi pathology in nervous system disorders. Frontiers in Neuroscience, 9. https://doi.org/10.3389/fnins.2015.00397

Jacquot, G., Maidou-Peindara, P., & Benichou, S. (2010). Molecular and functional basis for the scaffolding role of the p50/dynamitin subunit of the microtubule-associated dynactin complex. The Journal of Biological Chemistry, 285(30), 23019–23031. https://doi.org/10.1074/jbc.M110.100602

Jäger, S., Cimermancic, P., Gulbahce, N., Johnson, J. R., McGovern, K. E., Clarke, S. C., Shales, M., Mercenne, G., Pache, L., Li, K., Hernandez, H., Jang, G. M., Roth,

S. L., Akiva, E., Marlett, J., Stephens, M., D'Orso, I., Fernandes, J., Fahey, M., … Krogan, N. J. (2011). Global landscape of HIV-human protein complexes. Nature, 481(7381), 365–370. https://doi.org/10.1038/nature10719

Jemal, A., Bray, F., Center, M. M., Ferlay, J., Ward, E., & Forman, D. (2011). Global cancer statistics. CA: A Cancer Journal for Clinicians, 61(2), 69–90. https://doi.org/10.3322/caac.20107

Johnson, C. M., & Fisher, D. J. (2013). Site-Specific, Insertional Inactivation of incA in Chlamydia trachomatis Using a Group II Intron. PLoS ONE, 8(12), e83989. https://doi.org/10.1371/journal.pone.0083989

Johnson, K. A., Tan, M., & Sütterlin, C. (2009). Centrosome abnormalities during a Chlamydia trachomatis infection are caused by dysregulation of the normal duplication pathway. Cellular Microbiology, 11(7), 1064–1073. https://doi.org/10.1111/j.1462-5822.2009.01307.x

Knowlton, A. E., Brown, H. M., Richards, T. S., Andreolas, L. A., Patel, R. K., & Grieshaber, S. S. (2011). Chlamydia trachomatis Infection Causes Mitotic Spindle Pole Defects Independently from its Effects on Centrosome Amplification. Traffic, 12(7), 854–866. https://doi.org/10.1111/j.1600-0854.2011.01204.x

Kokes, M., Dunn, J. D., Granek, J. A., Nguyen, B. D., Barker, J. R., Valdivia, R. H., & Bastidas, R. J. (2015). Integrating Chemical Mutagenesis and Whole-Genome Sequencing as a Platform for Forward and Reverse Genetic Analysis of Chlamydia. Cell Host & Microbe, 17(5), 716–725. https://doi.org/10.1016/j.chom.2015.03.014

Liu, Y., & Pelletier, L. (2019). A magic bullet for targeting cancers with supernumerary centrosomes. The EMBO Journal, 38(2), e101134. https://doi.org/10.15252/embj.2018101134

Lord, S. J., Velle, K. B., Mullins, R. D., & Fritz-Laylin, L. K. (2020). SuperPlots: Communicating reproducibility and variability in cell biology. Journal of Cell Biology, 219(6), e202001064. https://doi.org/10.1083/jcb.202001064

Lutter, E. I., Martens, C., & Hackstadt, T. (2012). Evolution and conservation of predicted inclusion membrane proteins in chlamydiae. Comparative and Functional Genomics, 2012, 362104. https://doi.org/10.1155/2012/362104

Malhotra, M., Sood, S., Mukherjee, A., Muralidhar, S., & Bala, M. (2013). Genital Chlamydia trachomatis: An update. The Indian Journal of Medical Research, 138(3), 303–316.

Mandell, G. L., Bennett, J. E., & Dolin, R. (Eds.). (2010). Mandell, Douglas, and Bennett's principles and practice of infectious diseases (7th ed). Churchill Livingstone/Elsevier.

Melkonian, K. A., Maier, K. C., Godfrey, J. E., Rodgers, M., & Schroer, T. A. (2007). Mechanism of dynamitin-mediated disruption of dynactin. The Journal of Biological Chemistry, 282(27), 19355–19364. https://doi.org/10.1074/jbc.M700003200

Milunović-Jevtić, A., Mooney, P., Sulerud, T., Bisht, J., & Gatlin, J. (2016). Centrosomal clustering contributes to chromosomal instability and cancer. Current Opinion in Biotechnology, 40, 113–118. https://doi.org/10.1016/j.copbio.2016.03.011

Mirrashidi, K. M., Elwell, C. A., Verschueren, E., Johnson, J. R., Frando, A., Von Dollen, J., Rosenberg, O., Gulbahce, N., Jang, G., Johnson, T., Jäger, S., Gopalakrishnan, A. M., Sherry, J., Dunn, J. D., Olive, A., Penn, B., Shales, M., Cox, J. S., Starnbach, M. N., … Engel, J. (2015). Global Mapping of the Inc-Human Interactome Reveals that Retromer Restricts Chlamydia Infection. Cell Host & Microbe, 18(1), 109–121. https://doi.org/10.1016/j.chom.2015.06.004

Mital, J., & Hackstadt, T. (2011). Diverse Requirements for Src-Family Tyrosine Kinases Distinguish Chlamydial Species. MBio, 2(2). https://doi.org/10.1128/mBio.00031-11

Mital, J., Lutter, E. I., Barger, A. C., Dooley, C. A., & Hackstadt, T. (2015). Chlamydia trachomatis inclusion membrane protein CT850 interacts with the dynein light chain DYNLT1 (Tctex1). Biochemical and Biophysical Research Communications, 462(2), 165–170. https://doi.org/10.1016/j.bbrc.2015.04.116

Moore, E. R., & Ouellette, S. P. (2014). Reconceptualizing the chlamydial inclusion as a pathogen-specified parasitic organelle: An expanded role for Inc proteins. Frontiers in Cellular and Infection Microbiology, 4. https://doi.org/10.3389/fcimb.2014.00157

Mueller, K. E., Plano, G. V., & Fields, K. A. (2014). New frontiers in type III secretion biology: The Chlamydia perspective. Infection and Immunity, 82(1), 2–9. https://doi.org/10.1128/IAI.00917-13

Nguyen, B. D., & Valdivia, R. H. (2012). Virulence determinants in the obligate intracellular pathogen Chlamydia trachomatis revealed by forward genetic

approaches. Proceedings of the National Academy of Sciences, 109(4), 1263–1268. https://doi.org/10.1073/pnas.1117884109

Palmer, K. J., Hughes, H., & Stephens, D. J. (2009). Specificity of cytoplasmic dynein subunits in discrete membrane-trafficking steps. Molecular Biology of the Cell, 20(12), 2885–2899. https://doi.org/10.1091/mbc.e08-12-1160

Pannu, V., Rida, P. C. G., Celik, B., Turaga, R. C., Ogden, A., Cantuaria, G., Gopalakrishnan, J., & Aneja, R. (2014). Centrosome-declustering drugs mediate a two-pronged attack on interphase and mitosis in supercentrosomal cancer cells. Cell Death & Disease, 5(11), e1538–e1538. https://doi.org/10.1038/cddis.2014.505

Perez-Riverol, Y., Csordas, A., Bai, J., Bernal-Llinares, M., Hewapathirana, S., Kundu, D. J., Inuganti, A., Griss, J., Mayer, G., Eisenacher, M., Pérez, E., Uszkoreit, J., Pfeuffer, J., Sachsenberg, T., Yılmaz, Ş., Tiwary, S., Cox, J., Audain, E., Walzer, M., … Vizcaíno, J. A. (2019). The PRIDE database and related tools and resources in 2019: Improving support for quantification data. Nucleic Acids Research, 47(D1), D442–D450. https://doi.org/10.1093/nar/gky1106

Pruneda, J. N., Bastidas, R. J., Bertsoulaki, E., Swatek, K. N., Santhanam, B., Clague, M. J., Valdivia, R. H., Urbé, S., & Komander, D. (2018). A Chlamydia effector combining deubiquitination and acetylation activities induces Golgi fragmentation. Nature Microbiology, 3(12), 1377–1384. https://doi.org/10.1038/s41564-018-0271-y

Quintyne, N. J., Gill, S. R., Eckley, D. M., Crego, C. L., Compton, D. A., & Schroer, T. A. (1999). Dynactin is required for microtubule anchoring at centrosomes. The Journal of Cell Biology, 147(2), 321–334. https://doi.org/10.1083/jcb.147.2.321

Quintyne, N. J., & Schroer, T. A. (2002). Distinct cell cycle–dependent roles for dynactin and dynein at centrosomes. Journal of Cell Biology, 159(2), 245–254. https://doi.org/10.1083/jcb.200203089

Rey-Ladino, J., Ross, A. G. P., & Cripps, A. W. (2014). Immunity, immunopathology, and human vaccine development against sexually transmitted Chlamydia trachomatis. Human Vaccines & Immunotherapeutics, 10(9), 2664–2673. https://doi.org/10.4161/hv.29683

Richards, T. S., Knowlton, A. E., & Grieshaber, S. S. (2013). Chlamydia trachomatis homotypic inclusion fusion is promoted by host microtubule trafficking. BMC Microbiology, 13(1), 185. https://doi.org/10.1186/1471-2180-13-185

Rieder, C. L., & Cole, R. W. (2002). Cold-shock and the Mammalian cell cycle. Cell Cycle (Georgetown, Tex.), 1(3), 169–175.

Robinson, J. T., Wojcik, E. J., Sanders, M. A., McGrail, M., & Hays, T. S. (1999). Cytoplasmic dynein is required for the nuclear attachment and migration of centrosomes during mitosis in Drosophila. The Journal of Cell Biology, 146(3), 597–608. https://doi.org/10.1083/jcb.146.3.597

Rockey, D. D., Scidmore, M. A., Bannantine, J. P., & Brown, W. J. (2002). Proteins in the chlamydial inclusion membrane. Microbes and Infection, 4(3), 333–340. https://doi.org/10.1016/s1286-4579(02)01546-0

Sanchez, A. D., & Feldman, J. L. (2017). Microtubule-organizing centers: From the centrosome to non-centrosomal sites. Current Opinion in Cell Biology, 44, 93–101. https://doi.org/10.1016/j.ceb.2016.09.003

Schindelin, J., Arganda-Carreras, I., Frise, E., Kaynig, V., Longair, M., Pietzsch, T., Preibisch, S., Rueden, C., Saalfeld, S., Schmid, B., Tinevez, J.-Y., White, D. J., Hartenstein, V., Eliceiri, K., Tomancak, P., & Cardona, A. (2012). Fiji: An open-source platform for biological-image analysis. Nature Methods, 9(7), 676–682. https://doi.org/10.1038/nmeth.2019

Schroer, T. A., & Verma, V. (2021). Cytoskeleton | Dynactin. In Encyclopedia of Biological Chemistry III (pp. 188–192). Elsevier. https://doi.org/10.1016/B978-0-12-819460-7.00186-9

Sixt, B. S., Bastidas, R. J., Finethy, R., Baxter, R. M., Carpenter, V. K., Kroemer, G., Coers, J., & Valdivia, R. H. (2017). The Chlamydia trachomatis Inclusion Membrane Protein CpoS Counteracts STING-Mediated Cellular Surveillance and Suicide Programs. Cell Host & Microbe, 21(1), 113–121. https://doi.org/10.1016/j.chom.2016.12.002

Smith, J. S., Bosetti, C., Muñoz, N., Herrero, R., Bosch, F. X., Eluf-Neto, J., Meijer, C. J. L. M., van den Brule, A. J. C., Franceschi, S., & Peeling, R. W. (2004). Chlamydia trachomatis and invasive cervical cancer: A pooled analysis of the IARC multicentric case-control study: C. Trachomatis and Invasive Cervical Cancer. International Journal of Cancer, 111(3), 431–439. https://doi.org/10.1002/ijc.20257

Sowa, M. E., Bennett, E. J., Gygi, S. P., & Harper, J. W. (2009). Defining the human deubiquitinating enzyme interaction landscape. Cell, 138(2), 389–403. https://doi.org/10.1016/j.cell.2009.04.042

Stephens, R. S., Kalman, S., Lammel, C., Fan, J., Marathe, R., Aravind, L., Mitchell, W., Olinger, L., Tatusov, R. L., Zhao, Q., Koonin, E. V., & Davis, R. W. (1998). Genome sequence of an obligate intracellular pathogen of humans: Chlamydia trachomatis. Science (New York, N.Y.), 282(5389), 754–759. https://doi.org/10.1126/science.282.5389.754

Sun, H. S., Sin, A. T.-W., Poirier, M. B., & Harrison, R. E. (2016). Chlamydia trachomatis Inclusion Disrupts Host Cell Cytokinesis to Enhance Its Growth in Multinuclear Cells. Journal of Cellular Biochemistry, 117(1), 132–143. https://doi.org/10.1002/jcb.25258

Sun, H. S., Wilde, A., & Harrison, R. E. (2011). Chlamydia trachomatis Inclusions Induce Asymmetric Cleavage Furrow Formation and Ingression Failure in Host Cells. Molecular and Cellular Biology, 31(24), 5011–5022. https://doi.org/10.1128/MCB.05734-11

Tan, M., & Sütterlin, C. (2014). The Chlamydia protease CPAF: Caution, Precautions And Function. Pathogens and Disease, 72(1), 7–9. https://doi.org/10.1111/2049-632X.12213

Teo, G., Liu, G., & Zhang, J. (2014). SAINTexpress: Improvements and additional features in Significance Analysis of INTeractome software. Journal of Proteomics, 100, 37–43. https://doi.org/10.1016/j.jprot.2013.10.023

Tirumala, N. A., & Ananthanarayanan, V. (2020). Role of Dynactin in the Intracellular Localization and Activation of Cytoplasmic Dynein. Biochemistry, 59(2), 156–162. https://doi.org/10.1021/acs.biochem.9b00772

Wang, Y., Kahane, S., Cutcliffe, L. T., Skilton, R. J., Lambden, P. R., & Clarke, I. N. (2011). Development of a Transformation System for Chlamydia trachomatis: Restoration of Glycogen Biosynthesis by Acquisition of a Plasmid Shuttle Vector. PLoS Pathogens, 7(9), e1002258. https://doi.org/10.1371/journal.ppat.1002258

Weber, M. M., Bauler, L. D., Lam, J., & Hackstadt, T. (2015). Expression and localization of predicted inclusion membrane proteins in Chlamydia trachomatis. Infection and Immunity, 83(12), 4710–4718. https://doi.org/10.1128/IAI.01075-15

Weber, M. M., Noriea, N. F., Bauler, L. D., Lam, J. L., Sager, J., Wesolowski, J., Paumet, F., & Hackstadt, T. (2016). A Functional Core of IncA Is Required for Chlamydia trachomatis Inclusion Fusion. Journal of Bacteriology, 198(8), 1347–1355. https://doi.org/10.1128/JB.00933-15

Wesolowski, J., Weber, M. M., Nawrotek, A., Dooley, C. A., Calderon, M., St. Croix, C. M., Hackstadt, T., Cherfils, J., & Paumet, F. (2017). Chlamydia Hijacks ARF GTPases To Coordinate Microtubule Posttranslational Modifications and Golgi Complex Positioning. MBio, 8(3). https://doi.org/10.1128/mBio.02280-16

Wittmann, T., & Hyman, T. (1998). Chapter 7 Recombinant p50/Dynamitin as a Tool to Examine the Role of Dynactin in Intracellular Processes. In Methods in Cell Biology (Vol. 61, pp. 137–143). Elsevier. https://doi.org/10.1016/S0091-679X(08)61978-0

World Health Organization. (2016). WHO guidelines for the treatment of chlamydia trachomatis. http://www.ncbi.nlm.nih.gov/books/NBK379707/

Yadav, S., & Linstedt, A. D. (2011). Golgi Positioning. Cold Spring Harbor Perspectives in Biology, 3(5), a005322–a005322. https://doi.org/10.1101/cshperspect.a005322

Zhu, H., Shen, Z., Luo, H., Zhang, W., & Zhu, X. (2016). Chlamydia Trachomatis Infection-Associated Risk of Cervical Cancer: A Meta-Analysis. Medicine, 95(13), e3077. https://doi.org/10.1097/MD.0000000000003077

FIGURE 2.1

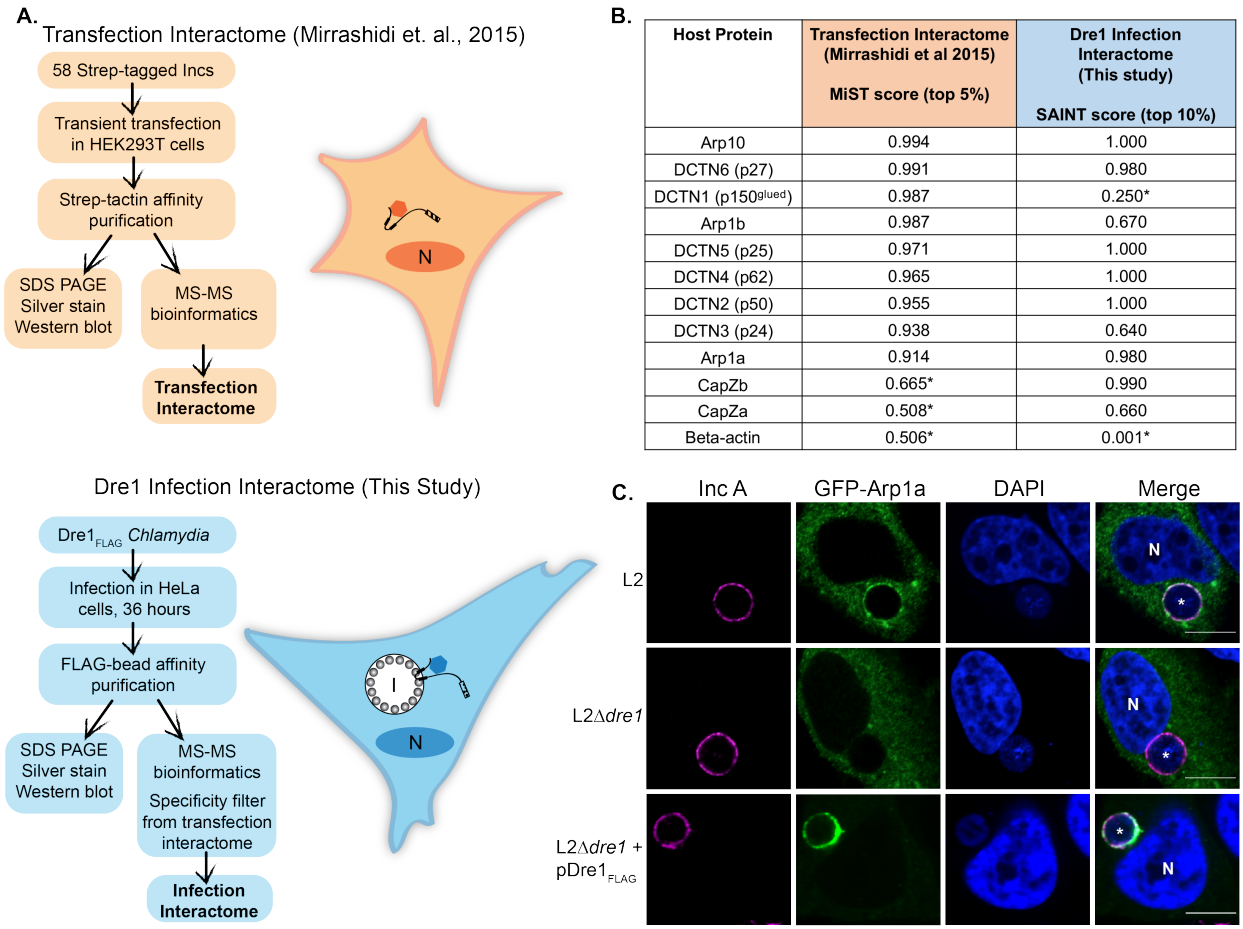

Host Protein	Transfection Interactome (Mirrashidi et al 2015) MiST score (top 5%)	Dre1 Infection Interactome (This study) SAINT score (top 10%)
Arp10	0.994	1.000
DCTN6 (p27)	0.991	0.980
DCTN1 (p150^{glued})	0.987	0.250*
Arp1b	0.987	0.670
DCTN5 (p25)	0.971	1.000
DCTN4 (p62)	0.965	1.000
DCTN2 (p50)	0.955	1.000
DCTN3 (p24)	0.938	0.640
Arp1a	0.914	0.980
CapZb	0.665*	0.990
CapZa	0.508*	0.660
Beta-actin	0.506*	0.001*

FIGURE 2.1. Dre1 recruits host dynactin to the inclusion during infection.

(A) Schematic of orthogonal AP-MS screens ("Transfection Interactome" and "Dre1 Infection Interactome") to identify host binding partners of Dre1.

(B) List of dynactin subunits that co-purified with transfected Dre1 in HEK293T cells and scored in the top 5% of all MiST scores (descending order; Transfection Interactome) and of dynactin subunits that co-purified with Dre1 during *C. trachomatis* infection and scored in the top 10% of SAINT scores (Infection Interactome). Host protein scores marked with an asterisk are outside the top 5% or 10% of scores by MiST or SAINT respectively, but are indicated because they were present in Dre1 eluates.

(C) Dre1 is required for recruitment of transfected GFP-Arp1a to the inclusion. HeLa cells infected for 24 hours with the indicated strains were fixed, and stained with anti-IncA (outlines inclusion membrane), transfected GFP-Arp1a (a dynactin subunit), and DAPI (to visualize nucleus and bacteria). Shown are single Z slices. N, nucleus. *, Inclusion. Scale bar, 10μm.

FIGURE 2.2

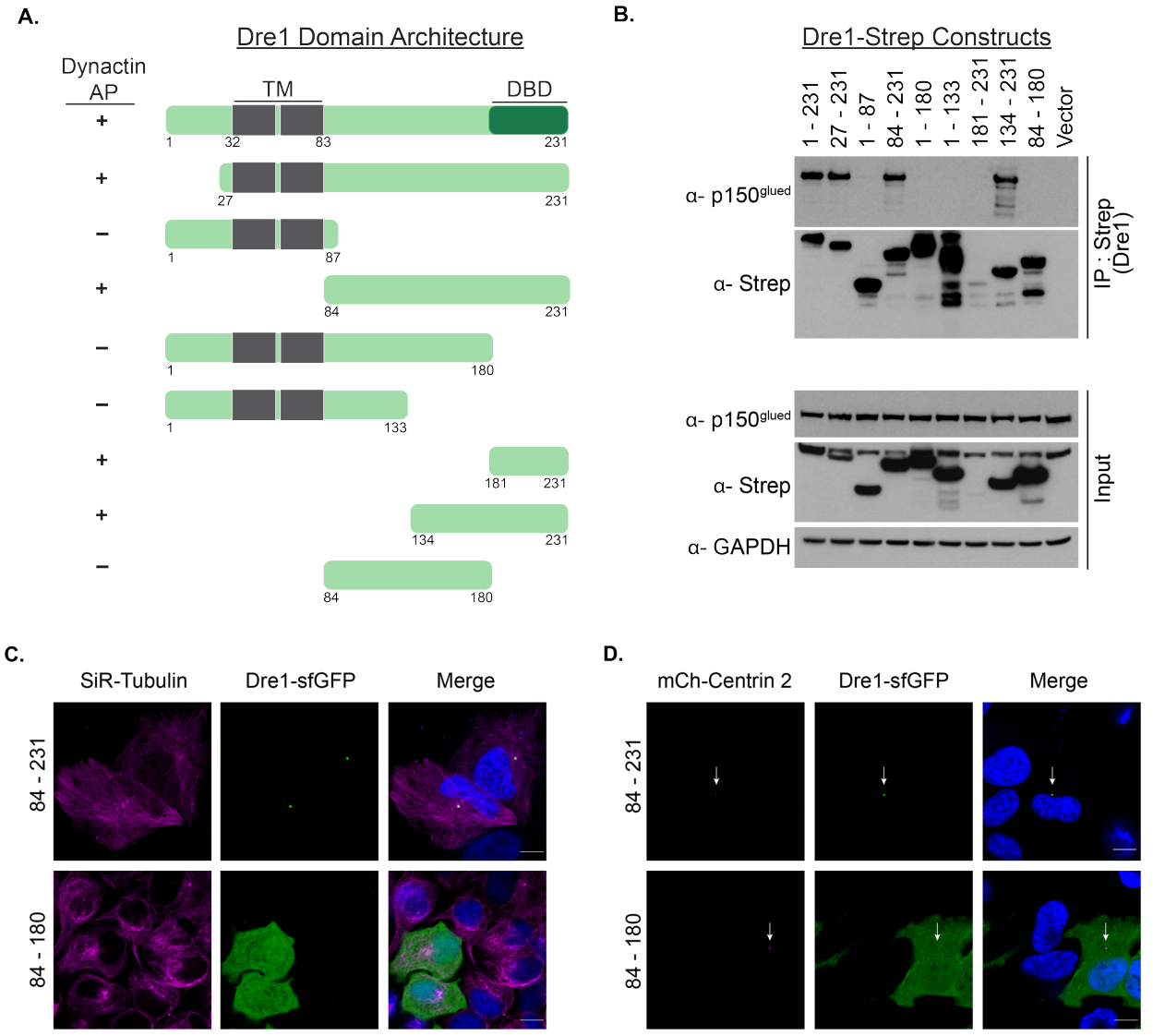

FIGURE 2.2. The C-terminal 50 amino acids of Dre1 are required for dynactin interaction and for recruitment of Dre1 to the centrosomal MTOC.

(A) Schematic of $Dre1_{Strep}$ constructs and summary of whether they interact with $p150^{glued}$. Transmembrane (TM) domain, grey. Dre1 Dynactin binding domain, (DBD), dark green.

(B) Immunoblot of $Dre1_{Strep}$ APs. HEK293T cells were transiently transfected with the indicated $Dre1_{Strep}$ constructs. Lysates were affinity purified with anti-Strep beads, and immunoblotted with the indicated antibodies. Input represents 0.02% of lysates. Cells transfected with empty vector serve as a negative control. Data shown are representative of three independent biological experiments.

(C, D) The C-terminus of transfected Dre1 is necessary for co-localization with Tubulin and Centrin 2. HeLa cells were transiently transfected with the indicated Dre1 constructs fused to superfolder GFP (sfGFP) and (C) stained with SiR-Tubulin dye to visualize MTs, or (D) co-transfected with mCherry-Centrin2 to visualize the centrosome (indicated with white arrows). Single Z slices acquired by live cell imaging are shown. Scale bar, 10μm.

FIGURE 2.3

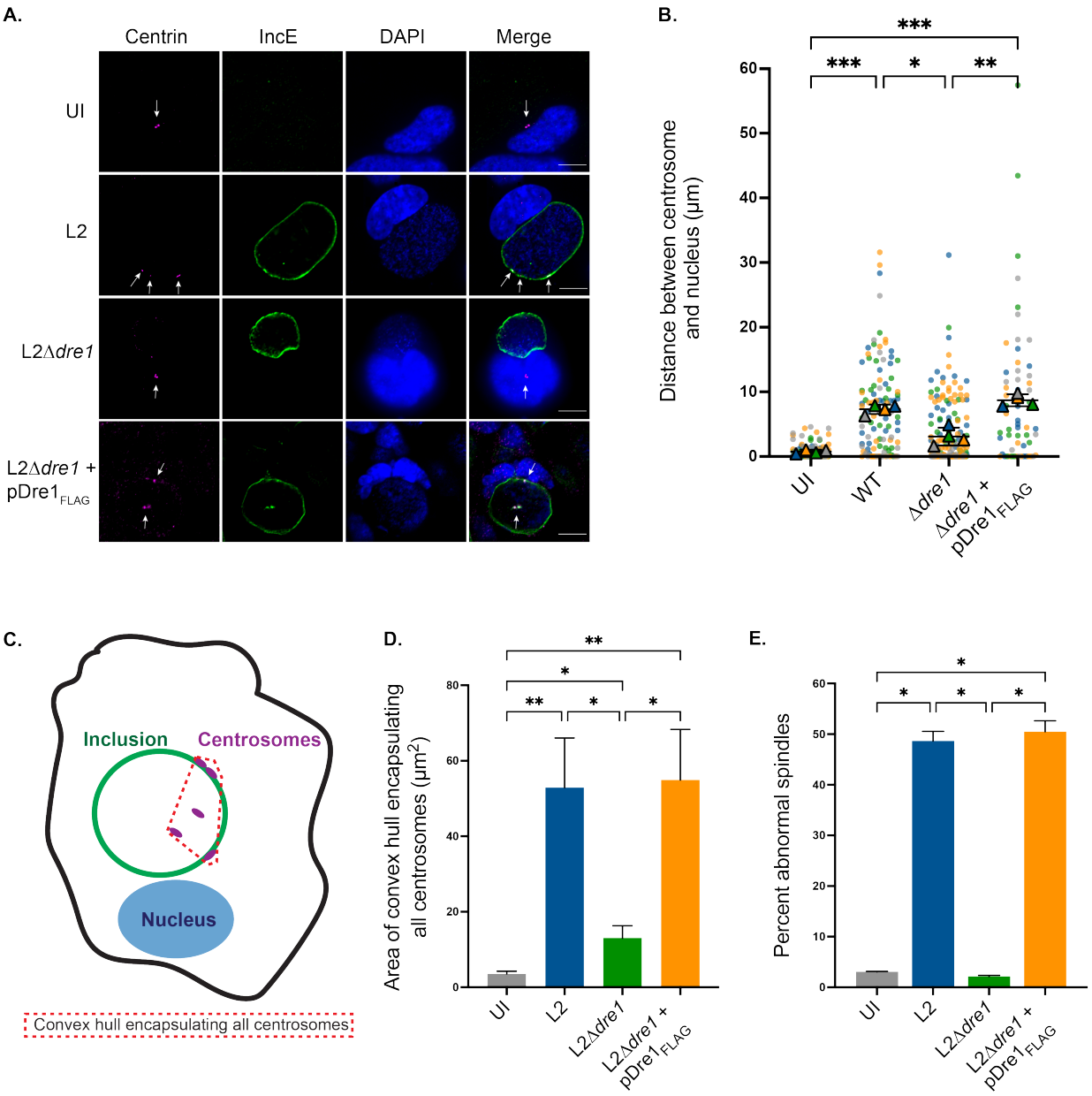

FIGURE 2.3. *C. trachomatis* modulates centrosome positioning during infection through Dre1.

(A) HeLa cells were infected for 36 hours with the indicated strains or left uninfected (UI), fixed and analyzed by confocal microscopy for the localization of endogenous Centrin (centrosome marker; magenta), IncE (inclusion membrane marker, green), and DAPI. Shown are single Z slices, arrows indicate centrosome position. Scale bar, 10 μm.

(B) Centrosome to nucleus distance in *C. trachomatis*-infected cells at 36 hpi was calculated from 3D reconstructions of Z-stacks. Data are represented as individual values

for centrosome:nucleus distance for each strain (small colored circles) and average distance for each of three independent biological replicates are represented as triangles (color coded by replicate). Overall average ± SD amongst biological replicates are represented as black bars. 300 cells per condition were counted over three biological replicates.

(C) Schematic depicting measurement of centrosome spread. Centrosome spread in HeLa cells infected for 36 hours was calculated by generating maximum intensity projections of 3D image stacks of non-mitotic cells, drawing a polygon connecting all centrosomes and then measuring the area of the convex hull generated from that polygon.

(D) Quantitation of centrosome spread. HeLa cells infected with the indicated strains for 36 hours were stained with antibodies to Centrin or γ-Tubulin and IncE. Centrosome spread was calculated in > 40 cells per condition, over three independent biological replicates. Data are represented as mean ± SD.

(E) Quantitation of percentage of mitotic cells with abnormal spindle formation. HeLa cells infected with the indicated strains for 36 hours were stained with antibodies to $p150^{glued}$ and γ-Tubulin to visualize spindles. Spindles with > 2 poles were scored as abnormal. 50 mitotic spindles were analyzed per condition, over three independent biological replicates. For infected samples, only cells with inclusions were quantified. Data are represented as mean ± SD. *p<0.05, **p<0.01, ***p<0.001, Welch's ANOVA.

FIGURE 2.4

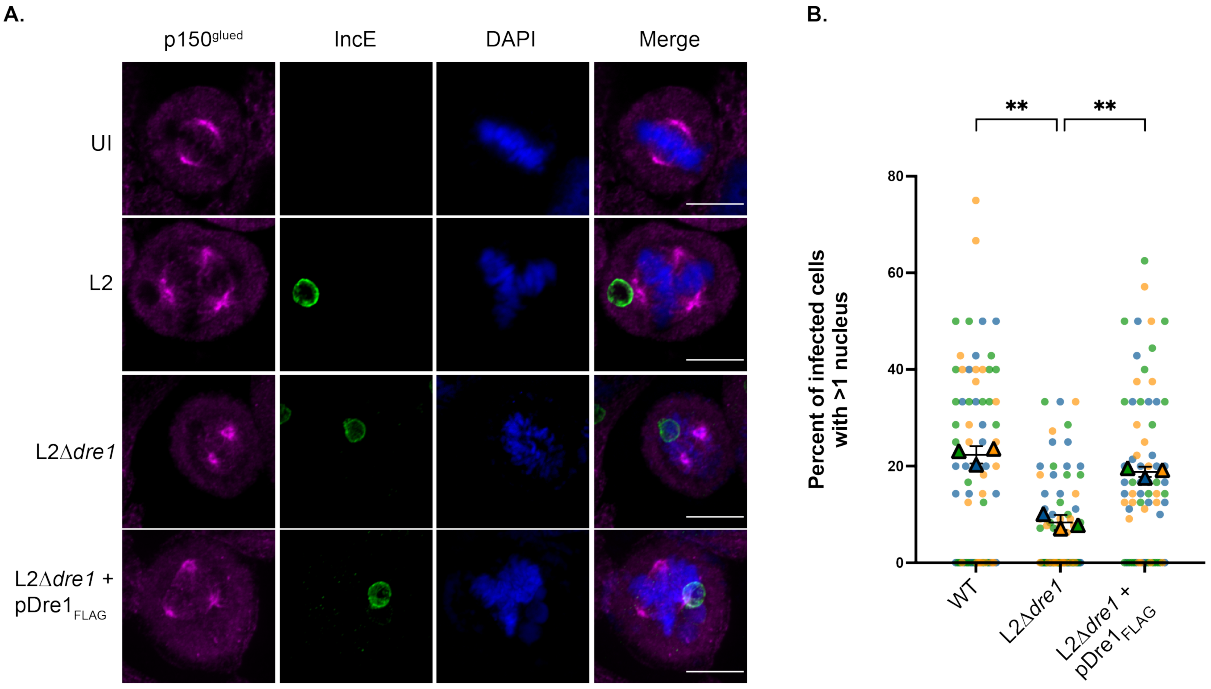

FIGURE 2.4. Dre1 positions the inclusion at spindle poles during host division and contributes to *C. trachomatis*-induced multinucleation.

(A) HeLa cells were infected with the indicated strains or left uninfected (UI) for 24 hours and analyzed by confocal microscopy for the localization of endogenous $p150^{glued}$ to visualize spindle poles (magenta), IncE to visualize the inclusion membrane (green), and DAPI. Shown are single Z slices. Scale bar, 10μm.

(B) Quantitation of multinucleation. HeLa cells were infected for 48 hours with the indicated *C. trachomatis* strains, and subsequently analyzed by confocal microscopy for the localization of MOMP (to visualize bacteria), DAPI (to visualize nuclei) and WGA 647 (to delineate the plasma membrane). 3D-reconstructions of 75 infected fields were scored for cells containing >1 nucleus for each strain over three replicates. Data are represented as individual percentages for each field (small colored circles) and average percentage for each of three independent biological replicates are represented as triangles (color coded by replicate). Overall average ± SD amongst biological replicates are represented as black bars. **p<0.01, Welch's ANOVA.

FIGURE 2.5

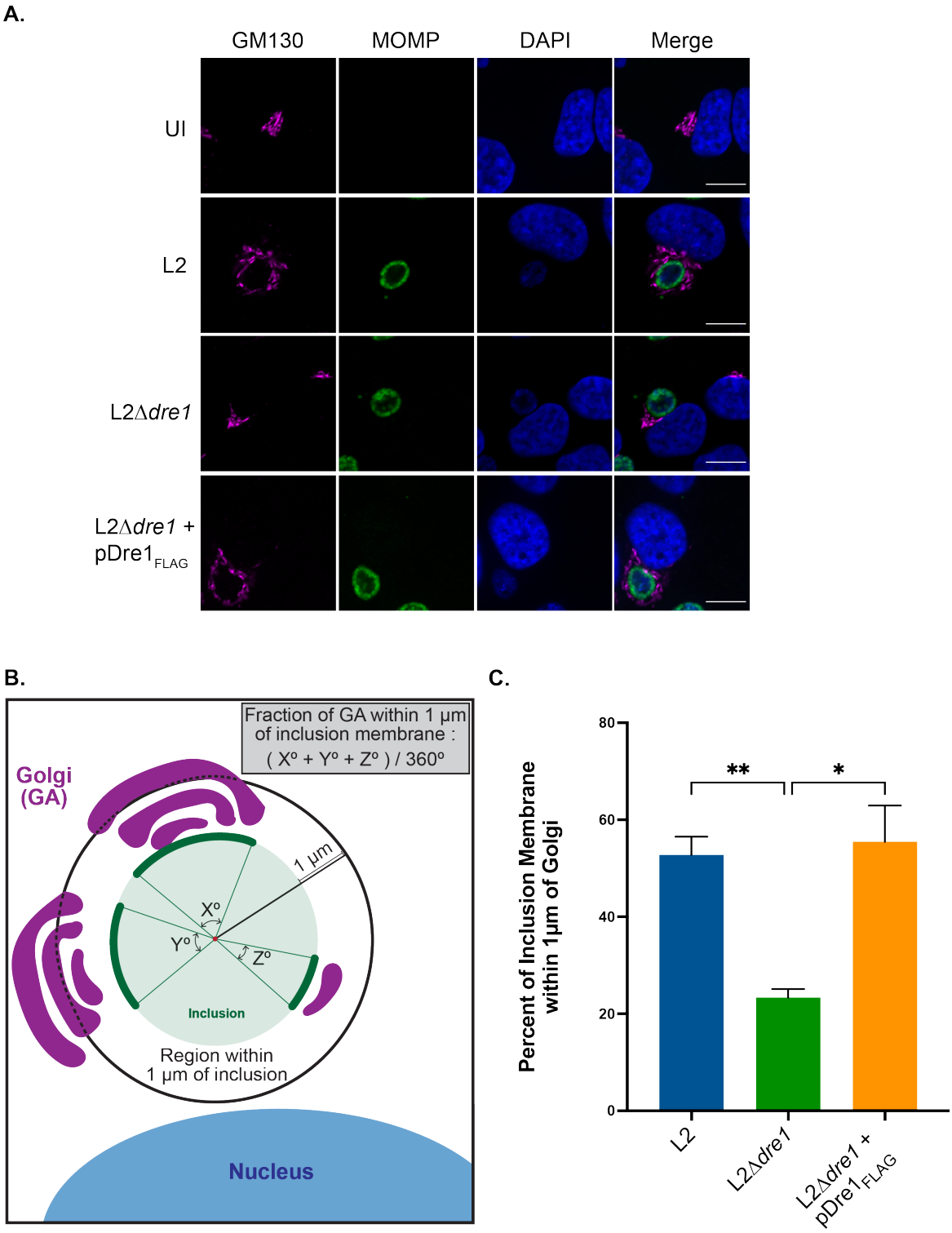
A.
GM130
MOMP
DAPI
Merge
UI
L2
L2Δdre1
L2Δdre1 +
pDre1FLAG
B.
Fraction of GA within 1 µm
of inclusion membrane :
(Xº + Yº + Zº) / 360º
Golgi
(GA)
1 µm
Xº
Yº
Zº
Inclusion
Region within
1 µm of inclusion
Nucleus
C.
Percent of Inclusion Membrane
within 1µm of Golgi
80
60
40
20
0
**
*
L2
L2Δdre1
L2Δdre1 +
pDre1FLAG

FIGURE 2.5. The Golgi Apparatus is recruited to the inclusion by Dre1.

(A) HeLa cells were infected with the indicated strains or left uninfected (UI) for 24 hours and analyzed by confocal microscopy for the localization of endogenous GM130 to visualize the GA (magenta), IncE to visualize the inclusion membrane (green), and DAPI. Shown are single Z slices. Scale bar, 10μm.

(B) Schematic depicting quantitation of GA recruitment to the inclusion. Maximum intensity projections were generated from Z-stacks and a circle was fitted to the inclusion membrane signal. A second, concentric circle was drawn with a radius 1 μm greater than the inclusion circle. The arc length of inclusion membrane corresponding to regions where GA signal falls between the outer and inner circles was determined, and this value was divided by 360°.

(C) Quantitation of GA recruitment in infected cells described in (A). For each condition > 100 infected cells across 3 independent biological replicates were counted and the average of the three replicates ± SD are represented. *p <0.05, **p<0.01, Welch's ANOVA.

FIGURE 2.6

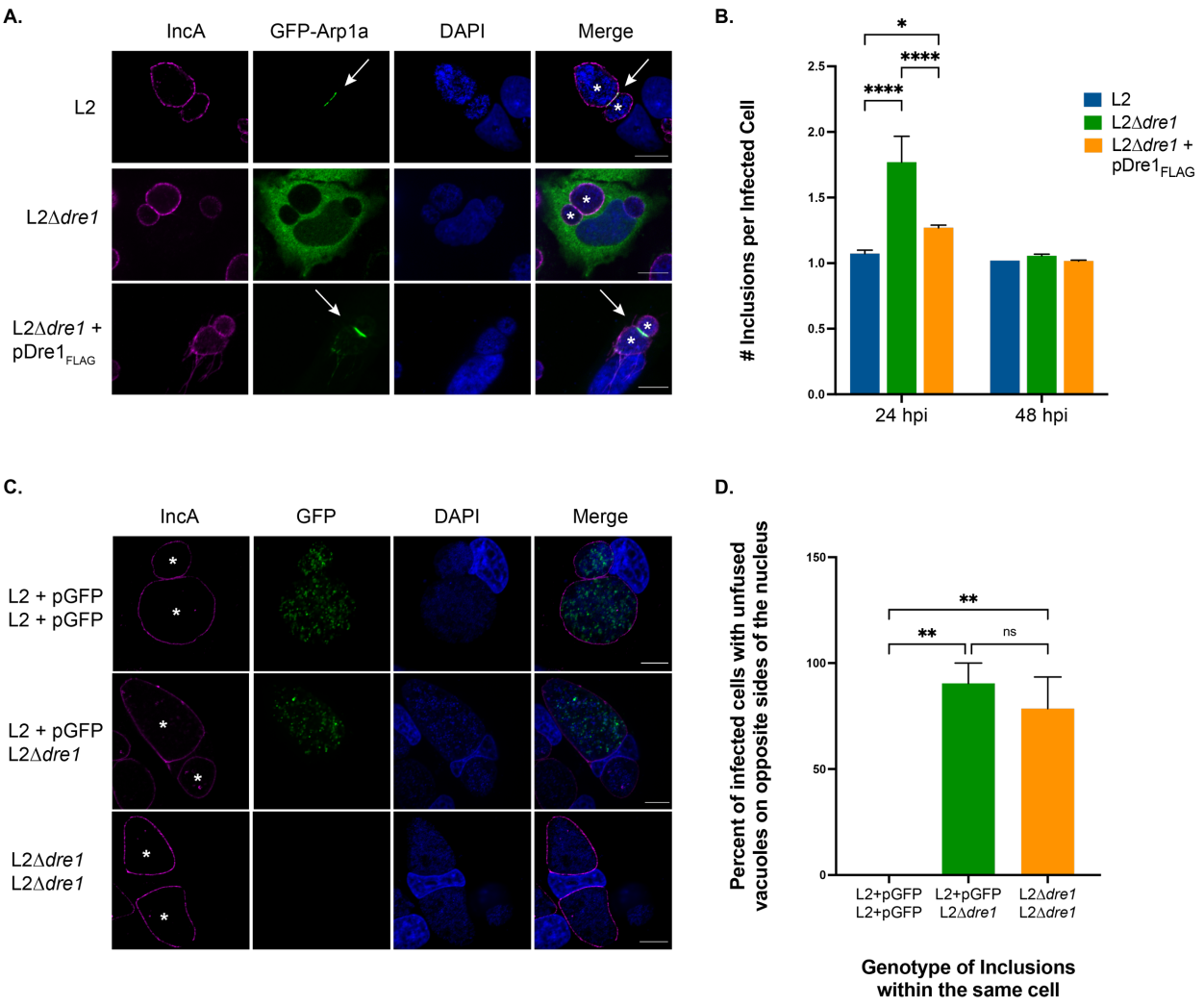

FIGURE 2.6. Dre1 is required for efficient inclusion fusion at centrosomal MTOCs.

(A) HeLa cells were infected with the indicated strains for 48 hours and analyzed by confocal microscopy for the localization of transfected GFP-Arp1a, endogenous IncA to visualize the inclusion membrane (magenta), and DAPI. Shown are single Z slices. Scale bar, 10μm.

(B) Quantitation of fusion defect. HeLa cells infected with the indicated strains were fixed at 24 or 48 hpi and stained with an antibody to IncA (to demarcate inclusions), WGA 647 (to identify plasma membrane), and DAPI. 120 cells were analyzed per condition, over three biological replicates. Data are represented as mean ± SD.

(C) HeLa cells were coinfected with L2+pGFP and L2Δ*dre1* for 48 hours and analyzed by confocal microscopy for the localization of GFP, IncA (magenta), and DAPI. Shown are single Z slices. Scale bar, 10μm.

(D) Quantitation of infected cells described in (C). 3D-reconstructions of 25 infected fields for each condition over three replicates were scored for cells containing multiple inclusions found on opposite sides of the nucleus from one another. Overall average ± SD amongst biological replicates are represented as black bars. *p<0.05, **p<0.01, ****p<0.0001, Welch's ANOVA.

FIGURE 2.7

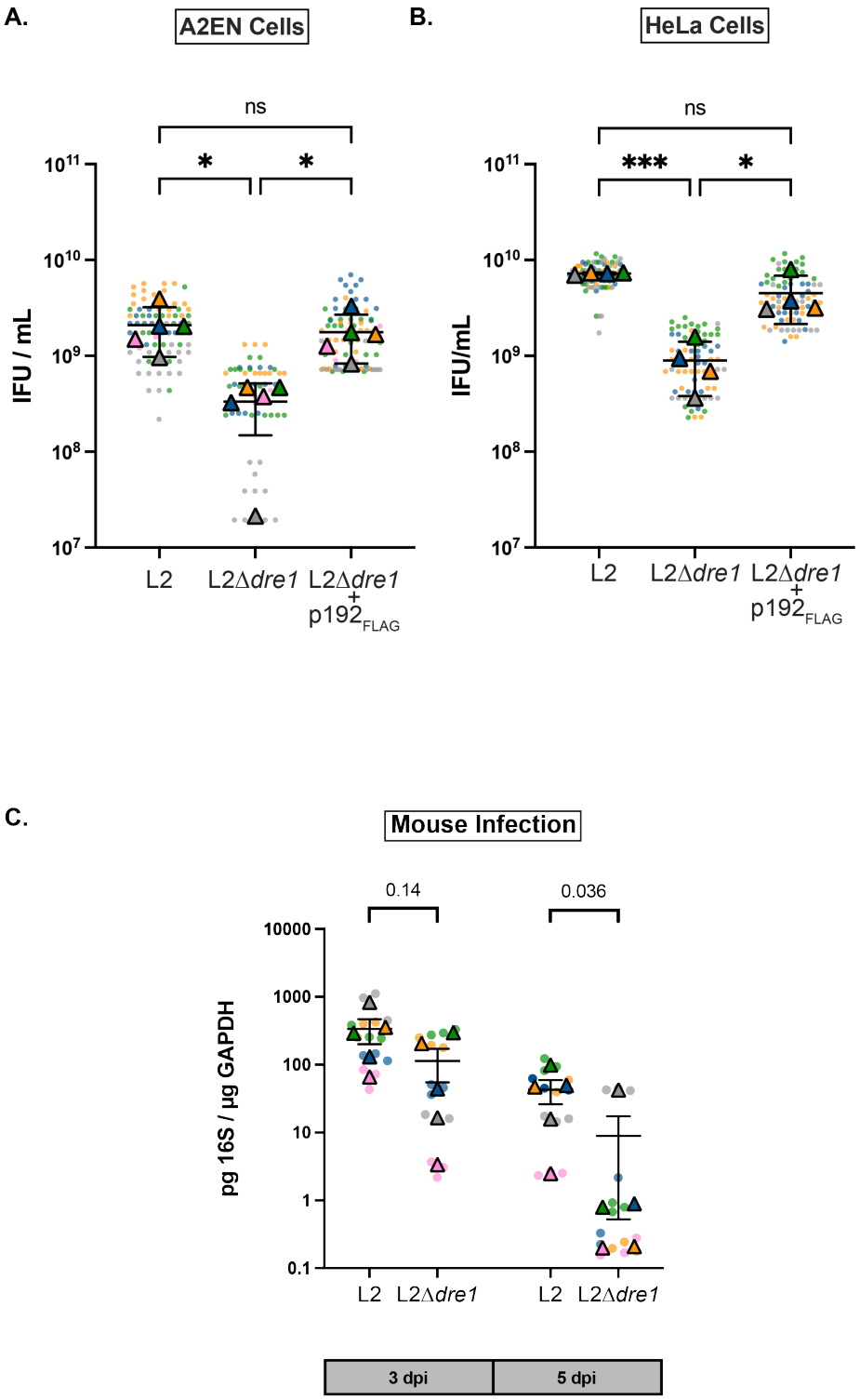
A.
A2EN Cells
ns
*
*
IFU / mL
10^{11}
10^{10}
10^{9}
10^{8}
10^{7}
L2
L2Δdre1
L2Δdre1 + p192FLAG
B.
HeLa Cells
ns
***
*
IFU/mL
C.
Mouse Infection
0.14
0.036
pg 16S / µg GAPDH
10000
1000
100
10
1
0.1
L2
L2Δdre1
L2
L2Δdre1
3 dpi
5 dpi

FIGURE 2.7. Dre1 is required for virulence in cell culture and a mouse model of upper genital tract infection

(A and B) Quantitation of infectious progeny at 48 hpi in pseudo-polarized A2EN cells (A) or in HeLa cells (B) infected with the indicated *C. trachomatis* strains. Confluent monolayers were infected with the indicated strains for 48 hours. EBs were extracted and used to infect fresh HeLa monolayers to enumerate infectious particles produced over the course of the primary infections. Data are mean ± SD from ≥ 4 independent experiments presented as a scatter plot where all measures (dots) and averages of each biological replicate (triangles) are color coded. *p<0.05, **p<0.01, ***p<0.001, Welch's ANOVA.

(C) Dre1-deficient bacteria are cleared faster from the mouse genital tract, as measured at 3- and 5- days post infection. Data are presented as a scatter plot with technical replicates (dots) and average value for each mouse (triangles) are color coded, n=5, Mann-Whitney U test.

FIGURE S2.1

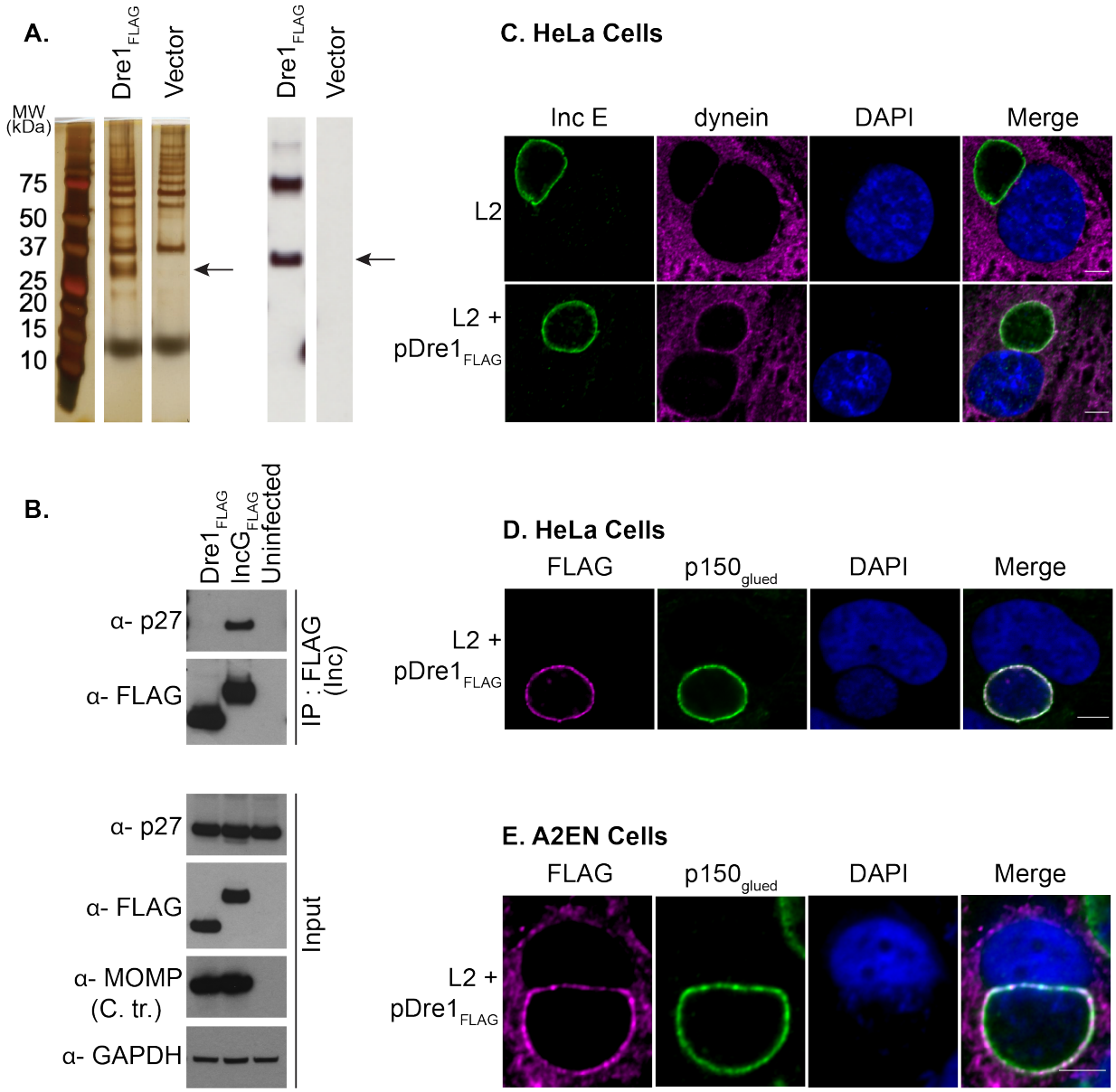

FIGURE S2.1. Dre1 interacts specifically with dynactin during infection.

(A) Silver stain and anti-FLAG immunoblot of HeLa cells infected with L2+pDre1$_{FLAG}$ or vector alone. Arrows indicate Dre1$_{FLAG}$ bands.

(B) FLAG immunoprecipitations of HeLa cells infected for 36 hours with *C. trachomatis* strains transformed with pDre1$_{FLAG}$, pIncG$_{FLAG}$, or uninfected. Eluates and total lysates were immunoblotted with the indicated antibodies.

(C) HeLa cells were infected with L2+pDre1$_{FLAG}$ or L2 for 24 hours and analyzed by confocal microscopy for the localization of endogenous dynein (DIC 74.1kDa), IncE, and DAPI.

(D) HeLa cells or **(E)** pseudo-polarized A2EN cells were infected with L2+pDre1$_{FLAG}$ for 24 hours and analyzed by confocal microscopy for the localization of endogenous p150^{glued} (a dynactin subunit), FLAG, and DAPI. All IF panels are single Z slices. Scale bar, 5μm.

FIGURE S2.2

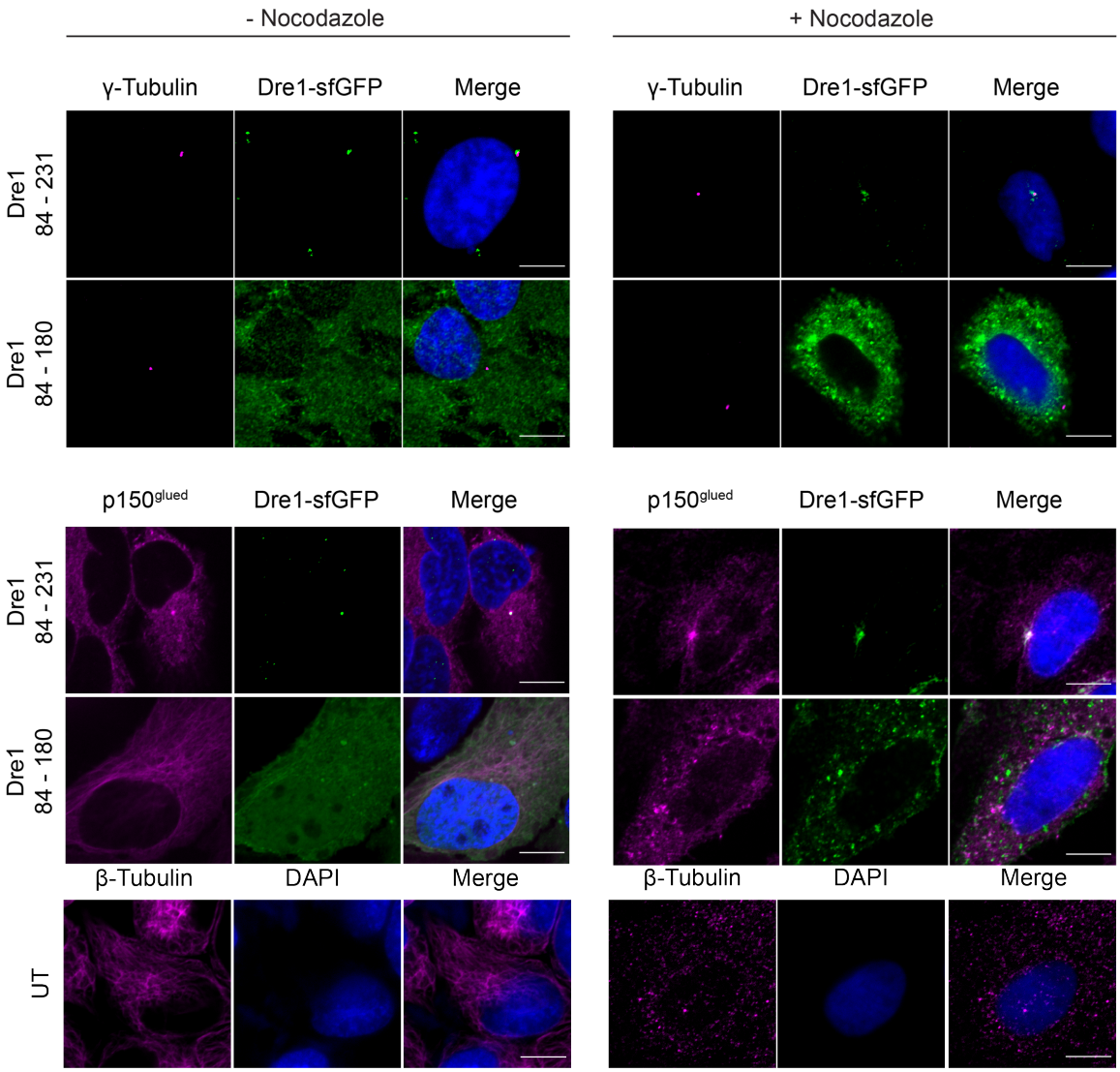

FIGURE S2.2. Dre1 localization at the centrosome does not depend on an intact MT network.

HeLa cells were transfected for 24 hours with binding (amino acids 84-231) or non-binding (amino acids 84-180aa) variants of $Dre1_{sfGFP}$, exposed to nocadazole (100 ng/mL) or DMSO for three hours, cold-shocked for 30 min on ice, and immediately fixed with 4% PFA, and stained with antibodies to endogenous γ-Tubulin, $p150^{glued}$, or β-tubulin (magenta), and DAPI. Untransfected HeLa cells (UT) were treated with nocodazole, fixed and stained for β-tubulin to confirm MT depolymerization. Shown are single Z slices. Scale bar, 10μm.

FIGURE S2.3

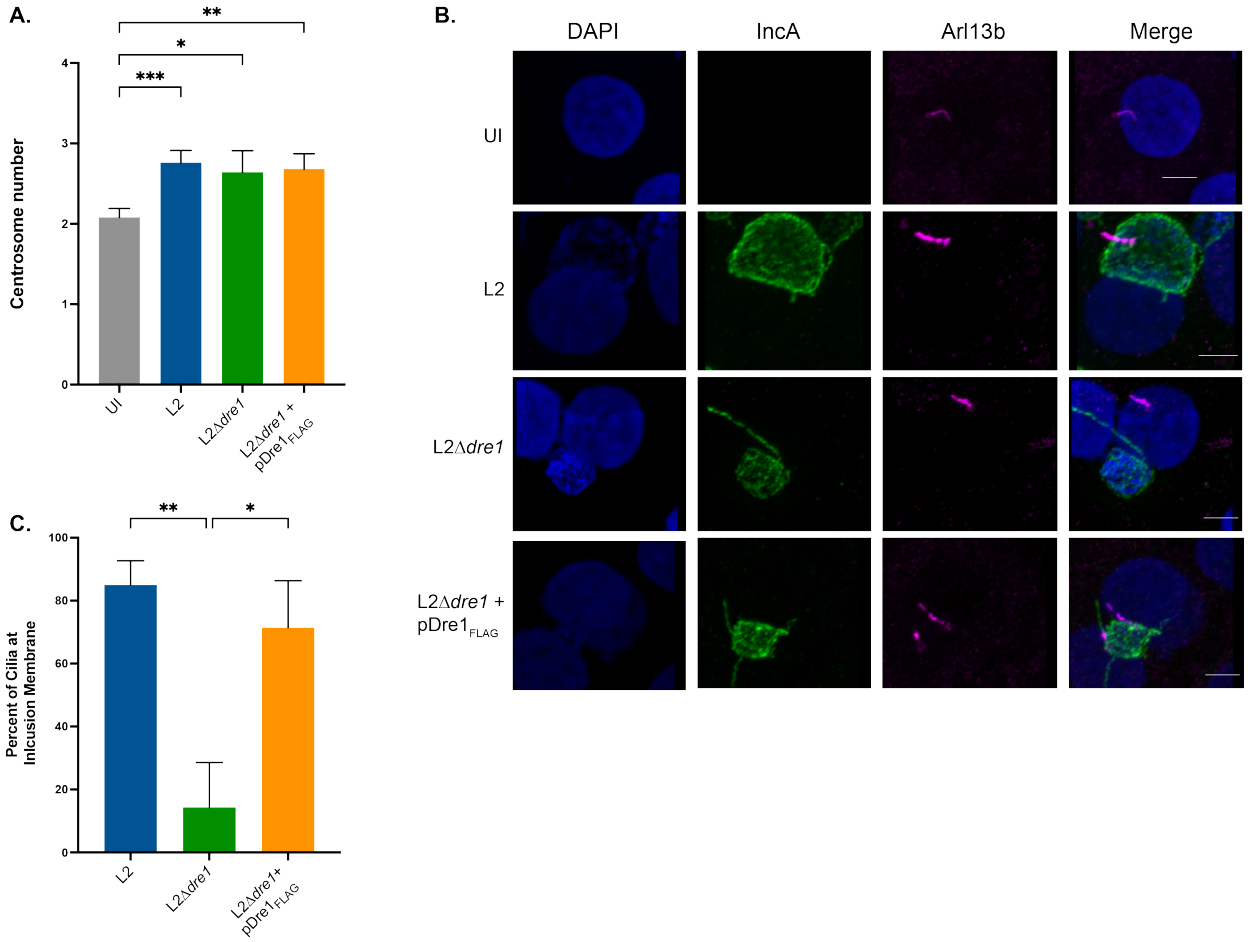

FIGURE S2.3. Dre1 modulates the position of primary cilia during infection, but is not involved in *C. trachomatis*-induced dysregulation of centrosome duplication.

(A) HeLa cells were infected with the indicated *C. trachomatis* strains for 36 hours and fixed. Centrosomes were visualized with antibodies to γ-Tubulin, Centrin, MOMP (major outer membrane of *C. trachomatis*), and DAPI. The average number of centrosomes in cells ± SD (n=3) is reported. 100 cells per condition per replicate were scored.

(B) Pseudo-polarized A2EN cells were infected with the indicated *C. trachomatis* strains for 24 hours, fixed, and stained with anti-Arl13b (magenta, to visualize primary cilia), anti-IncA (green, to visualize the inclusion membrane), and DAPI. Shown are single Z slices. Scale bar, 10μm.

(C) The percentage of cilia anchored at the inclusion membrane from the four different conditions is shown. 25 ciliated cells per condition were analyzed, over two biological replicates. Data are represented as mean ± SD. *p<0.05, **p<0.01, ***p<0.001, Welch's ANOVA.

FIGURE S2.4

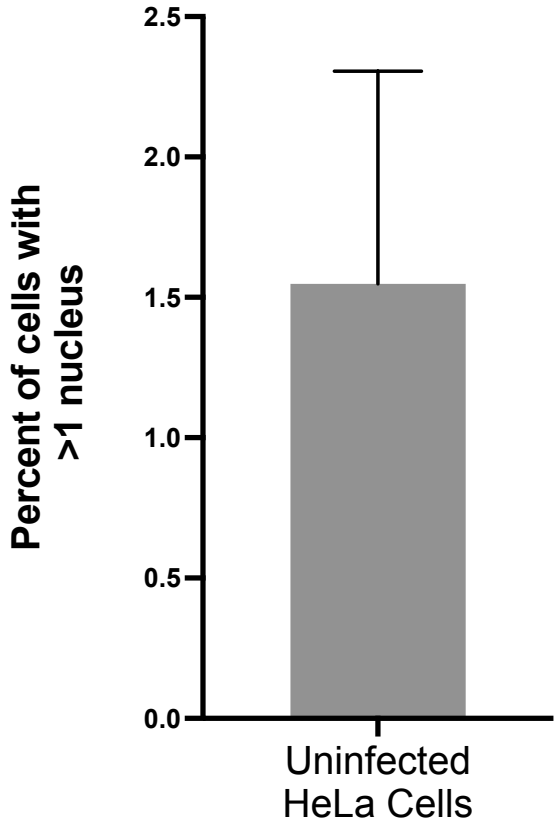

FIGURE S2.4. Basal rate of multinucleation in uninfected HeLa cells.

HeLa cells were seeded on coverslips and 48 hours later fixed and stained with DAPI to visualize nuclei and WGA 647 to delineate the plasma membrane. Approximately 1.5% of uninfected HeLa cells contained more than one nucleus. 120 cells were analyzed, over three biological replicates. Data are represented as mean ± SD.

FIGURE S2.5

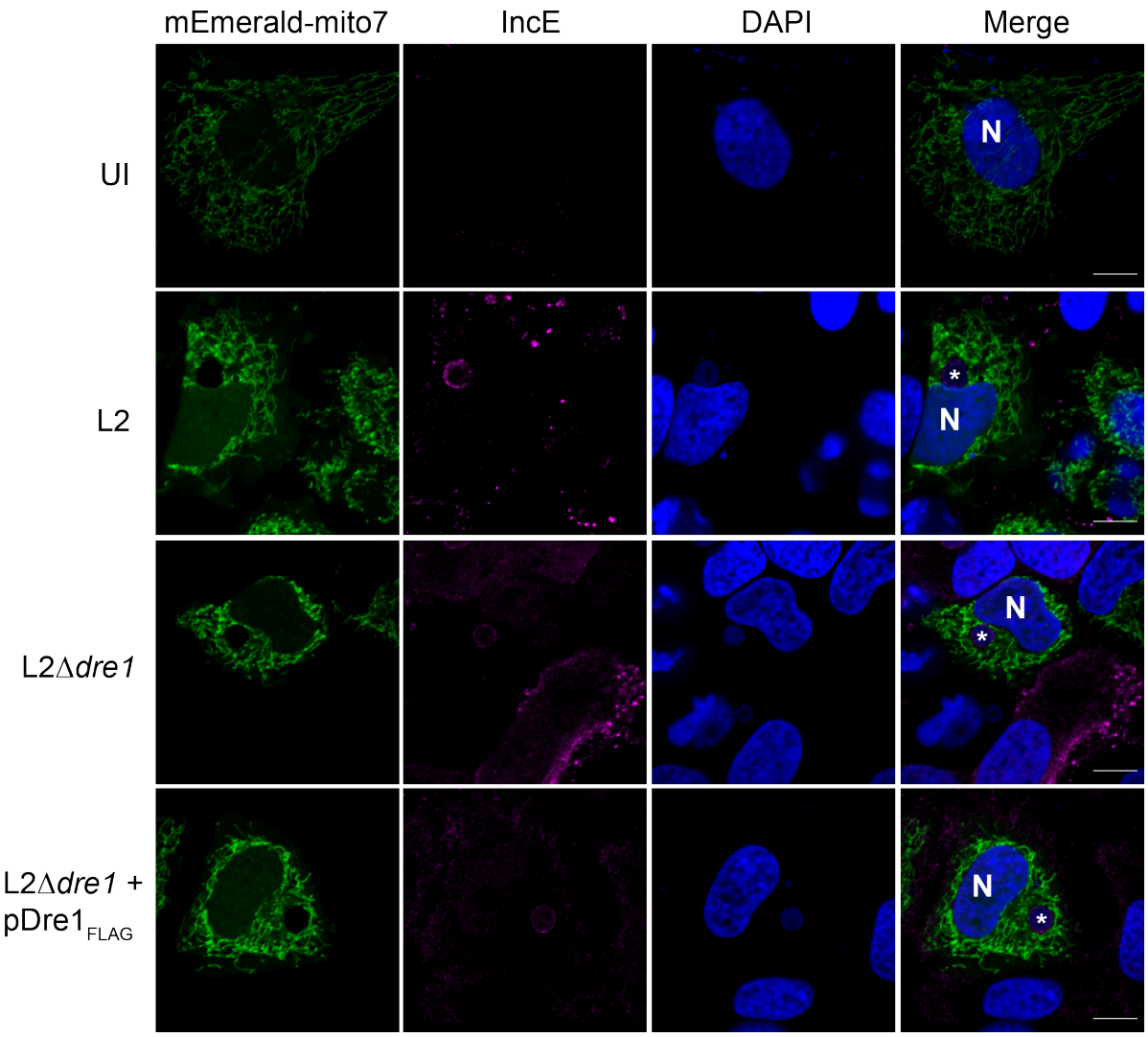

FIGURE S2.5. Dre1 does not alter mitochondrial position during infection.

HeLa cells were transfected with mEmerald-Mito7 (a mitochondrial marker) and then infected for 24 hours with the indicated strains, fixed, and stained with anti- IncE (magenta, to visualize inclusion membrane)) and DAPI (to visualize nuclei). N, nucleus. *, inclusion. Shown are single Z slices. Scale bar, 10μm.

FIGURE S2.6

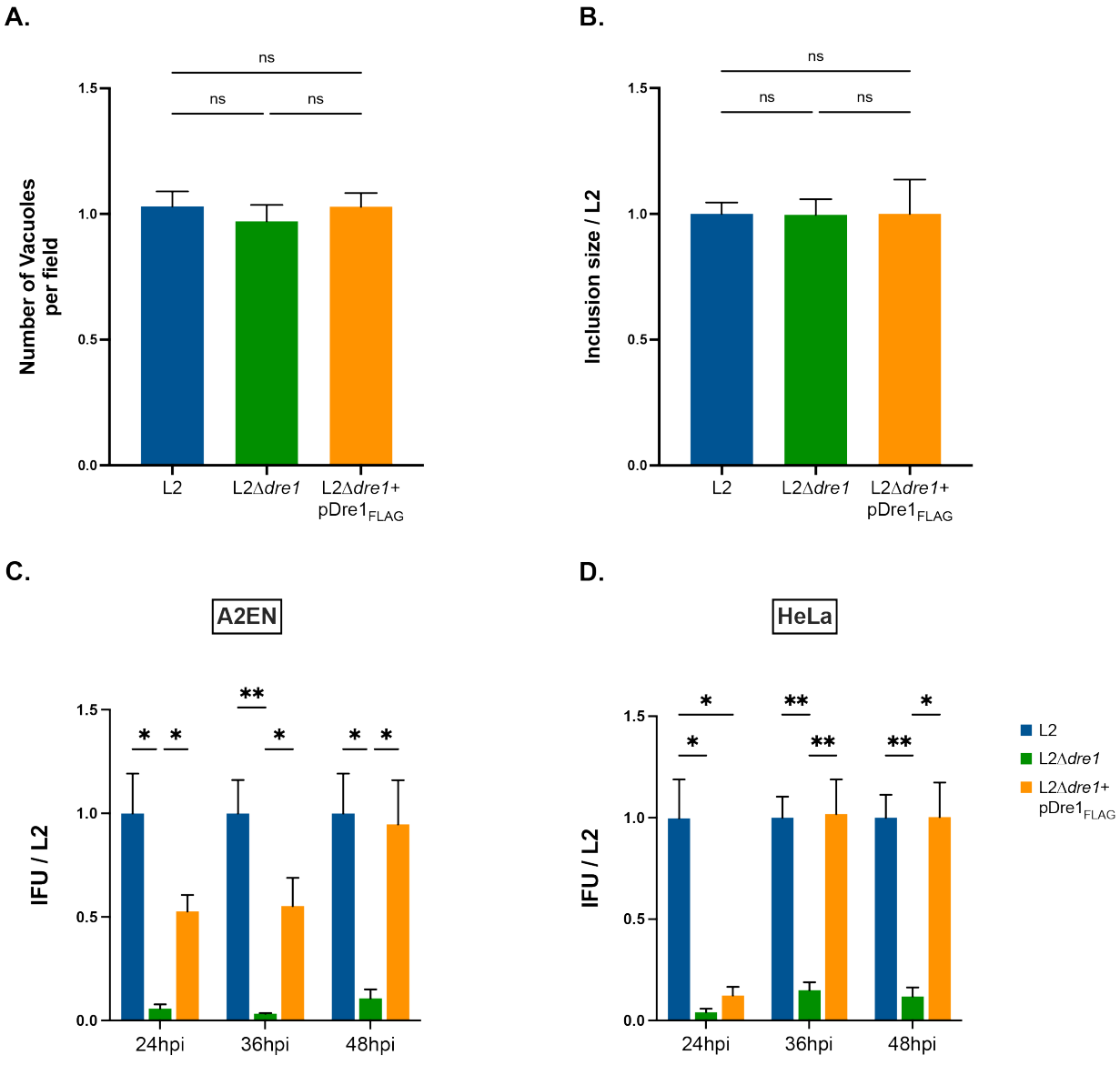

FIGURE S3.6. *C. trachomatis* L2Δ*dre1* exhibits a growth defect at later stages of the infectious cycle.

(A and B) Quantitation of (A) inclusion number and (B) inclusion area relative to L2-infections at 24hpi in HeLa cells. For (A) 35 fields per replicate for each condition were counted. For (B) 3D reconstructions for 35 inclusions per replicate for each condition were generated and measured using Fiji. Data are mean ± SD of three independent experiments.

(C and D) Quantitation of infectious progeny at 24, 36, and 48 hpi in (C) pseudo-polarized A2EN cells or in (D) HeLa cells infected with the indicated *C. trachomatis* strains. Relative IFUs for 24, 36, and 48 hpi are expressed as a fraction of L2. Data are mean ± SD from 4 independent experiments. *p<0.05, **p<0.01, ***p<0.001, Welch's ANOVA.

ADDITIONAL SUPPLEMENTAL MATERIAL

SUPPLEMENTARY FILE 2.1

Scoring for all PPIs identified through AP-MS (Transfection and Infection Interactomes). Related to Figure 2.1 and S2.1.

Worksheet 1, Transfection Interactome (all). Summary of MiST and CompPASS scores from $Dre1_{Strep}$-prey PPIs detected by AP-MS as well as individual MiST scores for abundance, reproducibility, and specificity. From Mirrashidi et. al., 2015.

Worksheet 2, Transfection Interactome (HC). Same as Worksheet 2, except that it only contains data for the high-confidence Dre1-host PPIs (as defined in Mirrashidi et. al., 2015.)

Worksheet 3, Infection Interactome (all). Spectral counts and SAINT scores with associated Bayesian False Discovery Rate scores (BFDR) for all $Dre1_{FLAG}$-host interactions identified during *C. trachomatis* infection.

SUPPLEMENTARY FILE 2.2

Whole genome sequencing identifying SNVs in *C. trachomatis* L2Δ*dre1* and parental strain compared to the published *C. trachomatis* L2 434/Bu genome sequence (accession no. AM884176).

SUPPLEMENTARY FILE 2.3

List of primers and strains used in this study.

CHAPTER THREE

STRUCTURAL ANALYSIS OF DRE1 IN COMPLEX WITH HOST DYNACTIN

"Just a conspiracy of cartographers, then?"
- Tom Stoppard

SUMMARY

Chlamydia trachomatis is an obligate intracellular pathogen that resides in a membrane-bound compartment, the inclusion. The bacteria secrete a unique class of proteins, Incs, which insert into the inclusion membrane and modulate the host-pathogen interface. We previously demonstrated that the *C.trachomatis* Inc, Dre1, binds host dynactin and through this interaction, recruits specific organelles associated with stable pools of dynactin to the inclusion membrane during infection. Furthermore, though dynactin is broadly distributed at various subcellular localizations, ectopically expressed Dre1 localizes specifically to the centrosomal MTOC. This result suggests that Dre1 targets centrosomal dynactin which is required for normal microtubule anchoring and/or focusing. In order to illuminate how Dre1 might discriminate different subpopulations of dynactin, we developed a cross-linking mass spectrometry (XL-MS) strategy that allowed us to map the binding interface between Dre1 and host dynactin. We present preliminary evidence that Dre1 binds along the Arp1 filament of the dynactin complex. Given that this subcomplex of dynactin mediates interaction with the motor protein dynein, as well as various adaptors, we speculate that binding at this interface might allow Dre1 to monitor or influence complex assembly. Furthermore, we demonstrate by negative stain electron microscopy (EM) that Dre1 co-purifies intact dynactin complexes. Combining the power of cryo EM and XL-MS during infection to elucidate the structure of Dre1 bound to the dynactin complex will undoubtedly provide new insights into dynactin regulation. This work underscores the power of using pathogens to further our understanding of disease-related cell biology.

INTRODUCTION

Motor proteins convert the chemical energy of ATP to mechanical energy, and thereby generate forces that are essential for a wide variety of cellular processes including cell motility, cell division, organelle positioning, and long-range transport of intracellular cargo (Tirumala & Ananthanarayanan, 2020). These proteins move processively along MTs, carrying cargo and organelles towards either the plus or minus ends of these polarized cytoskeletal filaments (Reck-Peterson et al., 2018). While mammalian cells encode nearly 40 plus-end directed kinesin motors, a single dynein motor is responsible for nearly all minus end directed trafficking in the cytoplasm (Reck-Peterson et al., 2018). Thus, an important area of investigation is elucidating how a single motor can transport such a diverse array of cargoes and how this process is regulated.

Dynactin was one of the earliest identified regulators of dynein activity. It was found to be required for vesicle movement along MTs (Gill et al., 1991; Schroer & Sheetz, 1991), and its interaction with dynein is enhanced in the presence of the adaptor, BICD2 (Splinter et al., 2012). Recent work has demonstrated that this adaptor, which is predominantly composed of long stretches of coiled coils, enhances processivity of the dynein/dynactin complex along MTs and facilitates cargo-binding (McKenney et al., 2014). In fact, most identified adaptors that specify cargo-binding or modulate processivity of the dynactin-dynein complex contain long coiled-coil domains (Reck-Peterson et al., 2018). Many intracellular pathogens target dynein to facilitate transit through the host cytosol (Ortiz Flores et al., 2019), however comparatively few pathogens target dynactin. Those that do include, Classical swine fever virus, which binds dynactin to facilitate localization at early

endocytic compartments, and foot and mouth disease virus, though phenotypic consequences of this interaction remain uncharacterized (Borca et al., 2019; Gladue et al., 2014). We speculate that the identified interaction between dynactin and Dre1 may be targeting a different cellular function of dynactin than its most commonly studied role as an activator for dynein processivity.

Dynactin is a large and complex assembly of proteins that is approximately 1.1 MDa in size. It contains more than 20 subunits, corresponding to 11 different proteins (Urnavicius et al., 2015). Dynactin is built around a filament composted of the actin-related protein, Arp1. This filament has polarity – and each end is capped by a different protein complex; either CapZa/b at the barbed end, or p62, p27, and p25 at the pointed end (Figure 3.2, Urnavicius et al., 2015). The shoulder domain sits on top of this filament and comprises two copies of $p150^{glued}$, four copies of p50/dynamitin, and two copies of p24 ((Reck-Peterson et al., 2018). Both $p150^{glued}$ and p50 extend peptides out from the body of the complex, and the $p150^{glued}$ extended domain has been implicated in MT binding (Waterman-Storer et al., 1995). We have shown that the *C. trachomatis* Inc, Dre1, co-purifies with all of these subunits during infection (Chapter 2).

Dynactin is required for most types of dynactin-based motility *in vivo*. Beyond its role in intracellular transport, it has been shown to be involved in MT binding, MT anchoring at organelles, organelle positioning, and even in binding specific cargo even in the absence of dynein (Schroer & Verma, 2021). Dre1 does not interact with any known dynein/dynactin adaptors, nor does it interact with any proteins that share structural

features with known adaptors (e.g. extended coiled-coil domains; Chapter 2, Mirrashidi et al., 2015)). Furthermore, we have shown that Dre1 is not required for trafficking of the inclusion from the cell periphery to the juxtanuclear position (Chapter 2). Given this evidence, we hypothesize that the primary role of the Dre1:dynactin interaction might be to target the MT-binding and MT-organizing functions of dynactin. Indeed, we observe that Dre1 localizes specifically at the centrosomal MTOC where there is a stable pool of dynactin throughout all stages of the cell cycle (Quintyne et al., 1999; Quintyne & Schroer, 2002) and that Dre1 mediates repositioning of multiple host organelles with dynactin-mediated MT organizing capacity.

In order to determine the molecular basis for the selectivity employed by Dre1 in targeting particular subpopulations of dynactin, we mapped the binding interface between Dre1 and dynactin. Given the complexity of the dynactin complex and associated binding partners, traditional methods (e.g. yeast two-hybrid, directed co-APs) that identify the direct binding partner(s) of Dre1 would require testing a prohibitively large number of combinations. Over the past fifteen years, cross-linking mass spectrometry (XL-MS) has developed into a robust and flexible tool that provides structural information in a wide variety of contexts (O'Reilly & Rappsilber, 2018). The cross-linking reaction covalently links proximal residues, providing a map of where proteins are in close contact. In this work we use the chemical DSSO (disuccinimidyl sulfoxide) to cross-link eluates containing purified Dre1 and host binding partners (Figure 3.1). We show preliminary evidence that Dre1 binds along the Arp1-filament of dynactin. Structural studies recently demonstrated that this dynactin subcomplex binds along the entire length of the dynein

light and intermediate chains, and that coiled-coil adaptors stabilize dynactin-dynein by associating along the boundary of this extended interface (Urnavicius et al., 2015). Binding at this nexus would allow Dre1 to monitor or dictate the composition of various dynactin-containing complexes.

We have shown that $Dre1_{CTD}$-Strep ectopically expressed in mammalian tissue culture cells interacts with all known dynactin subunits. Here, we demonstrate by negative stain EM that these complexes are intact. Thus, Dre1 might be a powerful tool enabling a simpler purification strategy for this large complex that doesn't require preparing samples from animal organs. In future work, we will use these purified complexes to perform higher resolution cryo EM, and to more confidently assess the interaction interface between Dre1 and dynactin. Combined with experiments aimed at performing cross-linking in C. trachomatis infected cells (Kaake et al., 2014), we hope to determine if Dre1 can distinguish and selectively interact dynactin in complex with particular adaptors or whether association with Dre1 alters the regulatory state or activity of dynactin. Taken together, this work will highlight the utility of pathogens in uncovering new information about host cell biology.

RESULTS

Dre1 binds the Arp1 filament of dynactin.

The structural details of the Dre1:dynactin interaction were characterized by chemical cross-linking mass spectrometry (MS) and integrated structural modeling. Here, disuccinimidyl sulfoxide (DSSO), a MS-cleavable, bifunctional amine-reactive small molecule, was used to cross-link proximal lysine residues of $Dre1_{CTD}$-Strep in complex with host dynactin. Cross-linked peptides were trypsin digested and resulting peptides analyzed by specialized LC-MS^3 experiments for identification of cross-linked residues. Application of this pipeline identified intra- and inter-linked peptides corresponding to 226 unique cross-linked residues (Supplementary Table 3.1). Lysine residues from Dre1 are involved in a total of 14 inter-subunit cross-links. Importantly, most of these cross-links are made between Dre1 and the Arp1 subunits that make up the actin-like filament of dynactin (Arp1, CapZa, and Arp10; Figure 3.2). Given that XL-MS captures structural information from a conformationally heterogeneous population of protein complexes that exist in solution, these links were mapped to a published 4.0 angstrom-resolution cryo EM structure of dynactin (Urnavicius et al., 2015). Segments of the published structure that are disordered were unable to be resolved, and thus, nearly half of the identified cross-links in our data set could not be matched onto a structure. Of the cross-links that fall within the protein domains structurally resolved and published, 83% of cross-links are satisfied, meaning that we have purified and cross-linked a dynactin complexes that match fairly well with the published structure (Supplementary Table 3.2). Discrepancies may indicate conformational changes in dynactin induced by Dre1, or they could be a function of the inherent flexibility of the dynactin complex. Repeating this experiment to

obtain higher coverage of the complex will distinguish between these possibilities. Here were present a model of the putative binding interface between Dre1 and the Arp1 filament of dynactin (Figure 3.2).

Dre1 co-purified intact dynactin complexes by NS-EM.

To further resolve the structure of Dre1 in complex with dynactin, we turned to cryo EM. After several failed attempts to purify various Dre1-Strep truncations and associated dynactin complexes from *E. coli* due to solubility issues (Figure 3.3), we turned to a mammalian-cell expression system. $Dre1_{CTD}$ (aa 84 – 231; see Figure 2.2 for domain architecture of Dre1) was selected due to its lack of transmembrane domains, its high expression levels in 293T cells, and its high-affinity interaction with dynactin as determined by western blot analysis using antibodies to endogenous dynactin ($p150^{glued}$, p27 subunits). Purified $Dre1_{CTD}$-Strep:dynactin complex from suspension HEK293 cells yielded high concentrations of solubilized protein (~1 μM), with discrete bands imaged by Coomassie that match published band patterns for dynactin purified from pig brains (Urnavicius et al., 2015). We performed negative stain EM (NS-EM) to assess the formation and stability of purified Dre1:dynactin complexes. In preliminary images, we observe that these complexes match fairly well with published structures of dynactin, and do not exhibit aggregative behaviors (Figure 3.3). We resolved electron density that corresponds to the Arp1 filament of dynactin, as well as to the shoulder domain. Given that these complexes appear to assemble appropriately on grids, we will next perform cryo EM to gain a higher resolution map of where Dre1 binds within these complexes and determine the direct binding partner of Dre1.

DISCUSSION

Structural analysis is a powerful tool for elucidating protein function and regulation. Here we utilize a two-pronged strategy to map the binding interface between Dre1 and dynactin. We combined the techniques of cross-linking mass spectrometry and cryo electron microscopy and present preliminary evidence that Dre1 binds along the Arp1 filament of dynactin. We demonstrate that Dre1 purifies intact, assembled dynactin complexes that are stable enough to resolve by negative-stain electron microscopy. These data provide a solid foundation from which to probe the molecular details of Dre1:dynactin complex assembly.

We report that Dre1 cross-links along the Arp1 filament of dynactin. Though nearly 50% of identified intra- and inter- molecular cross-links map to regions of dynactin that have not been structurally resolved, 83% of the cross-links that map to regions of dynactin that have been structurally resolved matched the published dynactin cryo EM structure (Urnavicius et al., 2015). In the future we will perform additional experiments, with cross-linkers that covalently link diverse amino acids to one another, in order to build a higher coverage map of the Dre1:dynactin interaction surface. Furthermore, we will perform analogous experiments in the context of infection (Figure 3.1) in order to determine whether inclusion membrane localized Dre1:dynactin complexes exhibit altered interactions, or whether they associate stably with additional binding partners.

Given that the Arp1 filament of dynactin modulates binding with dynein and a host of coiled-coil adaptor proteins, we were intrigued to see that Dre1 also appears to bind at

this busy interface. We speculate that this may be a mechanism by which Dre1 monitors or regulates complex assembly, and may be the molecular basis for how Dre1 distinguishes between different functions of dynactin. Future cryo EM experiments will be aimed at elucidating the how Dre1 modulates the Arp1 filament.

We have also begun to test whether association of Dre1 with dynactin stabilizes or displaces various adaptors and associated proteins. By immunoprecipitating dynactin in the presence or absence of Dre1, and analyzing the resulting proteomes by MS, we will begin to uncover which dynactin complexes Dre1 is targeting. As Dre1 does not co-purify with any known adaptors (Chapter 2; Mirrashidi et al., 2015), we speculate that Dre1 association may displace and/or replace certain adaptor functions. We will further assay how Dre1 modulates dynactin behavior by determining whether Dre1 added to processive dynein:dynactin:adaptor assemblies alters processivity along immobilized MTs, and whether Dre1 displaces dynein or adaptors from dynactin. Given our data that Dre1 localizes specifically at the centrosomal MTOC (Chapter 2) and not along MTs, it is possible that Dre1 stabilizes MT minus end-binding functions of dynactin. This could explain the ability of *C. trachomatis* to selectively reposition centrosomes and the GA (Chapter 2), which both have clusters of MT minus ends that are anchored by the MT binding function of dynactin p150^{glued} (Jaarsma & Hoogenraad, 2015; Quintyne et al., 1999). Together, these studies will determine the molecular mechanism by which a pathogen effector selectively targets or alters the regulation of dynactin functions.

Recent work has highlighted dynactin cellular functions that are independent of motor binding. Dynactin contributes to MT anchoring at sites where MT minus-ends converge, such as the centrosome. Furthermore, dynactin is able to cross-link microtubules to various cellular components. This functionality is dependent on the MT binding and cargo-binding capability of dynactin (Schroer & Verma, 2021). Dre1 might be specifically target this tethering function of dynactin to position the inclusion appropriately with respect to various cellular structures during infection.

The survival of an intracellular pathogen depends in large part on its ability to hijack established host protein machinery. Taken together, these experiments aim to resolve the molecular details and functional consequences of the interaction between Dre1 and dynactin. Understanding the role of a *C. trachomatis* effector in regulating the host dynactin complex provides specific information about how normal host processes are repurposed or used against the host during infection. Resolving these events may provide new targets for new therapeutics, as well as novel insights into fundamental eukaryotic processes.

MATERIALS AND METHODS

Cell Culture and Bacterial Propagation.

HeLa 229 and Vero cells were obtained from American Type Culture Collection (ATCC). HeLa cells were cultured and maintained in Eagle's Minimum Essential Medium (MEM; UCSF Cell Culture Facility) supplemented with 10% (v/v) fetal bovine serum (FBS) from Gemini at 37ºC in 5% $C0_2$. HEK293T cells (a generous gift from NJ Krogan, UCSF) and Vero cells were cultured and maintained in Dulbecco's modified Eagle's Medium (DMEM, UCSF Cell Culture Facility) supplemented with 10% (v/v) FBS at 37ºC in 5% $C0_2$. Cells were routinely tested for mycoplasma (Molecular Probes, M-7006). *C. trachomatis* serovar L2 (434/Bu) and derivative strains used in these studies are listed in Table S4. *C. trachomatis* was routinely propagated in either HeLa 229 epithelial cell monolayers or Vero cell monolayers as previously described (Elwell et al., 2011). HeLa cells were used for all experiments unless otherwise specified. Stellar™ chemically competent cells (Takara) were used to produce constructs for ectopic expression in mammalian cells, while *dam*$^-$*/dcm*$^-$ chemically competent *Escherichia coli* (NEB) were used to produce unmethylated constructs for transformation into *C. trachomatis*.

Plasmid construction.

The Dre1 gene and various deletion derivatives used for ectopic expression in mammalian cells were amplified from genomic *C. trachomatis* L2 (434/Bu) DNA and subcloned into the EcoRI and NotI sites in pcDNA4.0/2xStrepII (Jager et. al. 2011) using the primers indicated (Table S4). Dre1 constructs were verified by forward and reverse sequencing. Dre1 deletions were also subcloned into the EcoRI and BamHI sites in T789

(a pet28a variant with N-terminal 2xStrep-SNAP and C-terminal 10xHis tags; kindly provided by Ron Vale; UCSF). To express epitope-tagged Dre1 during *C. trachomatis* infection, Dre1 was amplified from genomic *C. trachomatis* L2 (434/Bu) DNA and subcloned into the NotI and SalI sites in the *E. coli/Chlamydia* pBOMB4 shuttle vector generously provided by Drs. Ted Hackstadt and Mary Weber (Bauler & Hackstadt, 2014).

Generation of *C. trachomatis* L2+pDre1$_{FLAG}$.

C. trachomatis L2 (434/Bu) was plaque purified. Plasmid DNA was isolated from *dam*$^{-}$*/dcm*$^{-}$ *E. coli* or *C. trachomatis* was transformed into *C. trachomatis* L2 as previously described with slight modifications (Johnson & Fisher, 2013; Wang et al., 2011). Briefly, 10µg of plasmid was mixed with 1 x 10^7 IFUs of C. trachomatis L2 and 1X Transformation Buffer (10 mM Tris pH 7.4 in 50mM $CaCl_2$) in 200 µl and incubated at room temperature for 30 minutes. The entire transformation mix was added to Vero cells seeded in 6-well plates (33.3µl/well). At 12 hpi, 5 mg/mL Ampicillin (Sigma) was added to select for transformed *Chlamydia*. After 3 initial passages, Ampicillin was increased to 50 mg/mL until transformed *Chlamydia* was expanded. Clonal populations of transformants were isolated under selection by plaque assay in Vero cells. The p2TK2-mCherry *E. coli*/*Chlamydia* shuttle vector encoding pTet-IncE-FLAG was previously generated in collaboration with the Derré lab (referred to herein as C. trachomatis L2+pIncE$_{FLAG;}$ Mirrashidi et al., 2015). (see Table S1 for a list of constructed *C. trachomatis* strains).

Strep affinity purifications.

For Strep affinity purifications, approximately 6 x 10^6 HEK293T cells were seeded in each of 20 x 10 cm^2 plates, and were transfected using Avalanche-Omni Transfection Reagent (EZ Biosystems), following manufacturer's instructions. At 48 h after transfection cells were detached with 10 mM EDTA/D-PBS, washed with PBS, and lysed with 10 mL of ice-cold Lysis Buffer (50mM Tris-HCl pH 7.5, 150mM NaCl, 1mM EDTA, 0.5% NP-40, PhosStop, Roche Complete Protease Inhibitor) at 4ºC for 30 minutes while rotating. Lysates were incubated with 30 uL of Strep-Tactin Sepharose beads (IBA) in 1 mL of Final Wash Buffer and incubated overnight, rotating at 4°C. Beads were washed three times in 1 mL of Wash Buffer (50mM Tris-HCl pH 7.5, 150mM NaCl, 1mM EDTA, 0.05% NP-40) and then once in Final Wash Buffer (50mM Tris-HCl pH 7.5, 150mM NaCl, 1mM EDTA). Samples were eluted in 45 µl of 10 mM $_D$-desthiobiotin (IBA) in Final Wash Buffer for 25 minutes at room temperature with continuous gentle agitation. Eluates were stained with Instant Blue (Expedeon) and immunoblotted with anti-$p150^{glued}$, anti-Strep, and anti-GAPDH antibodies.

Alkyne-A-DSBSO based cross-linking mass spectrometry analysis (XL-MS) during *C. trachomatis* infection.

8 x 6-well plates of 80% confluent HeLa cells were infected with either *C. trachomatis* L2+pDre1$_{FLAG}$ or C. trachomatis L2+pIncE$_{FLAG}$ at a MOI of 1.5 for 40 hours. At 36 hpi, 10 µM MG132 (Cayman) was added to infected cells. Cells were washed gently with PBS, and the cross-linker Alkyne-A-DSBSO (A-Bis; Burke et al., 2015) diluted to 2 mM in PBS was added to infected cells directly on the plates. 400 µl of A-Bis was added to each well,

and cells were incubated at 37ºC, 5% CO_2 for 1 hour under gentle agitation. Cross-linker was exchanged three times for fresh cross-linker. Cross-linking reaction was stopped after 1 hour by adding 0.125M glycine to the wells and incubating for 5 minutes at room temperature. Glycine and cross-linker was then aspirated from cells. Cells were lifted in 10mM EDTA/PBS for 10 minutes, and pelleted at 400g, 4ºC for 3 minutes. Cells were lysed in 8M Urea Lysis Buffer (8M urea, 5mM DTT, 150mM NaCl, 50mM Tris-HCl pH 7.5, 1% SDS, PhosStop, Roche Complete Protease Inhibitor) for 10 min on ice, and then sonicated on setting 3 with 3x5 second pulses with ~15 second rests in between, on ice.

FLAG immunoprecipitations.

Lysates were diluted to 2M urea using Final Wash Buffer, and were then incubated with 60µl anti-FLAG magnetic beads (Millipore Sigma) rotating overnight at 4ºC. Beads were washed six times in Wash Buffer, changing tubes each time, and then twice in Final Wash Buffer. Samples were eluted in 45µl of Elution Buffer (100µg/mL FLAG peptide, 1% Rapigest in Final Wash Buffer; Millipore Sigma) for 25 minutes at room temperature with continuous gentle agitation. All purifications were performed in triplicate and assayed by anti-FLAG immunoblot using enhanced chemiluminescence (Amersham Biosciences) or by silver stain (Pierce). For FLAG immunoprecipitations not analyzed by MS, eluates were analyzed by immunoblot analysis with the following antibodies: anti-FLAG, anti-MOMP, anti-GAPDH, and anti-p27.

DSSO-based cross-linking mass spectrometry analysis (XL-MS).

Individual preparations of Dre1:dynactin were cross-linked using increasing molar ratios of DSSO (Thermo Fisher Scientific), for 5, 10, or 30 minutes at 4 or 37^{o}C. Cross-linked proteins were separated on 4–20% TGX gradient SDS-PAGE gels (Bio-Rad), stained with MS-safe AcquaStain (Bulldog Bio), and cross-linked product bands excised and submitted for in gel reduction, alkylation, and trypsin digestion. Extracted peptides were separated online by Thermo Easy nLC 1000 by reverse-phase HPLC (75 μm × 30 cm fused silica packed with 1.9-μm Reprosil-Pur C18 AQ resin (Dr. Maisch-GmbH) column), running a linear gradient of 5–30% B in 50min, 35–95% B in 5 min, and 95% B for 4 min at a flow rate of 300 nL/min (buffer A: 100% H2O/0.1% FA; buffer B: 100% ACN/0.1% FA). For each sample, XL-MS3 data was acquired on Thermo Orbitrap Elite using two similar data dependent acquisition experiments where a single acquisition cycle consisted of: 1) one full MS1 scan (350–1500 m/z, 120,0000 resolution, AGC target of 1×106); 2) top two data-dependent MS2 scans (15,000 resolution, AGC target of 5×104, normalized collision energy = 22%); and 3) top three (or four) MS3 scans (ion count target 104, normalized collision energy = 35%). Precursor ions (charge state ≥4+) were dynamically excluded for 20 seconds (tolerance of 10 ppm). Charge state and dynamic exclusion were applied to MS2 but turned off for MS3 acquisition.

Raw data was extracted to MGF format using MSConvert51, with MS3 data used for protein and peptide searches. Searches were performed by batch-tag feature of a locally installed version of Protein Prospector (v. 5. 19. 1, University of California San Francisco), with DSSO remnant mass modifications set as variable modifications (e.g. Alkene, Sulfenic-acid, and Thiol). Peptide reports were generated using the Search Compare

feature of Protein Prospector, and dead-end, intra-linked, and inter-linked peptides identified by in-house software program XL-Discoverer (part of new XLTools suite). Summarization and confidence assignment of inter-linked peptides was performed by in house scripts that reduce ambiguous assignments and distribute redundant counts.

Protein purification from *E. coli*.

Dre1 constructs containing N-terminal 2xStrep and SNAP tags were fused to a C-terminal 10xHis-MBP tag for expression in *E. coli*. Cells were grown in TB at 37ºC overnight, diluted 1:100 and grown to OD600 of 0.4 - 0.6. Temperatures were reduced to 18ºC and expression was induced with 1 mM IPTG, incubated overnight at 18ºC, shaking at 200rpm. Cells were pelleted for 15mn at 4000g at 4ºC and lysed by sonication. Lysates were clarified by centrifugation for 30min at 20,000g, 4ºC. Proteins were purified using 100 µl of a 50% slurry of Ni-NTA resin 2X (Sigma). Proteins were eluted 3X with 100µl elution buffer (2.5X PBS, 50mM imidazole). SDS-PAGE gel was run and stained with Coomassie to assess solubility.

Negative stain electron microscopy.

Eluates from Strep affinity purified $Dre1_{CTD}$-Strep in complex with dynactin (in Final Wash Buffer) were negatively stained with uranyl formate (pH ~6.0) on thin-carbon layered 400-mesh copper grids (Klim Verba) that were glow discharged before sample was applied. Samples were imaged using a 76 Tecnai T12 Spirit TEM (FEI) operated at 120 keV. Micro- graph images were acquired with ~1.5-µm defocus on a 4k × 4k CCD camera (Gatan) at a magnification of 67,000× with a pixel size of 1.73 Å.

Antibodies and reagents.

Primary antibodies were obtained from the following sources: mouse anti-p150^{glued} (BD Biosciences, 610473), mouse anti-FLAG (Millipore, F3165), rabbit anti-FLAG (Millipore, F7425), mouse anti-GAPDH (Millipore, MAB374), rabbit anti-p27 (DCTN6, Proteintech, 16947-1-AP), goat anti-MOMP L2 (Fitzgerald, 20C-CR2104GP), rabbit anti-Strep TagII HRP (Novagen, 71591–3). Nocodazole was purchased from Sigma (M1404). SiR-tubulin 647 was purchased from Cytoskeleton, Inc. Wheat-germ agglutinin 647 was purchased from Life Technologies (W32466). Heparin sodium salt was purchased from Sigma (H3393). (S)-MG132 was purchased from Cayman Chemicals (10012628). Type 1 Collagen (ThermoFisher, A1048301). Rapigest was purchased from Waters (186001860).

ACKNOWLEDGEMENTS

I thank the Krogan lab: in particular Robyn Kaake for her enthusiasm for this project, and advice over the years. I also sincerely thank Komal Pawar and Klim Verba, for joining in on the Dre1 fun. Thank you to the many, many people who have listened while I drone on and one about the amazing insights that pathogens reveal about host cell biology: Alex Long, Noah Randolph-Flagg, Anne Pipathsouk, Rick McKenney, members of the Engel Lab (especially Cherilyn Elwell), Amy Diallo, and Sophie Dumont. I also thank the National Institute of Health and the National Science Foundation for funding.

REFERENCES

Bauler, L. D., & Hackstadt, T. (2014). Expression and Targeting of Secreted Proteins from Chlamydia trachomatis. Journal of Bacteriology, 196(7), 1325–1334. https://doi.org/10.1128/JB.01290-13

Borca, M. V., Vuono, E. A., Ramirez-Medina, E., Azzinaro, P., Berggren, K. A., Singer, M., Rai, A., Pruitt, S., Silva, E. B., Velazquez-Salinas, L., Carrillo, C., & Gladue, D. P. (2019). Structural Glycoprotein E2 of Classical Swine Fever Virus Interacts with Host Protein Dynactin Subunit 6 (DCTN6) during the Virus Infectious Cycle. Journal of Virology, 94(1), e01642-19. https://doi.org/10.1128/JVI.01642-19

Burke, A. M., Kandur, W., Novitsky, E. J., Kaake, R. M., Yu, C., Kao, A., Vellucci, D., Huang, L., & Rychnovsky, S. D. (2015). Synthesis of two new enrichable and MS-cleavable cross-linkers to define protein-protein interactions by mass spectrometry. Organic & Biomolecular Chemistry, 13(17), 5030–5037. https://doi.org/10.1039/c5ob00488h

Elwell, C. A., Jiang, S., Kim, J. H., Lee, A., Wittmann, T., Hanada, K., Melancon, P., & Engel, J. N. (2011). Chlamydia trachomatis Co-opts GBF1 and CERT to Acquire Host Sphingomyelin for Distinct Roles during Intracellular Development. PLoS Pathogens, 7(9), e1002198. https://doi.org/10.1371/journal.ppat.1002198

Gill, S. R., Schroer, T. A., Szilak, I., Steuer, E. R., Sheetz, M. P., & Cleveland, D. W. (1991). Dynactin, a conserved, ubiquitously expressed component of an activator of vesicle motility mediated by cytoplasmic dynein. The Journal of Cell Biology, 115(6), 1639–1650. https://doi.org/10.1083/jcb.115.6.1639

Gladue, D. P., O'Donnell, V., Baker-Bransetter, R., Pacheco, J. M., Holinka, L. G., Arzt, J., Pauszek, S., Fernandez-Sainz, I., Fletcher, P., Brocchi, E., Lu, Z., Rodriguez, L. L., & Borca, M. V. (2014). Interaction of foot-and-mouth disease virus nonstructural protein 3A with host protein DCTN3 is important for viral virulence in cattle. Journal of Virology, 88(5), 2737–2747. https://doi.org/10.1128/JVI.03059-13

Jaarsma, D., & Hoogenraad, C. C. (2015). Cytoplasmic dynein and its regulatory proteins in Golgi pathology in nervous system disorders. Frontiers in Neuroscience, 9. https://doi.org/10.3389/fnins.2015.00397

Jäger, S., Cimermancic, P., Gulbahce, N., Johnson, J. R., McGovern, K. E., Clarke, S. C., Shales, M., Mercenne, G., Pache, L., Li, K., Hernandez, H., Jang, G. M., Roth, S. L., Akiva, E., Marlett, J., Stephens, M., D'Orso, I., Fernandes, J., Fahey, M., … Krogan, N. J. (2011). Global landscape of HIV-human protein complexes. Nature, 481(7381), 365–370. https://doi.org/10.1038/nature10719

Johnson, C. M., & Fisher, D. J. (2013). Site-Specific, Insertional Inactivation of incA in Chlamydia trachomatis Using a Group II Intron. PLoS ONE, 8(12), e83989. https://doi.org/10.1371/journal.pone.0083989

Kaake, R. M., Wang, X., Burke, A., Yu, C., Kandur, W., Yang, Y., Novtisky, E. J., Second, T., Duan, J., Kao, A., Guan, S., Vellucci, D., Rychnovsky, S. D., & Huang, L. (2014). A New in Vivo Cross-linking Mass Spectrometry Platform to Define Protein–Protein Interactions in Living Cells. Molecular & Cellular Proteomics, 13(12), 3533–3543. https://doi.org/10.1074/mcp.M114.042630

McKenney, R. J., Huynh, W., Tanenbaum, M. E., Bhabha, G., & Vale, R. D. (2014). Activation of cytoplasmic dynein motility by dynactin-cargo adapter complexes.

Science (New York, N.Y.), 345(6194), 337–341. https://doi.org/10.1126/science.1254198

Mirrashidi, K. M., Elwell, C. A., Verschueren, E., Johnson, J. R., Frando, A., Von Dollen, J., Rosenberg, O., Gulbahce, N., Jang, G., Johnson, T., Jäger, S., Gopalakrishnan, A. M., Sherry, J., Dunn, J. D., Olive, A., Penn, B., Shales, M., Cox, J. S., Starnbach, M. N., … Engel, J. (2015). Global Mapping of the Inc-Human Interactome Reveals that Retromer Restricts Chlamydia Infection. Cell Host & Microbe, 18(1), 109–121. https://doi.org/10.1016/j.chom.2015.06.004

O'Reilly, F. J., & Rappsilber, J. (2018). Cross-linking mass spectrometry: Methods and applications in structural, molecular and systems biology. Nature Structural & Molecular Biology, 25(11), 1000–1008. https://doi.org/10.1038/s41594-018-0147-0

Ortiz Flores, R. M., Distel, J. S., Aguilera, M. O., & Berón, W. (2019). The role of microtubules and the dynein/dynactin motor complex of host cells in the biogenesis of the Coxiella burnetii-containing vacuole. PLOS ONE, 14(1), e0209820. https://doi.org/10.1371/journal.pone.0209820

Quintyne, N. J., Gill, S. R., Eckley, D. M., Crego, C. L., Compton, D. A., & Schroer, T. A. (1999). Dynactin is required for microtubule anchoring at centrosomes. The Journal of Cell Biology, 147(2), 321–334. https://doi.org/10.1083/jcb.147.2.321

Quintyne, N. J., & Schroer, T. A. (2002). Distinct cell cycle–dependent roles for dynactin and dynein at centrosomes. Journal of Cell Biology, 159(2), 245–254. https://doi.org/10.1083/jcb.200203089

Schroer, T. A., & Sheetz, M. P. (1991). Two activators of microtubule-based vesicle transport. The Journal of Cell Biology, 115(5), 1309–1318. https://doi.org/10.1083/jcb.115.5.1309

Schroer, T. A., & Verma, V. (2021). Cytoskeleton | Dynactin. In Encyclopedia of Biological Chemistry III (pp. 188–192). Elsevier. https://doi.org/10.1016/B978-0-12-819460-7.00186-9

Splinter, D., Razafsky, D. S., Schlager, M. A., Serra-Marques, A., Grigoriev, I., Demmers, J., Keijzer, N., Jiang, K., Poser, I., Hyman, A. A., Hoogenraad, C. C., King, S. J., & Akhmanova, A. (2012). BICD2, dynactin, and LIS1 cooperate in regulating dynein recruitment to cellular structures. Molecular Biology of the Cell, 23(21), 4226–4241. https://doi.org/10.1091/mbc.E12-03-0210

Tirumala, N. A., & Ananthanarayanan, V. (2020). Role of Dynactin in the Intracellular Localization and Activation of Cytoplasmic Dynein. Biochemistry, 59(2), 156–162. https://doi.org/10.1021/acs.biochem.9b00772

Urnavicius, L., Zhang, K., Diamant, A. G., Motz, C., Schlager, M. A., Yu, M., Patel, N. A., Robinson, C. V., & Carter, A. P. (2015). The structure of the dynactin complex and its interaction with dynein. Science (New York, N.Y.), 347(6229), 1441–1446. https://doi.org/10.1126/science.aaa4080

Wang, Y., Kahane, S., Cutcliffe, L. T., Skilton, R. J., Lambden, P. R., & Clarke, I. N. (2011). Development of a Transformation System for Chlamydia trachomatis: Restoration of Glycogen Biosynthesis by Acquisition of a Plasmid Shuttle Vector. PLoS Pathogens, 7(9), e1002258. https://doi.org/10.1371/journal.ppat.1002258

Waterman-Storer, C. M., Karki, S., & Holzbaur, E. L. (1995). The p150Glued component of the dynactin complex binds to both microtubules and the actin-related protein centractin (Arp-1). Proceedings of the National Academy of Sciences of the United States of America, 92(5), 1634–1638. https://doi.org/10.1073/pnas.92.5.1634

FIGURE 3.1

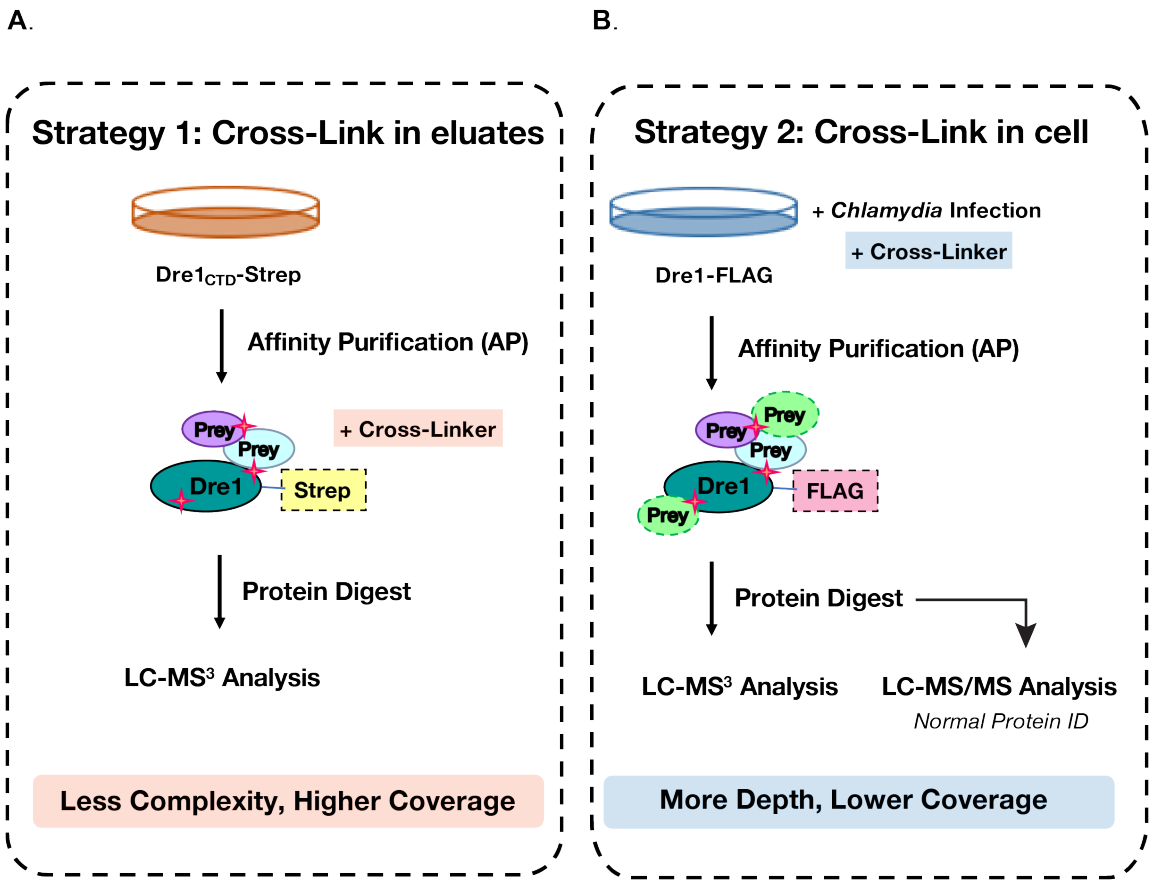

FIGURE 3.1. Two methodologies for using cross-linking MS to map the binding interface of Dre1 and dynactin.

(A) $Dre1_{CTD}$-Strep (residues 84 – 231, see Figure 2.2A) is ectopically expressed in adherent HEK293T cells for 48 hours. Dre1 and host binding partners are affinity purified using Strep-Tactin Sepharose beads. With a yield of ~1 µM of protein per experiment. Eluates are cross-linked using a 1:500 molar ratio of protein:DSSO. Cross-linked eluates are then subjected to an in-solution trypsin digest, and analyzed by MS. As Dre1 and host targets are isolated from the cell/lysates prior to cross-linking, a higher fraction of cross-linker is available to link Dre1 to host targets.

(B) HeLa Cells are infected with L2+$pDre1_{FL}$-FLAG for ~36 hours. Cell-permeable cross-linker (2.0 mM Alkyne-A-DSBSO) is added for 1 hour at 37°C, 5% CO_2. Cross-linked cells are lysed and affinity purified using magnetic-FLAG beads. Eluates are then subjected to an in-solution trypsin digest, and analyzed by MS. As cells are cross-linked during infection, interactions with transiently associated proteins may be stabilized and identified. Furthermore, this strategy generates interaction maps that occur at the inclusion membrane in the context of infection. A higher concentration of cross-linker is required as its activity is distributed throughout all proteins in the cell.

FIGURE 3.2

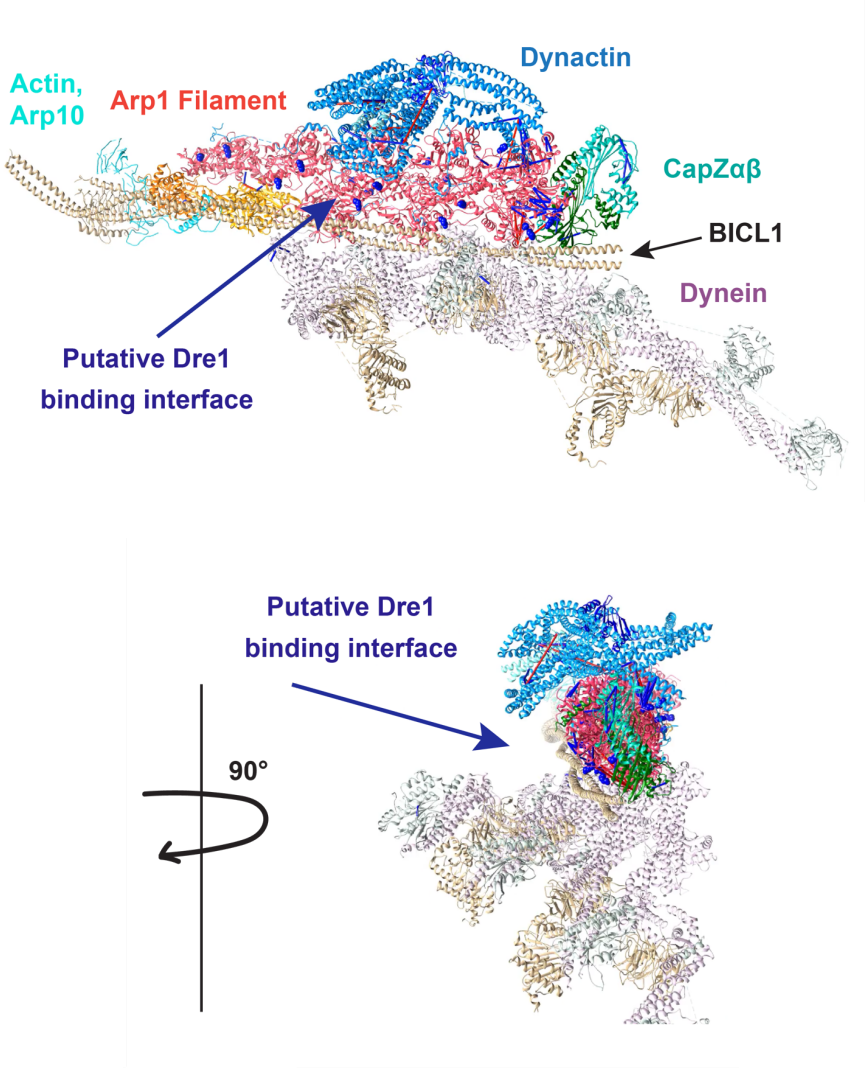

FIGURE 3.2. Dre1$_{CTD}$-Strep binds along the Arp1 filament of dynactin.

Dre1$_{CTD}$-Strep and the host dynactin complex were affinity purified from HEK293T cells, cross-linked with DSSO, and analyzed by LC-MS^3. Resulting cross-links were mapped onto the published 4.0 angstrom-resolution cryo-EM dynactin-dynein structure (Urnavicius et al., 2015). Dynactin subcomplexes are labeled, and regions of the structure that cross-link to Dre1 are indicated by blue spheres. 50% of Dre1 cross-links map to regions of subunits missing from the structure, likely because these regions of the complex are more flexible. 82% of the Dre1 cross-links to sections of the published dynactin structure were able to be successfully mapped. Dre1 cross-links to dynactin along the extended Arp1 filament.

FIGURE 3.3

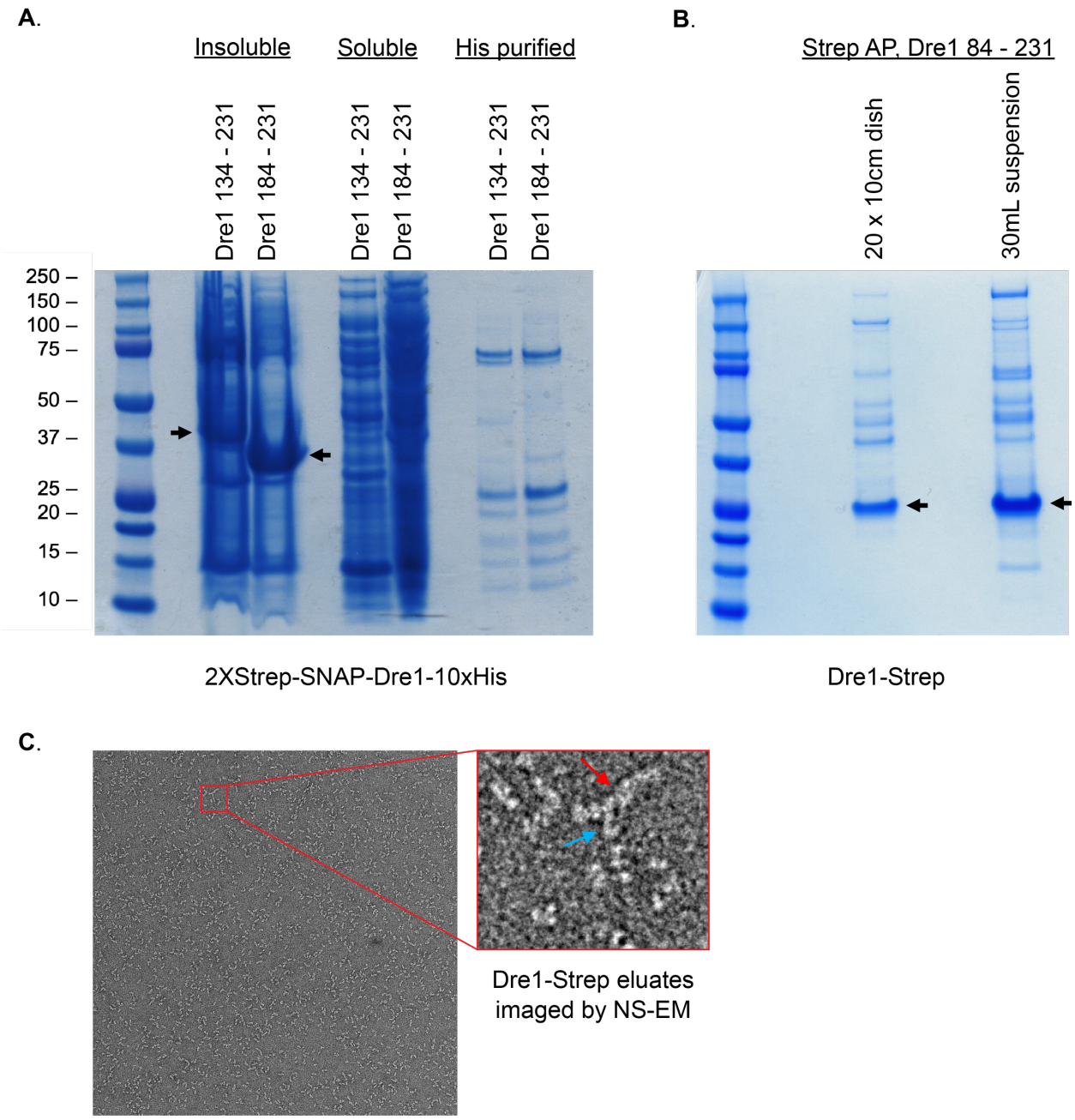

FIGURE 3.3. Performing cryo electron microscopy (EM) on Dre1$_{Strep}$ eluates to elucidate the structure of dynactin in complex with Dre1.

(**A**) Purification of 2xStrep-SNAP-Dre1-10xHis tagged Dre1 from *E. coli* for *in vitro* studies, including cryo electron microscopy (cryo-EM). BL-21 cells expressing the indicated deletion constructs of Dre1 were lysed, lysates were clarified, and immobilized to Ni-NTA resin. Beads were washed extensively, and the complexes were subjected to

SDS-PAGE and visualized by Coomassie blue staining. Arrow, Dre1. Molecular weight markers are indicated. Dre1 constructs were largely insoluble.

(**B**) Dre1$_{CTD}$-Strep (residues 84-231) was expressed for 48 hours in 20x10cm^2 plates of adherent HEK293T cells or in 30 mL of suspension-grown Expi293 cells. Cells were pelleted, lysed, and affinity purified using Strep-Tactin Sepharose beads. Purified complexes were subjected to SDS-PAGE and visualized by Coomassie blue staining. 1% of lysates were loaded in each lane. Dre1 and associated dynactin components are more concentrated in the 30 mL preps of suspension cells. This purification strategy will be used to isolate complexes for cryo-EM.

(**C**) Negative stain EM of eluates generated in (B) to screen for dynactin complex assembly. Right-angle light-scattering traces of ~100µg of total protein. Negatively-stained Arp1 filaments (red arrow) are clearly resolved, and the shoulder region (blue dynactin subunits in figure 3.2, blue arrow) can be detected. Inset is a higher magnification view of the boxed region.

CHAPTER FOUR

A NOVEL TYPE-THREE SECRETION SYSTEM INHIBITOR DIMINISHES CHLAMYDIA VIRULENCE

“If you surrendered to the wind, you could ride it.”
- Toni Morrison

SUMMARY

Antibiotic-resistant bacteria are an emerging global health threat. New antimicrobials are urgently needed. The injectisome type III secretion system (T3SS), required by dozens of Gram-negative bacteria for virulence but largely absent from nonpathogenic bacteria, is an attractive antimicrobial target. We previously identified synthetic cyclic peptomers, inspired by the natural product phepropeptin D, that inhibit protein secretion through the *Yersinia* Ysc and *Pseudomonas aeruginosa* Psc T3SSs but do not inhibit bacterial growth. Here, we describe the identification of an isomer, 4EpDN, that is 2-fold more potent (50% inhibitory concentration [IC50] of 4 μM) than its parental compound. Furthermore, 4EpDN inhibited the *Yersinia* Ysa and the *Salmonella* SPI-1 T3SSs, suggesting that this cyclic peptomer has broad efficacy against evolutionarily distant injectisome T3SSs. Indeed, 4EpDN strongly inhibited intracellular growth of *Chlamydia trachomatis* in HeLa cells, which requires the T3SS. 4EpDN did not inhibit the unrelated twin arginine translocation (Tat) system, nor did it impact T3SS gene transcription. Moreover, although the injectisome and flagellar T3SSs are evolutionarily and structurally related, the 4EpDN cyclic peptomer did not inhibit secretion of substrates through the *Salmonella* flagellar T3SS, indicating that cyclic peptomers broadly but specifically target the injectisome T3SS. 4EpDN reduced the number of T3SS needles detected on the surface of *Yersinia pseudotuberculosis* as detected by microscopy. Collectively, these data suggest that cyclic peptomers specifically inhibit the injectisome T3SS from a variety of Gram-negative bacteria, possibly by preventing complete T3SS assembly.

INTRODUCTION

Antibiotic resistance is of great concern to global public health. Bacterial pathogens have evolved numerous mechanisms to survive treatment with clinically available antibiotics (Santajit & Indrawattana, 2016). Alternative therapies against multidrug-resistant strains of so-called ESKAPE pathogens (*Enterococcus faecium*, *Staphylococcus aureus*, *Klebsiella pneumoniae*, *Acinetobacter baumannii*, *Pseudomonas aeruginosa*, and *Enterobacter* species) are urgently needed. Various strategies have been explored to avoid the so-called antimicrobial apocalypse (Ma et al., 2020). One promising approach is to inhibit bacterial virulence mechanisms to disarm pathogens without affecting nonpathogenic members of the microbiota or environmental bacteria (Calvert et al., 2018; Duncan et al., 2012). This approach has the potential to not only control infection but to do so in a way that preserves the integrity of the microbiome, which is beneficial for human health and is often the source of antibiotic resistance genes (Mohajeri et al., 2018; Relman & Lipsitch, 2018).

The type III secretion system (T3SS), a needle-like injectisome apparatus, is required for virulence in many Gram-negative pathogens, including *Salmonella*, *Yersinia*, *Chlamydia*, and the ESKAPE pathogen *P. aeruginosa*. The T3SS is largely absent from commensal bacteria, making it a good target for virulence blocker antimicrobials. Based on phylogenetic analysis of core T3SS proteins, T3SSs were classified into seven families (Abby & Rocha, 2012; Diepold & Armitage, 2015). However, T3SSs have many highly conserved structural components (Diepold & Wagner, 2014). T3SS genes are typically encoded on virulence plasmids or pathogenicity islands, indicative of horizontal gene

transfer (Gophna et al., 2003); therefore, phylogeny of T3SSs does not follow organismal phylogeny. Phylogenetic analysis suggests that the injectisome T3SS evolved from the flagellar system (Abby & Rocha, 2012; Diepold & Armitage, 2015). Indeed, the flagellar basal body is a secretion system, referred to as the flagellar T3SS, that secretes flagellin and other cargo into the extracellular space in order to build the flagellar filament to power motility. The flagellar and injectisome T3SSs share several conserved basal body and export apparatus components (Diepold & Wagner, 2014). However, the injectisome T3SS does not mediate motility, but instead delivers effector proteins into target host cells.

The T3SS is one of the most complex protein assemblies in prokaryotes involving multiple proteins assembled in an ordered manner. All T3SSs are composed of an external, hollow needle attached to a basal body made up of the outer membrane secretin SctC (Wagner & Diepold, 2020) and the inner membrane component SctD (YscD in *Yersinia*) (Diepold et al., 2010), as well as the export apparatus SctRSTUVJ (Diepold et al., 2011). Following the formation of the two SctC and SctD membrane rings, the cytosolic complex composed of YscKQLNO associates with the membrane rings and export apparatus to make an active secretion system (Diepold et al., 2010). The early substrates, such as SctF (called YscF in *Yersinia*), are then secreted (Diepold et al., 2012), allowing SctF to polymerize to form the T3SS needle. The middle substrates, the needle tip protein SctA and translocators SctE and SctB, are then secreted and make contact with host cells to trigger secretion of the late substrates, the effector proteins that alter host defenses (Wagner & Galán, 2020). A number of regulators of the T3SS have been described in different bacteria, including those whose secretion by the T3SS alters their cytoplasmic

concentration and therefore their activity. One example is *Pseudomonas* ExsE, which sequesters the T3SS master regulator EsxA through a partner switching mechanism, until host cell contact is made and ExsE is secreted, relieving ExsA repression and potentiating an increase in T3SS gene transcription (Rietsch et al., 2005; Urbanowski et al., 2005).

A number of small molecules, antibodies, and vaccines have been studied for T3SS targeted therapies (Fasciano et al., 2019). Despite showing promising effects on the T3SS in vitro and in animal models, only one antibody-based therapy has entered clinical trials. A bispecific antibody, MEDI3902, against the *P. aeruginosa* T3SS needle tip protein PcrV (SctA) and the Psl exopolysaccharide is effective against both acute and chronic infection models and is in phase II clinical trials for prevention of ventilator-associated pneumonia (DiGiandomenico et al., 2014; Tabor et al., 2018). However, antibodies must be administered intravenously, so chemical inhibitors of the T3SS are needed.

As narrow-spectrum antimicrobials require more precise diagnostics, broad-spectrum T3SS inhibitors would be more valuable clinically than those only able to target one bacterial species. In addition, most mammalian pathogens that utilize a T3SS require their T3SS only during growth within, but not outside, the host animal. However, the *Chlamydiae*, which cause lung, genital, and eye infections, are obligate intracellular bacteria, and their T3SS is strictly required for their growth (Häcker, 2018). Interestingly, the *Chlamydia* T3SS belongs to its own T3SS family (Abby & Rocha, 2012; Diepold & Armitage, 2015). Here, we identify a derivative of a synthetic cyclic peptomer family of T3SS inhibitors (Lam et al., 2018) that can inhibit the T3SS machinery of three

evolutionarily distinct T3SS families used by five different bacterial species to cause human disease, including the Ysc (*P. aeruginosa* Psc, *Y. pseudotuberculosis* Ysc), Inv-Mxi-Spa (*Y. enterocolitica* Ysa, *Salmonella enterica* serovar Typhimurium SPI-1), and *Chlamydiales* (*Chlamydia trachomatis*) families. While having significant breath of activity among various injectisome T3SSs, these inhibitors do not affect bacterial growth or other secretion systems such as the flagellar T3SS or the twin-arginine translocation system.

RESULTS

Structure-activity relationship study of cyclic peptomers.

Previously, we identified a group of cyclic peptomers that inhibited secretion of substrates from *Y. pseudotuberculosis* and *P. aeruginosa* T3SSs but did not inhibit bacterial growth, motility, or HeLa cell metabolism (Lam et al., 2017). These results suggested a potential for development of the cyclic peptomers as pathogen-specific virulence blockers. Based on dose-response curves and concentration of half maximal inhibition (IC50) of the *P. aeruginosa* T3SS, 1EpDN (previously named EpD1,2N) was chosen for structure-activity relationship (SAR) analysis. The compounds used in SAR analysis are listed in Table 1.

We first assessed the effect of alanine replacement at each of the six positions of the parent scaffold, 1EpDN. Note that because peptoids have side chains appended to a nitrogen atom rather than carbon as in amino acids, positions 1 and 2 were synthesized with N-methylglycine, also known as sarcosine (Sar), as the peptoid equivalent of alanine (Ala). Ala or Sar replacement at any of the six positions resulted in significant loss of activity, suggesting that all side chains contribute to the activity (see Figure S4.1 in the supplemental material). Next, we carried out a stereochemistry scan, in which different combinations of l- and d-amino acids at positions 3 to 6 were generated. The parent compound, 1EpDN, has propylamine, and benzylamine at positions 1 and 2, and d-Leu, l-Ile, l-Leu, and d-Phe at positions 3 to 6. For the stereochemistry scan, we will refer to 1EpDN as PBDLLD. While most stereoisomers had the same or reduced T3SS inhibitory activity, 4EpDN (PBLLDD) showed improved activity, with an IC50 of ~4 μM compared to the parent compound IC50 of ~8 μM (Figure 4.1A and B). Replacement of position 1

(4EpDN 1Sar) or position 2 (4EpDN 2Sar) with Sar significantly reduced activity of 4EpDN (Figure 4.2A and B). 4EpDN and 4EpDN 2Sar were used as an active compound and a negative control, respectively, in most follow-up experiments. Importantly, 4EpDN and 4EpDN 2Sar did not affect bacterial viability in broth culture (Figure S4.2).

Cyclic peptomers do not inhibit secretion through the twin-arginine translocation (Tat) system.

In order to determine if the cyclic peptomer 4EpDN inhibits the activity of secretion systems completely unrelated to the T3SS, we sought to assess the impact of cyclic peptomers on the twin arginine translocation (Tat) system. We chose to use *Y. pseudotuberculosis* for this because its Tat secretion system is well studied (Avican et al., 2017; Lavander et al., 2006). The Tat system translocates fully folded substrates across the inner membrane, while the T3SS translocates partially unfolded substrates across the inner, outer, and target host cell membranes (Green & Mecsas, 2016). To monitor Tat secretion system activity, a reporter strain expressing an IPTG (isopropyl-β-d-thiogalactopyranoside)-inducible β-lactamase TEM-1 domain fused to the signal peptide of the SufI Tat substrate (Avican et al., 2017) was constructed. Following IPTG induction, β-lactamase confers resistance to the β-lactam peptidoglycan-targeting antibiotic penicillin G when the SufI-β-lactamase reporter has successfully translocated into the periplasm (Figure 4.3A). The presence of known Tat inhibitors, Bay 11-7082 or N-phenylmaleimide (Bageshwar et al., 2016), strongly reduced growth of bacteria after 4 and 6 h, while growth of bacterial cultures treated with cyclic peptomers was similar to

that of the dimethyl sulfoxide (DMSO) control (Figure 4.3B and C). These results suggested that 4EpDN does not inhibit the Tat secretion system.

The 4EpDN cyclic peptomer inhibits secretion of T3SS substrates from the Inv-Mxi-Spa T3SS family but does not inhibit secretion through the flagellar T3SS.

The T3SSs were classified into seven families based on phylogenetic analysis (Abby & Rocha, 2012; Diepold & Armitage, 2015). We previously showed that cyclic peptomers inhibited the Ysc T3SS family found in *P. aeruginosa* and *Yersinia* (Figure 4.1 and 4.2) (Lam et al., 2017). In order to test whether cyclic peptomers are active against other T3SS families, we evaluated the effect of cyclic peptomers on the Inv-Mxi-Spa T3SS in *Y. enterocolitica* and *Salmonella enterica* serovar Typhimurium.

The *Y. enterocolitica* Ysa system, a chromosomally encoded T3SS, is distinct from the *Yersinia* Ysc T3SS and contributes *to Y. enterocolitica* colonization of the terminal ileum and gastrointestinal-associated tissues (Bent et al., 2013; Venecia & Young, 2005). A *Y. enterocolitica* mutant that lacks expression of the Ysa T3SS (ΔysaT) was used as a negative control, while a mutant lacking the Ysc T3SS (ΔyscL) (Young & Young, 2002) was used to evaluate the effect of compounds specifically on the Ysa system. Secretion of the Ysa effector protein YspF was quantified. 4EpDN inhibited secretion of YspF in a dose-dependent manner, while 4EpDN 2Sar did not affect its secretion (Figure 4.4). Together, these results suggest that cyclic peptomers are active against both the Ysc and Ysa T3SSs in *Yersinia*.

In order to evaluate whether the cyclic peptomers are active against T3SSs distinct from the Ysc T3SS outside the *Yersinia* genus, we tested cyclic peptomer efficacy in *Salmonella*. *Salmonella* employs two T3SSs during infection, with the SPI-1 T3SS belonging to the Inv-Mxi-Spa T3SS family (Abby & Rocha, 2012; Diepold & Armitage, 2015). Inhibition of SPI-1 T3SS effector protein SipC and SipA (Hallstrom & McCormick, 2016; Lilic et al., 2003; Singh et al., 2018) secretion by 4EpDN was observed at ~1 μM and ~1.4 μM, respectively, while 4EpDN 2Sar showed inhibition of SipC and SipA secretion only at concentrations greater than 30 μM (Figure 4.5). It has previously been shown that compound aggregates can act as promiscuous inhibitors with nonspecific activity (McGovern et al., 2002, 2003). To rule out that 4EpDN activity was due to compound aggregation, we chose to measure *Salmonella* type III secretion in the presence of detergent. Comparison of various nonionic detergents (NP-40, Tween 20, and Triton X-100) at different concentrations suggested that Tween 20 at 0.003% was the highest concentration of detergent to have a minimal effect on secretion of effector proteins (Figure S4.3); therefore, Tween 20 at this concentration was used for further analysis. Addition of Tween 20 did not reduce activity of 4EpDN but slightly increased it (Figure 4.5), suggesting that activity of the cyclic peptomers does not result from aggregated compounds.

As 4EpDN inhibited both the Ysc and Inv-Mxi-Spa T3SS families, we tested whether this cyclic peptomer could inhibit the flagellar T3SS, which is the most distantly related T3SS family based on previous phylogenetic analysis (Abby & Rocha, 2012). Conveniently, *Salmonella* expresses the SPI-1 and its flagellar system under the same conditions in

vitro (rich media). This allowed us to investigate effects of cyclic peptomers on both the SPI-1 T3SS and flagellar systems under the same culture conditions. Because of the conservation between the injectisome and flagellar T3SSs, flagellar substrates can be secreted through both systems. Therefore, secretion of flagellar substrates (FliC and FliD) was quantified in both wild-type (WT) and ΔSPI-1 strains to distinguish secretion through both the SPI-1 T3SS and flagellar system (WT strain) or only through the flagellar system alone (ΔSPI-1 strain). 4EpDN inhibited FliC and FliD secretion in WT *Salmonella* at concentrations of ≥60 μM and ≥3.75 μM, respectively (Figure S4.4), consistent with the ability of the SPI-1 T3SS being able to secrete flagellar substrates. However, 4EpDN only inhibited FliC and FliD secretion at high concentrations (≥60 μM) in the ΔSPI-1 mutant, with unfavorable dose-response curves compared to WT *Salmonella*. This suggests that the inhibitory effect of 4EpDN on FliD secretion in the WT strain was mainly through inhibition of its secretion through the SPI-1 T3SS. 4EpDN 2Sar had no significant effect on FliC secretion or FliD secretion. These data suggest that the cyclic peptomer 4EpDN does not significantly inhibit substrate secretion through the flagellar T3SS in *Salmonella* but strongly inhibits the SPI-1 T3SS under the same conditions.

The 4EpDN cyclic peptomer affects the T3SS needle.

In order to determine how 4EpDN might inhibit type III secretion, we tested whether the cyclic peptomer inhibits assembly of the T3SS. We chose to use *Yersinia* for these experiments because of the existing microscopy tools to monitor assembly of T3SS components. The T3SS basal body must be assembled prior to T3SS substrate secretion (Deng et al., 2017; Diepold, 2019; Diepold et al., 2010). In *Yersinia*, the T3SS basal body

component YscD (SctD) is an inner membrane ring protein that is conserved among injectisome T3SSs, but has low sequence homology with the flagellar ortholog FliG (Diepold & Wagner, 2014). The absence of YscD at the inner membrane prevents assembly of other T3SS machinery (YscL, YscK, YscQ) (Diepold et al., 2010, 2017) and secretion of T3SS substrates (Kudryashev et al., 2013). We used a *Y. enterocolitica* strain expressing a YscD allele translationally fused with enhanced green fluorescent protein (EGFP) to visualize the effect of compounds on YscD assembly (Diepold et al., 2010). 4EpDN caused only a modest reduction in the number of YscD puncta (Figure S4.5). Once the T3SS basal body is assembled and functional, the next stage of T3SS assembly is polymerization of the T3SS needle subunit SctF (YscF in *Yersinia*) to form the T3SS needle (Diepold et al., 2012). To determine whether the cyclic peptomers affect T3SS needle formation, we used an anti-YscF antibody to measure the number of YscF puncta at the bacterial surface by immunofluorescence microscopy. We found a 2-fold reduction in YscF puncta in the presence of 60 μM 4EpDN compared to the DMSO control (Figure 4.6A to C). These data suggest that cyclic peptomers affect the assembly or stability of T3SS needles, ultimately dampening secretion of effector proteins.

The 4EpDN cyclic peptomer does not inhibit transcription and secretion of the negative regulator ExsE.

The cyclic peptomers did not decrease expression of T3SS genes in *Salmonella* or *Pseudomonas* (Figure S4.6), suggesting that they do not act at the level of T3SS gene expression. In some bacteria with T3SSs, such as *Yersinia* and *Pseudomonas*, secretion of negative regulators through the T3SS leads to upregulation of T3SS gene expression

(Bergman et al., 1991; Pettersson et al., 1996; Rietsch et al., 2005; Rimpiläinen et al., 1992; Urbanowski et al., 2005; Williams & Straley, 1998). Thus, the observation that the cyclic peptomers did not affect *Pseudomonas* T3SS gene expression is surprising. To investigate this discrepancy, we observed the effect of 4EpDN on the *P. aeruginosa* negative regulator ExsE, which when secreted, relieves repression of the ExsA T3SS master regulator (Rietsch et al., 2005). 4EpDN significantly inhibited secretion of the effector protein ExoU by ~75% at either 9 or 60 μM, while 4EpDN 2Sar had no effect (Figure 4.7). In contrast, 4EpDN did not significantly inhibit ExsE secretion at 9 μM and only inhibited ExsE secretion ~40% at 60 μM. This result explains the lack of impact of 4EpDN on the ExsE, which negatively regulates ExsA-mediated transcription. A major difference between ExsE and ExoU in terms of their protein properties is their size; ExsE is ~9 kDa, while ExoU is ~74 kDa. Taken together, these data suggest that 4EpDN may inhibit secretion of larger T3SS cargo more robustly than smaller cargo.

Cyclic peptomers block *Chlamydia* infection.

In order to evaluate whether the 4EpDN cyclic peptomer can disarm bacterial virulence, we examined the effect of this compound on *Chlamydia* infection, as this pathogen requires the T3SS for infection and growth within human cells. The chlamydial life cycle involves two major bacterial forms, the extracellular infectious elementary bodies (EBs) and the intracellular replicative reticulate bodies (RBs). EBs are infectious and abundant around 48 h post infection (hpi). RBs are noninfectious and abundant at 24 hpi. Upon entry, EBs discharge preloaded T3SS effectors and are taken up into a membrane-bound compartment (the inclusion) where they differentiate into RBs, secrete additional T3SS

effectors and replicate, and then redifferentiate into EBs. The initial stages of infection were assessed by quantifying the number of inclusions per cell at 24 hpi. In contrast, production of infectious progeny, which assays RB-EB redifferentiation and release of EBs, was assayed by collecting EBs at 48 hpi, infecting fresh monolayers for 24 hpi. INP0400, a known T3SS inhibitor was used as a control (Muschiol et al., 2006). 4EpDN but not 4EpDN 2Sar decreased primary inclusion formation ~50% but inhibited formation of infectious progeny ~98% (Figure 4.8). These data show that the 4EpDN cyclic peptomer can completely block the chlamydial life cycle in human cells, which is dependent on the T3SS.

DISCUSSION

In this study, we showed that the cyclic peptomer 4EpDN is a broad-spectrum injectisome T3SS inhibitor that disrupts T3SS assembly and secretion of T3SS effectors. 4EpDN inhibits secretion through the T3SS of a number of pathogens, including the nosocomial ESKAPE pathogen *Pseudomonas aeruginosa*, enteropathogenic *Yersinia*, and *Salmonella*, with IC50 in the low μM range. 4EpDN does not inhibit secretion from two other secretion systems—the flagellar T3SS and the Tat system. The 4EpDN cyclic peptomer has only a small effect on assembly of the basal body component YscD in the plasma membrane but inhibits T3SS needle assembly. Importantly, 4EpDN can completely block the ability of the obligate intracellular pathogen Chlamydia trachomatis to propagate in human cells, which requires the T3SS.

Through alanine and stereochemistry scans, we identified 4EpDN, a cyclic peptomer with an IC50 of 4 μM in inhibiting secretion of T3SS effector proteins in *P. aeruginosa* and 1 μM in inhibiting the *Salmonella* SPI-1 T3SS. Compared to previously published T3SS inhibitors (Table 2), this low μM activity is encouraging. The only published T3SS inhibitors with comparable IC50 are the phenoxyacetamides (MBX 2359 and its optimized derivatives), which inhibit *P. aeruginosa* T3SS secretion at 1 to 3 μM (Bowlin et al., 2014). Stereoisomers of 1EpDN showed a wide range of potencies, suggesting that differences in their three-dimensional structures affect their biological activity. 9EpDN is a true enantiomer of 1EpDN, with an IC50 of ~13 μM, a lower potency than the 1EpDN parental compound's ~8 μM. Importantly, the activity of these isomers does not positively correlate with solubility (Figure S4.7, Table S4.1), indicating that the observed activity is due to a

specific molecular reaction rather than a nonspecific biophysical effect due to aggregation. Furthermore, the presence of nonionic detergent did not adversely affect the activity of compounds. These data suggest that 4EpDN is an active cyclic peptomer with specific T3SS inhibitory activity.

Secretion of protein substrates through the injectisome T3SS, the flagellar system, and the Tat system require the proton motive force (P. A. Lee et al., 2006; P.-C. Lee & Rietsch, 2015; Paul et al., 2008). Although cyclic peptomers inhibited secretion from the injectisome T3SS, they did not inhibit the Tat system and only weakly inhibited flagellar substrate secretion, suggesting that the proton motive force is unaffected, as we previously suggested (Lam et al., 2017), and that the cyclic peptomers do not inhibit bacterial secretion in general. These results suggest that cyclic peptomers act as broad-spectrum, but specific, inhibitors of the injectisome T3SS.

The 4EpDN cyclic peptomer demonstrated efficacy against the T3SSs of *P. aeruginosa*, *Y. pseudotuberculosis*, *Y. enterocolitica*, *Salmonella enterica* Typhimurium, and *Chlamydia trachomatis*, with an IC50 in the range of 1 μM (for the *Salmonella* SPI-1 T3SS) to ~16 μM (for the *Y. pseudotuberculosis* Ysa T3SS) (Table 2). Based on phylogenetic analysis of core T3SS proteins, T3SSs group into seven T3SS families, five of which contain T3SSs from human pathogens (Troisfontaines & Cornelis, 2005). 4EpDN has efficacy against T3SSs from at least three of these T3SS families, the Ysc (Ysc and Psc), Inv-Mxi-Spa (SPI-1 and Ysa), and *Chlamydiales*. Interestingly, the flagellar ATPase from *Escherichia coli* falls at the root of the phylogenetic tree (Auvray et al., 2002), distinct from

other T3SS families. As 4EpDN impacted secretion through the flagellar T3SS significantly less than through the injectisome T3SS in the same bacterial species and under the same culture and experimental conditions, we reason that the pathway targeted by cyclic peptomers is common to all injectisome T3SSs but absent from the flagellar system.

The T3SS is a complex system of ~20 different proteins and is assembled in a hierarchical manner prior to secretion of effector proteins (Deng et al., 2017; Wagner et al., 2018). The T3SS of *Yersinia*, *Pseudomonas*, *Salmonella*, and *Chlamydia* share a number of orthologous basal body components that must be assembled before secretion can occur. However, 4EpDN only slightly reduced localization of the inner membrane ring protein YscD to the *Yersinia* cell envelope. But 4EpDN significantly inhibited the ability of the *Yersinia* T3SS needle to bind anti-YscF antibodies by approximately 2-fold. In contrast, T3SS effector secretion was inhibited 4-fold at the same concentration, suggesting that inhibition of T3SS assembly may not be the only mechanism by which 4EpDN blocks T3SS activity. Interestingly, it is possible that the 4EpDN cyclic peptomer is more effective at inhibiting secretion of large T3SS cargo (such as ExoU, ~74 kDa) compared to smaller cargo (such as ExsE, ~9 kDa). As the YscF needle subunit is also ~9 kDa, this may explain why T3SS needle detection at the bacterial surface is not as robustly inhibited as ExoU secretion. It is possible that the 4EpDN cyclic peptomer interacts with the lumen of the T3SS needle, impacting large cargo secretion more than small cargo secretion. Alternatively, 4EpDN may disrupt normal assembly of the T3SS needle subunit, resulting in nonfunctional needles that cause dramatic effects on the

secretion of effectors. It is also possible that both phenomena contribute to the observed effects.

4EpDN strongly inhibited *Chlamydia* from infecting HeLa cells during primary infection and subsequently completely prevented *Chlamydia* from infecting additional host cells. At the early stage of *Chlamydia* infection, T3SS plays major roles in invasion, EB to RB differentiation, and replication through pre-synthesized T3SS effectors and early and midcycle effectors (Elwell et al., 2016). These effectors mediate nutrient acquisition and maintain the viability of the host cell. A decrease in inclusion number at the end of the midcycle (in primary infection) suggests inhibition of one or more of the above processes. At the late stage of infection (~24 to 72 hpi), the RB to EB transition occurs, and late-cycle effectors are generated and packaged in progeny EB to prepare for the next infection cycle (Elwell et al., 2016; Saka et al., 2011). 4EpDN has a particularly strong effect on the secondary infection (assayed at 48 hpi), suggesting that the cyclic peptomer may inhibit secretion of pre-synthesized *C. trachomatis* effectors. This highlights the potential of cyclic peptomers to prevent the spread of *Chlamydia* infection. *Chlamydia* relies on its T3SS effector proteins to interact with host factors, such as the actin cytoskeleton, Golgi network, endoplasmic reticulum, and microtubule network, to mediate invasion and intracellular growth (Elwell et al., 2016). It is possible that compounds that inhibit these host pathways could interfere with *Chlamydial* growth (Al-Zeer et al., 2014; Derré, 2015; Kumar & Valdivia, 2008). However, microscopic analysis of many cellular structures in HeLa cells in the presence of 4EpDN did not show any gross changes to the actin cytoskeleton, Golgi network, endoplasmic reticulum, or microtubule network at the

concentration used in our *Chlamydia* infection (Figure S4.8). *C. trachomatis* infection may cause infertility in female patients and eye damage, in addition to lung infections (Häcker, 2018). Antibiotics, such as β-lactam antibiotics, are a common way to treat *Chlamydia* infection, but the chance of recurrence is high (Klöckner et al., 2018; Miller, 2006). Current vaccine development efforts are under way, but multiple challenges remain (Phillips et al., 2019). There is increased demand for drugs against *Chlamydia* due to antibiotic resistance (Krupp & Madhivanan, 2015). The strong efficacy of cyclic peptomers highlights their potential for development as an anti-*chlamydial* drug.

Overall, the cyclic peptomer 4EpDN specifically targets the injectisome T3SS of Gram-negative bacteria. As the T3SS is important to overcome host defense mechanisms, inhibition of this virulence mechanism may augment the function of the host immune system to clear infection. Thus, the cyclic peptomer has potential to be used as a prophylactic to prevent infections with T3SS-expressing pathogens or in combination with antibiotics to treat existing infections. The strong inhibitory effect of 4EpDN on *C. trachomatis* infection of human cells suggests the possibility of using this compound as a topical prophylactic against *Chlamydia* genital infection. Further pharmacokinetics studies will establish the stability of this and related compounds in the host, expanding the potential of the cyclic peptomers to be used as therapeutics against additional infections.

FUTURE DIRECTIONS

Given that *C. trachomatis* is an obligate intracellular pathogen that requires a functional T3SS for growth, we utilized a selection strategy to identify 4EpDN-resistant *C. trachomatis* isolates that arise over the course of passaging in the presence of 4EpDN at the MIC95. Resistant mutants will then be sequenced to identify SNPs that confer resistance to 4EpDN and these mutants will be used to map the mechanism of T3SS inhibition by 4EpDN.

We first determined the MIC of 4EpDN against *C. trachomatis* by infecting HeLa cells with *Chlamydia* in the presence of 2-fold serial dilutions of inhibitor. Infectious progeny was quantified at 48 hpi, and revealed that the MIC95 of 4EpDN was ~9 μM. To generate *C. trachomatis* mutants resistant to 4EpDN, we adopted a previously published strategy developed to isolate spontaneous drug resistant *Chlamydia* mutants (Engstrom et. al., 2014, Engstrom et. al., 2015). HeLa cells were infected with *C. trachomatis* in the presence of drug, infections were incubated for 48-60 hours (to give the bacteria the maximum amount of time to replicate), and then infectious progeny was isolated. Initial infections were performed in triplicate. We serially passaged each of the three replicates 10-20 times, and isolates were plaque purified (Nguyen and Valdivia, 2012) at passages 5, 10, 15, and 20. Clonal isolates that exhibited stable resistance were then amplified for sequencing to identify any SNPs linked with resistance. As this method relies on spontaneous mutations, we expect at most only a small number of SNPs to arise unrelated to selective pressure by the presence of the T3SS inhibitor. For example, only

a single SNP was observed in a *C. trachomatis* strain that underwent 20 passages in the absence of selection (Engstrom et al. 2014).

We have identified and isolated a mutant that exhibited increased resistance to 4EpDN by passage 10 (see Figure 4.9). As *C. trachomatis* relies on a functional T3SS to establish an intracellular replicative niche, this selection strategy will provide strong evolutionary pressure to evade the activity of 4EpDN. Mapping SNPs that confer resistance to this drug will likely provide mechanistic insight into the inhibition of T3SS by 4EpDN. In this work we have leveraged *Chlamydia's* absolute T3SS requirement to elucidate the activity of a drug with potential as a prophylactic against *Chlamydia* infection, as well as broader therapeutic potential as a potent antimicrobial.

MATERIALS AND METHODS

Bacterial strains and culture conditions.

The bacterial strains and cell lines used in this study are listed in Table 3. All cultures were grown with shaking at 250 rpm unless otherwise noted. *Y. pseudotuberculosis* was grown in 2×YT (2× yeast extract and tryptone) at 26°C overnight. To induce the T3SS, the cultures were subcultured to an optical density at 600 nm (OD600) of 0.2 into low-calcium medium (2×YT with 20 mM sodium oxalate and 20 mM MgCl2). *Y. enterocolitica* was grown in brain heart infusion (BHI) medium at 26°C overnight. The Ysc T3SS in *Y. enterocolitica* was induced using low-calcium BHI (BHI with 20 mM sodium oxalate and 20 mM MgCl2). The Ysa T3SS was induced as described previously (Young & Young, 2002) using L medium (1% tryptone, 0.5% yeast extract) with 290 mM NaCl at 26°C. *P. aeruginosa* and *S. enterica* were grown in Luria-Bertani (LB) medium overnight at 37°C. For *P. aeruginosa*, the T3SS was induced using low-calcium medium (LB with 5 mM EGTA and 20 mM MgCl2). SPI-1 T3SS secretion was assessed after subculturing into fresh LB at 37°C unless noted otherwise. *C. trachomatis* serovar L2 (LGV 434) was propagated in HeLa 229 cells. *C. trachomatis* EBs were harvested from infected cells and purified using a Renografin step-gradient as previously described (Caldwell et al., 1981). HeLa cells (ATCC) were cultured in Dulbecco's modified Eagle's medium (DMEM) with 10% fetal bovine serum (FBS). All cell lines were incubated at 37°C with 5% CO2.

Bacterial viability assay.

Overnight cultures of WT *P. aeruginosa* (PAO1) or *Y. pseudotuberculosis* were back-diluted 1:40 in LB or in 2×YT, respectively, and grown for 1.5 h at 37°C (*Pseudomonas*)

or 26°C (*Yersinia*). Then, 384-well plates were prepared with one-half final volume of medium, compounds, and 10% vol/vol resazurin-based alamarBlue high-sensitivity (HS) cell viability reagent (catalog number A50101; Invitrogen). After incubation, the cultures were centrifuged for 5 min at 14,800 rpm. Supernatant was removed, and the pellets were resuspended in medium. Cultures were then normalized to an OD600 of 0.0005 and added to the prepared 384-well plates. Plates were incubated in a plate reader (PerkinElmer Envision 2105) at 37°C (*Pseudomonas*) or room temperature (*Yersinia*), and fluorescence was measured every hour for 12 h.

Preparation of bacteria for T3SS induction.

Visualization of secreted proteins was carried out as described previously (Green & Mecsas, 2016). Briefly, *Y. pseudotuberculosis*, *P. aeruginosa*, or *S. enterica* was grown in T3SS-inducing medium (as described above) in the presence of cyclic peptomers or an equivalent volume of DMSO at 37°C for 2 h for *Y. pseudotuberculosis* Ysc T3SS, 3 h for *P. aeruginosa*, 4 h for *S. enterica*, or at 26°C for 6 h for the *Y. enterocolitica* Ysa T3SS. The cultures were normalized to bacterial density (OD600) and then centrifuged for 15 min at 14,800 rpm. The supernatants were transferred to new tubes and mixed with trichloroacetic acid (TCA) to a final volume of 10% by vortexing vigorously for 30 s. Samples were incubated on ice for 1 h and then spun down at 4°C for 15 min at 13,200 rpm. The supernatants were carefully removed, and pelleted proteins were washed with acetone and spun down at 4°C for 15 min at 13,200 rpm for a total of three washes. The pellet was then resuspended in final sample buffer (FSB) and 20% dithiothreitol (DTT) and boiled for 15 min prior to SDS-PAGE. Tween 20 was added to the

bacterial culture at the same time as the compounds in S. enterica secretion assays at 0.003% (vol/vol).

T3SS secretion cargo quantification.

Image Lab software (Bio-Rad) was used to quantify T3SS cargo protein bands relative to those of DMSO-treated controls. The WT *Y. pseudotuberculosis* YopE, *P. aeruginosa* ExoU, or *S. enterica* SipA, SipC, FliC, and FliD bands in DMSO control samples were set to 1.00. To evaluate type III secretion of ExsE in *P. aeruginosa*, Western blotting against T3SS cargo was carried out using a polyvinylidene difluoride (PVDF) membrane (Millipore). Prior to blocking, membranes were incubated with acetone at 4°C for 30 min with gentle shaking. Membranes were then moved to Tris-buffered saline with 0.1% Tween 20 (TBST) and heated to 50°C for 30 min. Blots were blocked in 2.5% nonfat milk for 1 h at room temperature and incubated with anti-ExsE at 4°C overnight with gentle shaking. Blots were washed three times for 5 min each in TBST. Horseradish peroxidase conjugated secondary antibody was then incubated for 1 h at room temperature. Signals were detected with a luminol kit (catalog number sc-2048; Santa Cruz Biotechnology, Inc.) after washing. ExsE, BSA, RpoA, and SipC were visualized with anti-ExsE antibody (courtesy of Timothy Yahr) (20% tris-tricine gel), anti-BSA (catalog number 2A3E6; Santa Cruz Biotechnology, Inc.), anti-RpoA (gift from Melanie Marketon) (7.5% tris-glycine gel), and anti-SipC (catalog number ABIN335178; Antibodies-online, Inc.) (10% tris-glycine gel), respectively.

YscD visualization assay.

Y. enterocolitica expressing YscD-EGFP was cultured overnight in BHI supplemented with nalidixic acid (35 μg/ml) and diaminopimelic acid (80 μg/ml) at 26°C with shaking (12), followed by subculturing into low-calcium BHI medium (20 mM NaOX, 20 mM MgCl2, 0.4% glycerol) with nalidixic acid and diaminopimelic acid to an OD600 of 0.2 for 1.5 h. Compounds or an equivalent volume of DMSO was added prior to inducing the T3SS. After 3 h at 37°C with shaking, cells were pelleted and resuspended in M9 medium supplemented with diaminopimelic acid, and compounds, spotted onto a 0.1% agarose pad supplemented with diaminopimelic acid and compounds and imaged live at ×63/1.4 oil magnification using a Zeiss AxioImager widefield microscope. Analysis of YscD puncta was carried out in Imaris 8 using spot tracking analysis with the same arbitrary threshold to call bacterial cells and puncta for all samples. Samples were prepared blinded, and each sample was imaged at the same 10 selected views covering the entire sample.

YscF needle staining assay.

Y. pseudotuberculosis was cultured, and the T3SS was induced as described above. Compounds or an equivalent volume of DMSO was added prior to inducing the T3SS. Cells were fixed by mixing 500 μl of bacterial culture with 800 μl 4% paraformaldehyde (PFA), 1 μl of 25% gluteraldehyde, and 40 μl of 0.5 M sodium phosphate. The mixture was gently inverted repeatedly to mix and left at room temperature for 15 min before being moved to ice for an additional 30 min. Cells were pelleted gently at 5,000 × g for 3 min at 4°C. Pellets were gently resuspended and washed with ice-cold phosphate-buffered saline (PBS) for a total of three times. The final pellet was resuspended in GTE buffer

(50 mM glucose, 25 mM Tris base, pH 8.0, and 10 mM EDTA). Cells were spotted and spread onto a coverslip and allowed to partially dry. Then, 1% bovine serum albumin (BSA) in phosphate-buffered saline with 0.1% Tween 20 (PBST) was added to the coverslips and left overnight, gently shaking at 4°C. The BSA/PBST block was removed, and anti-YscF antibody was diluted in 1% BSA/PBST and added to the coverslips. Coverslips were incubated with anti-YscF antibody for 4 h at 4°C while gently shaking. Anti-YscF antibody was removed, and coverslips were washed with PBST three times for 5 min each. mCherry-tagged secondary antibody was diluted in 1% BSA/PBST, added to the coverslips, and incubated in the dark at 4°C for 2 h while gently shaking. Secondary antibody was removed, and coverslips were washed with PBST three times for 5 min each. Hoescht 33342 (Thermo Fisher Scientific) was diluted in PBST, added to the coverslips, and incubated in the dark for 20 min at room temperature while gently shaking. Hoescht stain was washed away by washing the coverslips 3 times with PBST for 5 min each. Coverslips were mounted to slides using ProLong Gold (Life Technologies). Slides were imaged at ×63/1.4 oil magnification using a Zeiss AxioImager widefield microscope. Analysis of YscF puncta was carried out in Imaris 8 using spot tracking analysis with the same arbitrary threshold to call bacterial cells and puncta for all samples. Analysis was performed in batches for all conditions within a replicate.

mRNA quantification by qPCR.

Overnight *P. aeruginosa* (PA103 or PAO1) cultures were subcultured and shifted to T3SS-inducing conditions (see above) in the presence of 60 μM 1EpDN, 60 μM 1EpDN 2Sar, or 50 μM MBX1641. Samples were taken after 3 h of induction. Overnight

Salmonella cultures were subcultured into fresh LB with 0.3 M NaCl at 37°C in the presence of 9 μM 4EpDN, 4EpDN 2Sar, or equivalent DMSO. Samples were taken after 2 h and 4 h of induction. Samples were stored in RNAprotect reagent (Qiagen) and processed within a week. Total RNA was isolated using an RNAeasy kit (Qiagen) according to the manufacturer's instructions, followed by two rounds of Turbo DNase (Thermo Fisher scientific) treatment. A total of 2 μg of RNA was used to make cDNA, and quantitative PCRs (qPCRs) were run with SYBR green PCR master mix (Applied Biosystems). DNA helicase (dnaB) and 16S rRNA genes were used as a reference for *P. aeruginosa* and *Salmonella* samples, respectively. Two to three technical replicates were averaged for each sample. The primers used are listed in Table S2. Results were analyzed using Bio-Rad CFX software.

Tat assay.

To make Tat targeting constructs, plasmid pMMB67EH (ATCC 37622) was digested with KpnI. TEM1 of β-lactamase was PCR-amplified from yopH-Bla (courtesy of Melanie Marketon) using primers oHL210 and oHL217 (Table S2), and sufI signal peptide DNA was PCR-amplified from genomic DNA of *Y. pseudotuberculosis* with primers oHL218 and oHL219 (Table S2). The digested pMMB67EH, TEM1, and sufI signal peptide DNA were assembled into a plasmid (sufI-Bla) using Gibson assembly.

WT *Yersinia* or tatB::Tn carrying sufI-Bla was grown in 2×YT supplemented with 15 μg/ml gentamicin at 26°C with shaking. Overnight cultures were subcultured to an OD600 of 0.1 and grown for 1.5 h at 26°C with shaking. Then, 5 mM IPTG was added to the culture for

0.5 h to allow for expression and translocation of SufI-Bla. Penicillin G (25 µg/ml) was added to the cultures. Cultures were then treated with cyclic peptomers or DMSO, and the OD600 was measured every hour up to 8 h.

Chlamydia infection and imaging.

Primary infections. HeLa cell monolayers were infected with C. trachomatis serovar L2 at a multiplicity of infection (MOI) of 1.0 in the presence of one of the following compounds at 9 µM: DMSO, 4EpDN, or 4EpDN 2Sar. Cells were incubated for 24 h in the presence of the above-listed compounds at 37°C and then fixed with 4% paraformaldehyde (PFA). Cells were stained for IncA (Chlamydia inclusion membrane marker), DNA (with DAPI), and MOMP (Chlamydia major outer membrane protein) simultaneously. This method of staining allows visualization of the inclusion independent of MOMP synthesis or transport. The percentage of cells infected (i.e., stained positively for the listed Chlamydia markers) in the presence of the compounds was quantified using confocal microscopy. Quantifications of inclusion take into account both DAPI staining and indirect immunofluoresence with an antibody to MOMP. Ten randomly selected fields of view were measured per experiment. The data represent three biological replicates.

Secondary infections. HeLa cell monolayers were infected with *C. trachomatis* serovar L2 at an MOI of 1.0 in the presence of one of the following compounds at 9 µM: DMSO, 4EpDN, or 4EpDN 2Sar. Cells were incubated for 48 h in the presence of the above-listed compounds at 37°C. Infected cells were then lysed, and the lysate was applied to fresh HeLa monolayers to enumerate infectious particles. These secondary infections were

fixed in 4% PFA at 24 hpi and were stained against MOMP and DNA. The infectious units per ml (IFU/ml) were calculated by averaging the number of infected cells in each of 10 randomly selected fields of view at ×40 magnification on a confocal microscope and multiplying this by the appropriate dilution and area factors. The data represent four biological replicates.

Cytological profiling (CP).

Briefly, HeLa cells were cultured and seeded into 384-well plates at 2,500 cells/well. After 48 h, compounds were added using a Janus MDT robot (PerkinElmer). Two stain sets were used—stain set 1, Hoechst, EdUrhodamine, anti-phosphohistone H3, and GM130; stain set 2, Hoechst, fluorescein isothiocyanate (FITC)-alpha tubulin, rhodamine-phalloidin, and calnexin. For stain set 1, cells were incubated with 20 μM EdUrhodamine for 1 h prior to fixing in 4% formaldehyde solution in PBS for 20 min. Cells were then washed with PBS and permeabilized with 0.5% Triton X-100 in PBS for 10 min before blocking with 2% BSA in PBS solution for at least 1 h. Following this, cells were incubated with primary antibodies overnight at 4°C. The following day, excess primary antibody was washed off with PBS and Alexa-488, and Alexa-647 secondary antibodies and Hoechst solution were incubated for 1 h. Plates were washed with PBS and preserved with 0.1% sodium azide in PBS solution prior to imaging. For stain set 2, cells were fixed with a 4% formaldehyde solution in PBS for 20 min. Cells were then washed with PBS and permeabilized with 0.5% Triton X-100 in PBS for 10 min before blocking with 2% BSA in PBS solution for at least 1 h. Following this, cells were incubated with primary antibodies overnight at 4°C. After blocking, the cells were washed and then incubated with FITC

conjugated anti-alpha tubulin antibody and rhodamine-phalloidin overnight at 4°C. The following day, the cells were washed and then incubated with secondary Alexa-647 and Hoechst stain for 1 h. Plates were washed with PBS and preserved with 0.1% sodium azide in PBS solution prior to imaging.

Two images per well were captured with an ImageXpress Micro XLS automated epiflourescent microscope (Molecular Devices). Images were then processed as described in Woehrmann et al., 2013. Briefly, initial image processing was performed using MetaXpress image analysis software, using built-in morphometry metrics, the multiwavelength cell scoring, transfluor, and micronuclei modules. Custom-written scripts were used to compare the treated samples with the DMSO control wells and then to convert each feature to a histogram difference (HD) score. This produced a 452-feature vector CP fingerprint. Compound treatment wells were labeled as dead if the cell count for the treatment well was <10% of the median cell count in the treatment plate. In addition to the CP fingerprint, feature cell counts (nuclei, EdU S-phase, and phospho-histone H3) were used to determine the effects of compounds on HeLa cell replication.

Synthesis of cyclic peptomers.

Peptides were synthesized using standard Fmoc solid-phase peptide synthesis, utilizing the submonomer approach for peptoid synthesis (Zuckermann et al., 1992), either at room temperature or with microwave assistance. Cyclization was done in solution at a high dilution. Fmoc-Xaa (10 mmol) was added to a flame-dried round-bottomed flask and dried in a vacuum desiccator with phosphorous pentoxide overnight. Then, 50 ml of dry

dichloromethane (DCM) was cannula-transferred into the flask, followed by 2.5 ml of N,N-diisopropylethylamine (DIPEA) transferred via syringe. After sonication for 10 min, 5 g of 2-chlorotrityl resin was added under a stream of nitrogen and allowed to shake for 4 h. The resin was capped with a 15-ml solution of 1:2:17 methanol (MeOH):DIPEA:dimethylformamide (DMF) (3 times for 15 min each). The resin was washed with DMF (3 times with 15 ml each) followed by DCM (3 times with 15 ml each). The loading value was calculated by determining the mass increase of dried, loaded resin.

Amino acid coupling at room temperature.

Four equivalents (eq) of Fmoc-Xaa, 8 eq of DIPEA, and 4 eq of 1-[Bis(dimethylamino)methylene]-1H-1,2,3-triazolo[4,5-b]pyridinium 3-oxide hexafluorophosphate, hexafluorophosphate azabenzotriazole tetramethyl uronium (HATU) were added to the resin in DMF. The reaction mixture was agitated via shaking for 45 min and then drained. The resin was washed with DMF (3 times with 3 ml each) and DCM (3 times with 3 ml each). The reaction was monitored by liquid chromatography-mass spectrometry (LC-MS) and repeated until the starting material was no longer observed. For microwave conditions, a solution of 4 eq of Fmoc-Xaa, 4 eq of HATU, and 6 eq of DIPEA in DMF was allowed to pre-react for 5 min. This solution was added to the deprotected peptide on-resin and allowed to react for 10 min at 50°C under microwave heating. The solution was drained, and the resin was washed with DMF (3 times with 3 ml each) and DCM (3 times with 3 ml each). The reaction was monitored by LC-MS and repeated until the starting material was no longer observed.

Coupling of BrAcOH at room temperature.

A solution of 10 eq of bromoacetic acid (BrAcOH) and 5 eq of N,N-diisopropylcarbodiimide (DIC) in DMF was allowed to prereact for 10 min. This solution was added to the deprotected peptide on-resin. The reaction mixture was agitated via shaking for 45 min and then drained. The resin was washed with DMF (3 times with 3 ml each) and DCM (3 times with 3 ml each). The reaction was monitored by LC-MS and repeated until the starting material was no longer observed. The reaction was monitored by LC-MS and repeated until the starting material was no longer observed.

Peptoid side chain addition.

A solution of 5 eq of the desired amine was prepared in a minimum volume of DMF. The resin containing the BrAc-peptide was swollen with DCM for 5 min prior to reaction. The amine was added, and the reaction mixture was agitated via shaking for 3 to 20 h. The solution was drained, and the resin was washed with DMF (3 times with 3 ml each) and DCM (3 times with 3 ml each). The reaction was monitored by LC-MS and repeated until the starting material was no longer observed.

Removal of the N-Fmoc protection group at room temperature.

A solution of 2% piperidine and 2% 1,8-diazabicyclo[5.4.0]undec-7-ene (DBU) in DMF was added to the resin. The reaction mixture was agitated via shaking for 20 min and then drained. The resin was washed with DMF (3 times with 3 ml each) and DCM (3 times with 3 ml each). For microwave conditions, a solution of 2% piperidine and 2% DBU in DMF was added to the resin. The reaction mixture was allowed to react for 5 min at 50°C under

microwave heating and then drained. The resin was washed with DMF (3 times with 3 ml each) and DCM (3 times with 3 ml each).

Peptide cleavage.

Complete linear peptides were cleaved off the resin in 5 resin volumes of 2.5% trifluoroacetic acid (TFA) in DCM for 4 min, three times, with a 5-resin-volume DCM wash between steps. Solvent was removed under N2, followed by dissolution in acetone or DCM and evaporation under reduced pressure. Residual TFA was removed in vacuo overnight.

Cyclization with COMU.

Linear peptides were dissolved in 20 ml of dry acetonitrile (ACN) with 4 eq of DIPEA and added dropwise (final concentration, 1 mg crude peptide per ml) to a solution of 1:1 tetrahydrofuran (THF)-ACN containing 2 eq of (1-cyano-2 ethoxy-2 oxoethylidenaminooxy) dimethylamino-morpholinocarbenium hexafluorophosphate (COMU). Reaction mixtures were stirred for 0.5 to 24 h, until complete cyclization was achieved as monitored by LC-MS. The reaction mixture was reduced in vacuo for purification via high pressure liquid chromatography (HPLC).

Purification of peptides.

COMU by-products were removed after solution-phase cyclization on a Biotage Isolera Prime system equipped with a SNAP Ultra-C18 30-g column eluting with H2O-acetonitrile

modified with 0.1% TFA. The mass spectra of all peptides are shown in Figure S4.9 in the supplemental material.

Proton NMR of peptides.

Peptides were analyzed through nuclear magnetic resonance (NMR) spectroscopy measured in ppm and were obtained on a 500-MHz spectrometer using CDCl3 (δ = 7.26) as an internal standard for 1H-NMR. Identity of compounds for SAR study was confirmed by LCMS and 1H-NMR (Figure S4.9).

Kinetic solubility.

A 15 mM stock of the compounds in DMSO was prepared, and 125 µl of M9 and DMEM (no antibiotics) was dispensed into a 96-well v-bottom plate. Then, 1 ml of 15 mM stock compound was added to make a solution of 120 µM final concentration with 0.8% DMSO. The solution was shaken at 37°C for ~2 h. The solution was passed over a 0.7- µM glass fiber filter. Then, the solution was diluted 1:4 in acetonitrile to crash out any proteins. The solution was centrifuged at 500 × g for 10 min. Avoiding the pellet, 10 µl of supernatant was added to a fresh plate with 90 µl of acetonitrile. The final dilution is 40 times lower. Next, 10 µl of 40× dilution of solution was injected on the Orbi-trap. A 1 µM standard was used for the ratiometric comparison, and the assay was done in triplicate.

Cyclic peptide manipulation.

Stock peptides were stored at 15 mM at −70°C. All treatment and control pairs, in all assays, had the same DMSO volumes. The compounds were prediluted in DMSO prior

to experiments for lower concentrations when they were performed in conjunction with higher concentration treatment to maintain the same volume of DMSO.

Statistical analysis.

Prism 9 (GraphPad Software, La Jolla, CA, USA) was used to calculate the mean, standard error of the mean, median, standard error of median, and one-way analysis of variance (ANOVA) values shown.

Using *C. trachomatis* to identify mutants resistant to 4EpDN.

We first assessed the MIC95 of 4EpDN on *C. trachomatis* re-infection. HeLa cells were grown in 96-well plates and infected at an MOI of 1. A two-fold serial dilution of 4EpDN was added to appropriate wells coincident with the addition of bacteria. Infectious progeny were quantified at 48 hpi using standard methods employed by the Engel lab (secondary infection of HeLa cells in the absence of 4EpDN followed by quantitation of number of vacuoles per cell as determined by indirect immunofluorescence (Mirrashidi et. al., 2015). The MIC95 was determined to be ~ 9μM of 4EpDN. To then select for *C. trachomatis* mutants resistant to 4EpDN, approximately $1x10^7$ HeLa cells were seeded in each of three T75 flasks (each flask is a biological replicate for the selection assay and resulting mutants from each replicate were not mixed). Each 85% confluent flask was infected with $1x10^8$ Rifampin-resistant *C. trachomatis* EBs (generously provided by R. Valdivia, Duke University) in the presence of 9 μM 4EpDN. Infected cells were incubated at 37°C, 5% CO_2 for 48 hours before being osmotically lysed in ddH_2O. Flasks were washed once quickly in 3mL ddH_2O, and were then incubated 10 minutes at 37°C, 5% CO_2 in 3mL

ddH_2O. Water lysed seed (P0 seed) was concentrated by centrifugation at 13,000 RPM for 15 minutes at 4°C, and resuspended in 1X SPG (Caldwell et. al., 1981). 90% of seed was used to infect fresh HeLa monolayers seeded in a 6-well plates to enable centrifugation of bacteria (in the presence of 9 μM 4pDN) onto cells. 10% of seed was preserved at -80°C. Infections were incubated at 37°C, 5% CO_2 for 48-60 hpi. EBs were then harvested through osmotic lysis (200μl of ddH_2O per well; P1 seed) and used to infect another HeLa monolayer in a 6-well plate. EBs were passaged in the presence of 9 μM 4EpDN at least 20 times. At P5, P10, P15, and P20, 15% of seed was used to plaque purify clonal mutant populations which were then reassessed for MIC95 to determine if they were resistant to 4EpDN compared to the parental *C. trachomatis* EBs.

Plaque purification.

Vero cells (ATCC; cultured in DMEM supplemented with 10% FBS) seeded in 6-well plates were infected with ~100 IFUs/well from each passage of EBs and, at 2 hpi, overlaid with DMEM/agarose (0.5% SeaKem LE agarose [Lonza], 1 DMEM, 10% FBS, 9 μM 4EpDN, 1X nonessential amino acids [GIBCO], 200 ng/ml cycloheximide [Sigma-Aldrich]). At 7–10 dpi, bacteria from small plaques were harvested and expanded in HeLa cells in the presence of 4EpDN.

Whole genome sequencing.

HeLa cells in 6-well plates were infected with each isolated strain exhibiting increased resistance to 4EpDN. At time of harvest, EBs were concentrated from cell lysates by centrifugation (21,000 x g, 5 min, 4°C) and resuspended in DNase I reaction buffer (NEB).

Residual host DNA was digested with 8 units of DNase I (NEB) for 1 hr at 37°C, and EBs were washed with PBS, pelleted, and resuspended in 180 ml of ATL buffer (QIAGEN). Total DNA was isolated with a QIAGEN DNeasy Blood and Tissue Kit (QIAGEN). A total of 2-25 ng/µl (collected in >15 µl of Buffer EB; QIAGEN) of total DNA was isolated from each resistant mutant, as well as from the parental *C. trachomatis* strain. Samples were shipped on cold-packs to the UC Davis Sequencing core. Samples were sequenced as a spike in on an Illumina MiSeq run with PE300 reads. Genomes were assembled to the published C. trachomatis L2 (434/Bu) genome (AM884176) and variants were identified using GATK (Broad Institute) and/or SPAdes (Center for Algorithmetric Biotechnology).

For Characterization of cyclic peptomers, including drawn structures, SMILE structures, molecular weight, LCMS Spectra, and 1H-NMR Spectra are shown, please see full supplemental material found at https://doi.org/10.1128/AAC.01690-20; and https://journals.asm.org/doi/suppl/10.1128/AAC.01690-20/suppl_file/aac.01690-20-s0001.pdf

Supplemental tables can be accessed online through ProQuest and include:

Table 4.1. Compounds synthesized and used in this study.

Table 4.2. Efficacy of cyclic peptomers and other type III secretion system inhibitors.

Table 4.3. Bacterial strains used in this study.

Table S4.1. Solubility of cyclic peptomers.

Table S4.2. Primers used in this study.

ACKNOWLEDGEMENTS

The authors acknowledge the National Institutes of Health grant R01AI141511 (to V.A. and R.S.L.) and K99AI139281 (to H.N.L.) for support. We thank Benjamin Abrams (University of California, Santa Cruz) for technical support on the YscD spot tracking analysis. We thank Timothy Yahr for the anti-ExsE antibody. We thank Anita Sil (University of California, San Francisco) for the use of her confocal microscope. We thank Raphael Valdivia (Duke University, North Carolina) for generously sharing Rif^R *C. trachomatis* L2. We thank Patrik Engstrom (University of California, Berkeley) for his advice and guidance in designing the selection assay to identify *C. trachomatis* mutants resistant to 4EpDN.

REFERENCES

Abby, S. S., & Rocha, E. P. C. (2012). The Non-Flagellar Type III Secretion System Evolved from the Bacterial Flagellum and Diversified into Host-Cell Adapted Systems. PLoS Genetics, 8(9), e1002983. https://doi.org/10.1371/journal.pgen.1002983

Aiello, D., Williams, J. D., Majgier-Baranowska, H., Patel, I., Peet, N. P., Huang, J., Lory, S., Bowlin, T. L., & Moir, D. T. (2010). Discovery and characterization of inhibitors of Pseudomonas aeruginosa type III secretion. Antimicrobial Agents and Chemotherapy, 54(5), 1988–1999. https://doi.org/10.1128/AAC.01598-09

Al-Zeer, M. A., Al-Younes, H. M., Kerr, M., Abu-Lubad, M., Gonzalez, E., Brinkmann, V., & Meyer, T. F. (2014). Chlamydia trachomatis remodels stable microtubules to coordinate Golgi stack recruitment to the chlamydial inclusion surface. Molecular Microbiology, 94(6), 1285–1297. https://doi.org/10.1111/mmi.12829

Anantharajah, A., Buyck, J. M., Sundin, C., Tulkens, P. M., Mingeot-Leclercq, M.-P., & Van Bambeke, F. (2017). Salicylidene Acylhydrazides and Hydroxyquinolines Act as Inhibitors of Type Three Secretion Systems in Pseudomonas aeruginosa by Distinct Mechanisms. Antimicrobial Agents and Chemotherapy, 61(6), e02566-16. https://doi.org/10.1128/AAC.02566-16

Anantharajah, A., Faure, E., Buyck, J. M., Sundin, C., Lindmark, T., Mecsas, J., Yahr, T. L., Tulkens, P. M., Mingeot-Leclercq, M.-P., Guery, B., & Van Bambeke, F. (2016). Inhibition of the Injectisome and Flagellar Type III Secretion Systems by INP1855 Impairs Pseudomonas aeruginosa Pathogenicity and Inflammasome Activation.

The Journal of Infectious Diseases, 214(7), 1105–1116. https://doi.org/10.1093/infdis/jiw295

Auvray, F., Ozin, A. J., Claret, L., & Hughes, C. (2002). Intrinsic membrane targeting of the flagellar export ATPase FliI: Interaction with acidic phospholipids and FliH. Journal of Molecular Biology, 318(4), 941–950. https://doi.org/10.1016/S0022-2836(02)00172-9

Avican, U., Doruk, T., Östberg, Y., Fahlgren, A., & Forsberg, Å. (2017). The Tat Substrate SufI Is Critical for the Ability of Yersinia pseudotuberculosis To Cause Systemic Infection. Infection and Immunity, 85(4), e00867-16. https://doi.org/10.1128/IAI.00867-16

Bageshwar, U. K., VerPlank, L., Baker, D., Dong, W., Hamsanathan, S., Whitaker, N., Sacchettini, J. C., & Musser, S. M. (2016). High Throughput Screen for Escherichia coli Twin Arginine Translocation (Tat) Inhibitors. PloS One, 11(2), e0149659. https://doi.org/10.1371/journal.pone.0149659

Bent, Z. W., Branda, S. S., & Young, G. M. (2013). The Yersinia enterocolitica Ysa type III secretion system is expressed during infections both in vitro and in vivo. MicrobiologyOpen, 2(6), 962–975. https://doi.org/10.1002/mbo3.136

Bergman, T., Håkansson, S., Forsberg, A., Norlander, L., Macellaro, A., Bäckman, A., Bölin, I., & Wolf-Watz, H. (1991). Analysis of the V antigen lcrGVH-yopBD operon of Yersinia pseudotuberculosis: Evidence for a regulatory role of LcrH and LcrV. Journal of Bacteriology, 173(5), 1607–1616. https://doi.org/10.1128/jb.173.5.1607-1616.1991

Bliska, J. B., Guan, K. L., Dixon, J. E., & Falkow, S. (1991). Tyrosine phosphate hydrolysis of host proteins by an essential Yersinia virulence determinant. Proceedings of the National Academy of Sciences of the United States of America, 88(4), 1187–1191. https://doi.org/10.1073/pnas.88.4.1187

Bowlin, N. O., Williams, J. D., Knoten, C. A., Torhan, M. C., Tashjian, T. F., Li, B., Aiello, D., Mecsas, J., Hauser, A. R., Peet, N. P., Bowlin, T. L., & Moir, D. T. (2014). Mutations in the Pseudomonas aeruginosa needle protein gene pscF confer resistance to phenoxyacetamide inhibitors of the type III secretion system. Antimicrobial Agents and Chemotherapy, 58(4), 2211–2220. https://doi.org/10.1128/AAC.02795-13

Bzdzion, L., Krezel, H., Wrzeszcz, K., Grzegorek, I., Nowinska, K., Chodaczek, G., & Swietnicki, W. (2017). Design of small molecule inhibitors of type III secretion system ATPase EscN from enteropathogenic Escherichia coli. Acta Biochimica Polonica, 64(1), 49–63. https://doi.org/10.18388/abp.2016_1265

Caldwell, H. D., Kromhout, J., & Schachter, J. (1981). Purification and partial characterization of the major outer membrane protein of Chlamydia trachomatis. Infection and Immunity, 31(3), 1161–1176. https://doi.org/10.1128/iai.31.3.1161-1176.1981

Calvert, M. B., Jumde, V. R., & Titz, A. (2018). Pathoblockers or antivirulence drugs as a new option for the treatment of bacterial infections. Beilstein Journal of Organic Chemistry, 14, 2607–2617. https://doi.org/10.3762/bjoc.14.239

Choi, W.-S., Lee, T. H., Son, S. J., Kim, T. G., Kwon, B.-M., Son, H.-U., Kim, S. U., & Lee, S.-H. (2017). Inhibitory effect of obovatol from Magnolia obovata on the Salmonella

type III secretion system. The Journal of Antibiotics, 70(11), 1065–1069. https://doi.org/10.1038/ja.2017.98

Deng, W., Marshall, N. C., Rowland, J. L., McCoy, J. M., Worrall, L. J., Santos, A. S., Strynadka, N. C. J., & Finlay, B. B. (2017). Assembly, structure, function and regulation of type III secretion systems. Nature Reviews. Microbiology, 15(6), 323–337. https://doi.org/10.1038/nrmicro.2017.20

Derré, I. (2015). Chlamydiae interaction with the endoplasmic reticulum: Contact, function and consequences. Cellular Microbiology, 17(7), 959–966. https://doi.org/10.1111/cmi.12455

Diepold, A. (2019). Assembly and Post-assembly Turnover and Dynamics in the Type III Secretion System. In S. Wagner & J. E. Galan (Eds.), Bacterial Type III Protein Secretion Systems (Vol. 427, pp. 35–66). Springer International Publishing. https://doi.org/10.1007/82_2019_164

Diepold, A., Amstutz, M., Abel, S., Sorg, I., Jenal, U., & Cornelis, G. R. (2010). Deciphering the assembly of the Yersinia type III secretion injectisome. The EMBO Journal, 29(11), 1928–1940. https://doi.org/10.1038/emboj.2010.84

Diepold, A., & Armitage, J. P. (2015). Type III secretion systems: The bacterial flagellum and the injectisome. Philosophical Transactions of the Royal Society of London. Series B, Biological Sciences, 370(1679), 20150020. https://doi.org/10.1098/rstb.2015.0020

Diepold, A., Sezgin, E., Huseyin, M., Mortimer, T., Eggeling, C., & Armitage, J. P. (2017). A dynamic and adaptive network of cytosolic interactions governs protein export

by the T3SS injectisome. Nature Communications, 8, 15940. https://doi.org/10.1038/ncomms15940

Diepold, A., & Wagner, S. (2014). Assembly of the bacterial type III secretion machinery. FEMS Microbiology Reviews, 38(4), 802–822. https://doi.org/10.1111/1574-6976.12061

Diepold, A., Wiesand, U., Amstutz, M., & Cornelis, G. R. (2012). Assembly of the Yersinia injectisome: The missing pieces. Molecular Microbiology, 85(5), 878–892. https://doi.org/10.1111/j.1365-2958.2012.08146.x

Diepold, A., Wiesand, U., & Cornelis, G. R. (2011). The assembly of the export apparatus (YscR,S,T,U,V) of the Yersinia type III secretion apparatus occurs independently of other structural components and involves the formation of an YscV oligomer. Molecular Microbiology, 82(2), 502–514. https://doi.org/10.1111/j.1365-2958.2011.07830.x

DiGiandomenico, A., Keller, A. E., Gao, C., Rainey, G. J., Warrener, P., Camara, M. M., Bonnell, J., Fleming, R., Bezabeh, B., Dimasi, N., Sellman, B. R., Hilliard, J., Guenther, C. M., Datta, V., Zhao, W., Gao, C., Yu, X.-Q., Suzich, J. A., & Stover, C. K. (2014). A multifunctional bispecific antibody protects against Pseudomonas aeruginosa. Science Translational Medicine, 6(262), 262ra155. https://doi.org/10.1126/scitranslmed.3009655

Duncan, M. C., Linington, R. G., & Auerbuch, V. (2012). Chemical Inhibitors of the Type Three Secretion System: Disarming Bacterial Pathogens. Antimicrobial Agents and Chemotherapy, 56(11), 5433–5441. https://doi.org/10.1128/AAC.00975-12

Duncan, M. C., Wong, W. R., Dupzyk, A. J., Bray, W. M., Linington, R. G., & Auerbuch, V. (2014). An NF-κB-based high-throughput screen identifies piericidins as inhibitors of the Yersinia pseudotuberculosis type III secretion system. Antimicrobial Agents and Chemotherapy, 58(2), 1118–1126. https://doi.org/10.1128/AAC.02025-13

Elwell, C., Mirrashidi, K., & Engel, J. (2016). Chlamydia cell biology and pathogenesis. Nature Reviews. Microbiology, 14(6), 385–400. https://doi.org/10.1038/nrmicro.2016.30

Engström, P., Krishnan, K. S., Ngyuen, B. D., Chorell, E., Normark, J., Silver, J., Bastidas, R. J., Welch, M. D., Hultgren, S. J., Wolf-Watz, H., Valdivia, R. H., Almqvist, F., & Bergström, S. (2015). A 2-Pyridone-Amide Inhibitor Targets the Glucose Metabolism Pathway of Chlamydia trachomatis. MBio, 6(1). https://doi.org/10.1128/mBio.02304-14

Engström, P., Nguyen, B. D., Normark, J., Nilsson, I., Bastidas, R. J., Gylfe, A., Elofsson, M., Fields, K. A., Valdivia, R. H., Wolf-Watz, H., & Bergström, S. (2013). Mutations in hemG mediate resistance to salicylidene acylhydrazides, demonstrating a novel link between protoporphyrinogen oxidase (HemG) and Chlamydia trachomatis infectivity. Journal of Bacteriology, 195(18), 4221–4230. https://doi.org/10.1128/JB.00506-13

Enquist, P.-A., Gylfe, A., Hägglund, U., Lindström, P., Norberg-Scherman, H., Sundin, C., & Elofsson, M. (2012). Derivatives of 8-hydroxyquinoline—Antibacterial agents that target intra- and extracellular Gram-negative pathogens. Bioorganic &

Medicinal Chemistry Letters, 22(10), 3550–3553. https://doi.org/10.1016/j.bmcl.2012.03.096

Fasciano, A. C., Shaban, L., & Mecsas, J. (2019). Promises and Challenges of the Type Three Secretion System Injectisome as an Antivirulence Target. EcoSal Plus, 8(2), ecosalplus.ESP-0032-2018. https://doi.org/10.1128/ecosalplus.ESP-0032-2018

Felise, H. B., Nguyen, H. V., Pfuetzner, R. A., Barry, K. C., Jackson, S. R., Blanc, M.-P., Bronstein, P. A., Kline, T., & Miller, S. I. (2008). An inhibitor of gram-negative bacterial virulence protein secretion. Cell Host & Microbe, 4(4), 325–336. https://doi.org/10.1016/j.chom.2008.08.001

Gauthier, A., Robertson, M. L., Lowden, M., Ibarra, J. A., Puente, J. L., & Finlay, B. B. (2005). Transcriptional inhibitor of virulence factors in enteropathogenic Escherichia coli. Antimicrobial Agents and Chemotherapy, 49(10), 4101–4109. https://doi.org/10.1128/AAC.49.10.4101-4109.2005

Gophna, U., Ron, E. Z., & Graur, D. (2003). Bacterial type III secretion systems are ancient and evolved by multiple horizontal-transfer events. Gene, 312, 151–163. https://doi.org/10.1016/s0378-1119(03)00612-7

Green, E. R., & Mecsas, J. (2016). Bacterial Secretion Systems: An Overview. Microbiology Spectrum, 4(1). https://doi.org/10.1128/microbiolspec.VMBF-0012-2015

Grishin, A. V., Luyksaar, S. I., Kapotina, L. N., Kirsanov, D. D., Zayakin, E. S., Karyagina, A. S., & Zigangirova, N. A. (2018). Identification of chlamydial T3SS inhibitors through virtual screening against T3SS ATPase. Chemical Biology & Drug Design, 91(3), 717–727. https://doi.org/10.1111/cbdd.13130

Guo, Z., Li, X., Li, J., Yang, X., Zhou, Y., Lu, C., & Shen, Y. (2016). Licoflavonol is an inhibitor of the type three secretion system of Salmonella enterica serovar Typhimurium. Biochemical and Biophysical Research Communications, 477(4), 998–1004. https://doi.org/10.1016/j.bbrc.2016.07.018

Häcker, G. (Ed.). (2018). Biology of Chlamydia (1st ed. 2018). Springer International Publishing : Imprint: Springer. https://doi.org/10.1007/978-3-319-71232-1

Hallstrom, K. N., & McCormick, B. A. (2016). The type three secreted effector SipC regulates the trafficking of PERP during Salmonella infection. Gut Microbes, 7(2), 136–145. https://doi.org/10.1080/19490976.2015.1128626

Hao, H., Aixia, Y., Lei, F., Nancai, Y., & Wen, S. (2010). Effects of baicalin on Chlamydia trachomatis infection in vitro. Planta Medica, 76(1), 76–78. https://doi.org/10.1055/s-0029-1185943

Harmon, D. E., Davis, A. J., Castillo, C., & Mecsas, J. (2010). Identification and characterization of small-molecule inhibitors of Yop translocation in Yersinia pseudotuberculosis. Antimicrobial Agents and Chemotherapy, 54(8), 3241–3254. https://doi.org/10.1128/AAC.00364-10

Hudson, D. L., Layton, A. N., Field, T. R., Bowen, A. J., Wolf-Watz, H., Elofsson, M., Stevens, M. P., & Galyov, E. E. (2007). Inhibition of Type III Secretion in Salmonella enterica Serovar Typhimurium by Small-Molecule Inhibitors. Antimicrobial Agents and Chemotherapy, 51(7), 2631–2635. https://doi.org/10.1128/AAC.01492-06

Jessen, D. L., Bradley, D. S., & Nilles, M. L. (2014). A type III secretion system inhibitor targets YopD while revealing differential regulation of secretion in calcium-blind

mutants of Yersinia pestis. Antimicrobial Agents and Chemotherapy, 58(2), 839–850. https://doi.org/10.1128/AAC.01170-13

Kang, J. E., Jeon, B. J., Park, M. Y., & Kim, B. S. (2020). Inhibitory Activity of Sedum middendorffianum-Derived 4-Hydroxybenzoic Acid and Vanillic Acid on the Type III Secretion System of Pseudomonas syringae pv. Tomato DC3000. The Plant Pathology Journal, 36(6), 608–617. https://doi.org/10.5423/PPJ.OA.08.2020.0162

Kang, J. E., Jeon, B. J., Park, M. Y., Yang, H. J., Kwon, J., Lee, D. H., & Kim, B. S. (2020). Inhibition of the type III secretion system of Pseudomonas syringae pv. Tomato DC3000 by resveratrol oligomers identified in Vitis vinifera L. Pest Management Science, 76(7), 2294–2303. https://doi.org/10.1002/ps.5764

Kauppi, A. M., Nordfelth, R., Uvell, H., Wolf-Watz, H., & Elofsson, M. (2003). Targeting bacterial virulence: Inhibitors of type III secretion in Yersinia. Chemistry & Biology, 10(3), 241–249. https://doi.org/10.1016/s1074-5521(03)00046-2

Kim, O. K., Garrity-Ryan, L. K., Bartlett, V. J., Grier, M. C., Verma, A. K., Medjanis, G., Donatelli, J. E., Macone, A. B., Tanaka, S. K., Levy, S. B., & Alekshun, M. N. (2009). N-hydroxybenzimidazole inhibitors of the transcription factor LcrF in Yersinia: Novel antivirulence agents. Journal of Medicinal Chemistry, 52(18), 5626–5634. https://doi.org/10.1021/jm9006577

Kimura, K., Iwatsuki, M., Nagai, T., Matsumoto, A., Takahashi, Y., Shiomi, K., Omura, S., & Abe, A. (2011). A small-molecule inhibitor of the bacterial type III secretion system protects against in vivo infection with Citrobacter rodentium. The Journal of Antibiotics, 64(2), 197–203. https://doi.org/10.1038/ja.2010.155

Klöckner, A., Bühl, H., Viollier, P., & Henrichfreise, B. (2018). Deconstructing the Chlamydial Cell Wall. Current Topics in Microbiology and Immunology, 412, 1–33. https://doi.org/10.1007/82_2016_34

Krupp, K., & Madhivanan, P. (2015). Antibiotic resistance in prevalent bacterial and protozoan sexually transmitted infections. Indian Journal of Sexually Transmitted Diseases and AIDS, 36(1), 3–8. https://doi.org/10.4103/0253-7184.156680

Kudryashev, M., Stenta, M., Schmelz, S., Amstutz, M., Wiesand, U., Castaño-Díez, D., Degiacomi, M. T., Münnich, S., Bleck, C. K., Kowal, J., Diepold, A., Heinz, D. W., Dal Peraro, M., Cornelis, G. R., & Stahlberg, H. (2013). In situ structural analysis of the Yersinia enterocolitica injectisome. ELife, 2, e00792. https://doi.org/10.7554/eLife.00792

Kumar, Y., & Valdivia, R. H. (2008). Actin and intermediate filaments stabilize the Chlamydia trachomatis vacuole by forming dynamic structural scaffolds. Cell Host & Microbe, 4(2), 159–169. https://doi.org/10.1016/j.chom.2008.05.018

Lam, H., Schwochert, J., Lao, Y., Lau, T., Lloyd, C., Luu, J., Kooner, O., Morgan, J., Lokey, S., & Auerbuch, V. (2017). Synthetic Cyclic Peptomers as Type III Secretion System Inhibitors. Antimicrobial Agents and Chemotherapy, 61(9), e00060-17. https://doi.org/10.1128/AAC.00060-17

Lavander, M., Ericsson, S. K., Bröms, J. E., & Forsberg, A. (2006). The twin arginine translocation system is essential for virulence of Yersinia pseudotuberculosis. Infection and Immunity, 74(3), 1768–1776. https://doi.org/10.1128/IAI.74.3.1768-1776.2006

Layton, A. N., Hudson, D. L., Thompson, A., Hinton, J. C. D., Stevens, J. M., Galyov, E. E., & Stevens, M. P. (2010). Salicylidene acylhydrazide-mediated inhibition of type III secretion system-1 in Salmonella enterica serovar Typhimurium is associated with iron restriction and can be reversed by free iron. FEMS Microbiology Letters, 302(2), 114–122. https://doi.org/10.1111/j.1574-6968.2009.01847.x

Lee, P. A., Tullman-Ercek, D., & Georgiou, G. (2006). The bacterial twin-arginine translocation pathway. Annual Review of Microbiology, 60, 373–395. https://doi.org/10.1146/annurev.micro.60.080805.142212

Lee, P.-C., & Rietsch, A. (2015). Fueling type III secretion. Trends in Microbiology, 23(5), 296–300. https://doi.org/10.1016/j.tim.2015.01.012

Li, J., Lv, C., Sun, W., Li, Z., Han, X., Li, Y., & Shen, Y. (2013). Cytosporone B, an inhibitor of the type III secretion system of Salmonella enterica serovar Typhimurium. Antimicrobial Agents and Chemotherapy, 57(5), 2191–2198. https://doi.org/10.1128/AAC.02421-12

Li, J., Sun, W., Guo, Z., Lu, C., & Shen, Y. (2014). Fusaric acid modulates Type Three Secretion System of Salmonella enterica serovar Typhimurium. Biochemical and Biophysical Research Communications, 449(4), 455–459. https://doi.org/10.1016/j.bbrc.2014.05.044

Lilic, M., Galkin, V. E., Orlova, A., VanLoock, M. S., Egelman, E. H., & Stebbins, C. E. (2003). Salmonella SipA polymerizes actin by stapling filaments with nonglobular protein arms. Science (New York, N.Y.), 301(5641), 1918–1921. https://doi.org/10.1126/science.1088433

Liu, Y., Zhang, Y., Zhou, Y., Wang, T., Deng, X., Chu, X., & Zhou, T. (2019). Cinnamaldehyde inhibits type three secretion system in Salmonella enterica serovar Typhimurium by affecting the expression of key effector proteins. Veterinary Microbiology, 239, 108463. https://doi.org/10.1016/j.vetmic.2019.108463

Lv, Q., Chu, X., Yao, X., Ma, K., Zhang, Y., & Deng, X. (2019). Inhibition of the type III secretion system by syringaldehyde protects mice from Salmonella enterica serovar Typhimurium. Journal of Cellular and Molecular Medicine, 23(7), 4679–4688. https://doi.org/10.1111/jcmm.14354

Lv, Q., Li, S., Wei, H., Wen, Z., Wang, Y., Tang, T., Wang, J., Xia, L., & Deng, X. (2020). Identification of the natural product paeonol derived from peony bark as an inhibitor of the Salmonella enterica serovar Typhimurium type III secretion system. Applied Microbiology and Biotechnology, 104(4), 1673–1682. https://doi.org/10.1007/s00253-019-10290-7

Lv, Q., Lv, Y., Dou, X., Wassy, S. L., Jia, G., Wei, L., Yu, Q., Deng, X., Zhang, C., & Wang, J. (2021). Myricetin inhibits the type III secretion system of Salmonella enterica serovar typhimurium by downregulating the Salmonella pathogenic island I gene regulatory pathway. Microbial Pathogenesis, 150, 104695. https://doi.org/10.1016/j.micpath.2020.104695

Ma, Y.-N., Chen, L., Si, N.-G., Jiang, W.-J., Zhou, Z.-G., Liu, J.-L., & Zhang, L.-Q. (2019). Identification of Benzyloxy Carbonimidoyl Dicyanide Derivatives as Novel Type III Secretion System Inhibitors via High-Throughput Screening. Frontiers in Plant Science, 10, 1059. https://doi.org/10.3389/fpls.2019.01059

Ma, Y.-X., Wang, C.-Y., Li, Y.-Y., Li, J., Wan, Q.-Q., Chen, J.-H., Tay, F. R., & Niu, L.-N. (2020). Considerations and Caveats in Combating ESKAPE Pathogens against Nosocomial Infections. Advanced Science (Weinheim, Baden-Wurttemberg, Germany), 7(1), 1901872. https://doi.org/10.1002/advs.201901872

Matsui, H., Eguchi, M., Ohsumi, K., Nakamura, A., Isshiki, Y., Sekiya, K., Kikuchi, Y., Nagamitsu, T., Masuma, R., Sunazuka, T., & Omura, S. (2005). Azithromycin Inhibits the Formation of Flagellar Filaments without Suppressing Flagellin Synthesis in Salmonella enterica Serovar Typhimurium. Antimicrobial Agents and Chemotherapy, 49(8), 3396–3403. https://doi.org/10.1128/AAC.49.8.3396-3403.2005

McGovern, S. L., Caselli, E., Grigorieff, N., & Shoichet, B. K. (2002). A common mechanism underlying promiscuous inhibitors from virtual and high-throughput screening. Journal of Medicinal Chemistry, 45(8), 1712–1722. https://doi.org/10.1021/jm010533y

McGovern, S. L., Helfand, B. T., Feng, B., & Shoichet, B. K. (2003). A specific mechanism of nonspecific inhibition. Journal of Medicinal Chemistry, 46(20), 4265–4272. https://doi.org/10.1021/jm030266r

Miller, K. E. (2006). Diagnosis and treatment of Chlamydia trachomatis infection. American Family Physician, 73(8), 1411–1416.

Mohajeri, M. H., Brummer, R. J. M., Rastall, R. A., Weersma, R. K., Harmsen, H. J. M., Faas, M., & Eggersdorfer, M. (2018). The role of the microbiome for human health: From basic science to clinical applications. European Journal of Nutrition, 57(Suppl 1), 1–14. https://doi.org/10.1007/s00394-018-1703-4

Morgan, J. M., Lam, H. N., Delgado, J., Luu, J., Mohammadi, S., Isberg, R. R., Wang, H., & Auerbuch, V. (2018). An Experimental Pipeline for Initial Characterization of Bacterial Type III Secretion System Inhibitor Mode of Action Using Enteropathogenic Yersinia. Frontiers in Cellular and Infection Microbiology, 8, 404. https://doi.org/10.3389/fcimb.2018.00404

Muschiol, S., Bailey, L., Gylfe, A., Sundin, C., Hultenby, K., Bergström, S., Elofsson, M., Wolf-Watz, H., Normark, S., & Henriques-Normark, B. (2006). A small-molecule inhibitor of type III secretion inhibits different stages of the infectious cycle of Chlamydia trachomatis. Proceedings of the National Academy of Sciences of the United States of America, 103(39), 14566–14571. https://doi.org/10.1073/pnas.0606412103

Nakasone, N., Higa, N., Toma, C., Ogura, Y., Suzuki, T., & Yamashiro, T. (2017). Epigallocatechin gallate inhibits the type III secretion system of Gram-negative enteropathogenic bacteria under model conditions. FEMS Microbiology Letters, 364(13). https://doi.org/10.1093/femsle/fnx111

Nesterenko, L. N., Zigangirova, N. A., Zayakin, E. S., Luyksaar, S. I., Kobets, N. V., Balunets, D. V., Shabalina, L. A., Bolshakova, T. N., Dobrynina, O. Y., & Gintsburg, A. L. (2016). A small-molecule compound belonging to a class of 2,4-disubstituted 1,3,4-thiadiazine-5-ones suppresses Salmonella infection in vivo. The Journal of Antibiotics, 69(6), 422–427. https://doi.org/10.1038/ja.2015.131

Nguyen, B. D., & Valdivia, R. H. (2012). Virulence determinants in the obligate intracellular pathogen Chlamydia trachomatis revealed by forward genetic

approaches. Proceedings of the National Academy of Sciences of the United States of America, 109(4), 1263–1268. https://doi.org/10.1073/pnas.1117884109

Nordfelth, R., Kauppi, A. M., Norberg, H. A., Wolf-Watz, H., & Elofsson, M. (2005). Small-molecule inhibitors specifically targeting type III secretion. Infection and Immunity, 73(5), 3104–3114. https://doi.org/10.1128/IAI.73.5.3104-3114.2005

Paul, K., Erhardt, M., Hirano, T., Blair, D. F., & Hughes, K. T. (2008). Energy source of flagellar type III secretion. Nature, 451(7177), 489–492. https://doi.org/10.1038/nature06497

Pendergrass, H. A., Johnson, A. L., Hotinger, J. A., & May, A. E. (2020). Fluorescence Detection of Type III Secretion Using a Glu-CyFur Reporter System in Citrobacter rodentium. Microorganisms, 8(12), 1953. https://doi.org/10.3390/microorganisms8121953

Pettersson, J., Nordfelth, R., Dubinina, E., Bergman, T., Gustafsson, M., Magnusson, K. E., & Wolf-Watz, H. (1996). Modulation of virulence factor expression by pathogen target cell contact. Science (New York, N.Y.), 273(5279), 1231–1233. https://doi.org/10.1126/science.273.5279.1231

Phillips, S., Quigley, B. L., & Timms, P. (2019). Seventy Years of Chlamydia Vaccine Research—Limitations of the Past and Directions for the Future. Frontiers in Microbiology, 10, 70. https://doi.org/10.3389/fmicb.2019.00070

Portnoy, D. A., Moseley, S. L., & Falkow, S. (1981). Characterization of plasmids and plasmid-associated determinants of Yersinia enterocolitica pathogenesis. Infection and Immunity, 31(2), 775–782. https://doi.org/10.1128/iai.31.2.775-782.1981

Rabin, S. D. P., & Hauser, A. R. (2005). Functional regions of the Pseudomonas aeruginosa cytotoxin ExoU. Infection and Immunity, 73(1), 573–582. https://doi.org/10.1128/IAI.73.1.573-582.2005

Rangel, S. M., Diaz, M. H., Knoten, C. A., Zhang, A., & Hauser, A. R. (2015). The Role of ExoS in Dissemination of Pseudomonas aeruginosa during Pneumonia. PLoS Pathogens, 11(6), e1004945. https://doi.org/10.1371/journal.ppat.1004945

Relman, D. A., & Lipsitch, M. (2018). Microbiome as a tool and a target in the effort to address antimicrobial resistance. Proceedings of the National Academy of Sciences, 115(51), 12902–12910. https://doi.org/10.1073/pnas.1717163115

Rietsch, A., Vallet-Gely, I., Dove, S. L., & Mekalanos, J. J. (2005). ExsE, a secreted regulator of type III secretion genes in Pseudomonas aeruginosa. Proceedings of the National Academy of Sciences of the United States of America, 102(22), 8006–8011. https://doi.org/10.1073/pnas.0503005102

Rimpiläinen, M., Forsberg, A., & Wolf-Watz, H. (1992). A novel protein, LcrQ, involved in the low-calcium response of Yersinia pseudotuberculosis shows extensive homology to YopH. Journal of Bacteriology, 174(10), 3355–3363. https://doi.org/10.1128/jb.174.10.3355-3363.1992

Saka, H. A., Thompson, J. W., Chen, Y.-S., Kumar, Y., Dubois, L. G., Moseley, M. A., & Valdivia, R. H. (2011). Quantitative proteomics reveals metabolic and pathogenic properties of Chlamydia trachomatis developmental forms. Molecular Microbiology, 82(5), 1185–1203. https://doi.org/10.1111/j.1365-2958.2011.07877.x

Santajit, S., & Indrawattana, N. (2016). Mechanisms of Antimicrobial Resistance in ESKAPE Pathogens. BioMed Research International, 2016, 2475067. https://doi.org/10.1155/2016/2475067

Sheremet, A. B., Zigangirova, N. A., Zayakin, E. S., Luyksaar, S. I., Kapotina, L. N., Nesterenko, L. N., Kobets, N. V., & Gintsburg, A. L. (2018). Small Molecule Inhibitor of Type Three Secretion System Belonging to a Class 2,4-disubstituted-4H-[1,3,4]-thiadiazine-5-ones Improves Survival and Decreases Bacterial Loads in an Airway Pseudomonas aeruginosa Infection in Mice. BioMed Research International, 2018, 1–13. https://doi.org/10.1155/2018/5810767

Singh, P. K., Kapoor, A., Lomash, R. M., Kumar, K., Kamerkar, S. C., Pucadyil, T. J., & Mukhopadhyay, A. (2018). Salmonella SipA mimics a cognate SNARE for host Syntaxin8 to promote fusion with early endosomes. The Journal of Cell Biology, 217(12), 4199–4214. https://doi.org/10.1083/jcb.201802155

Slepenkin, A., Enquist, P.-A., Hägglund, U., de la Maza, L. M., Elofsson, M., & Peterson, E. M. (2007). Reversal of the antichlamydial activity of putative type III secretion inhibitors by iron. Infection and Immunity, 75(7), 3478–3489. https://doi.org/10.1128/IAI.00023-07

Tabor, D. E., Oganesyan, V., Keller, A. E., Yu, L., McLaughlin, R. E., Song, E., Warrener, P., Rosenthal, K., Esser, M., Qi, Y., Ruzin, A., Stover, C. K., & DiGiandomenico, A. (2018). Pseudomonas aeruginosa PcrV and Psl, the Molecular Targets of Bispecific Antibody MEDI3902, Are Conserved Among Diverse Global Clinical Isolates. The Journal of Infectious Diseases, 218(12), 1983–1994. https://doi.org/10.1093/infdis/jiy438

Tree, J. J., Wang, D., McInally, C., Mahajan, A., Layton, A., Houghton, I., Elofsson, M., Stevens, M. P., Gally, D. L., & Roe, A. J. (2009). Characterization of the effects of salicylidene acylhydrazide compounds on type III secretion in Escherichia coli O157:H7. Infection and Immunity, 77(10), 4209–4220. https://doi.org/10.1128/IAI.00562-09

Troisfontaines, P., & Cornelis, G. R. (2005). Type III secretion: More systems than you think. Physiology (Bethesda, Md.), 20, 326–339. https://doi.org/10.1152/physiol.00011.2005

Tsou, L. K., Lara-Tejero, M., RoseFigura, J., Zhang, Z. J., Wang, Y.-C., Yount, J. S., Lefebre, M., Dossa, P. D., Kato, J., Guan, F., Lam, W., Cheng, Y.-C., Galán, J. E., & Hang, H. C. (2016). Antibacterial Flavonoids from Medicinal Plants Covalently Inactivate Type III Protein Secretion Substrates. Journal of the American Chemical Society, 138(7), 2209–2218. https://doi.org/10.1021/jacs.5b11575

Urbanowski, M. L., Lykken, G. L., & Yahr, T. L. (2005). A secreted regulatory protein couples transcription to the secretory activity of the Pseudomonas aeruginosa type III secretion system. Proceedings of the National Academy of Sciences of the United States of America, 102(28), 9930–9935. https://doi.org/10.1073/pnas.0504405102

Venecia, K., & Young, G. M. (2005). Environmental regulation and virulence attributes of the Ysa type III secretion system of Yersinia enterocolitica biovar 1B. Infection and Immunity, 73(9), 5961–5977. https://doi.org/10.1128/IAI.73.9.5961-5977.2005

Wagener, B. M., Anjum, N., Evans, C., Brandon, A., Honavar, J., Creighton, J., Traber, M. G., Stuart, R. L., Stevens, T., & Pittet, J.-F. (2020). α-Tocopherol Attenuates

the Severity of Pseudomonas aeruginosa-induced Pneumonia. American Journal of Respiratory Cell and Molecular Biology, 63(2), 234–243. https://doi.org/10.1165/rcmb.2019-0185OC

Wagner, S., & Diepold, A. (2020). A Unified Nomenclature for Injectisome-Type Type III Secretion Systems. Current Topics in Microbiology and Immunology, 427, 1–10. https://doi.org/10.1007/82_2020_210

Wagner, S., & Galán, J. E. (Eds.). (2020). Bacterial type III protein secretion systems. Springer. https://doi.org/10.1007/978-3-030-52123-3

Wagner, S., Grin, I., Malmsheimer, S., Singh, N., Torres-Vargas, C. E., & Westerhausen, S. (2018). Bacterial type III secretion systems: A complex device for the delivery of bacterial effector proteins into eukaryotic host cells. FEMS Microbiology Letters, 365(19). https://doi.org/10.1093/femsle/fny201

Wang, D., Zetterström, C. E., Gabrielsen, M., Beckham, K. S. H., Tree, J. J., Macdonald, S. E., Byron, O., Mitchell, T. J., Gally, D. L., Herzyk, P., Mahajan, A., Uvell, H., Burchmore, R., Smith, B. O., Elofsson, M., & Roe, A. J. (2011). Identification of bacterial target proteins for the salicylidene acylhydrazide class of virulence-blocking compounds. The Journal of Biological Chemistry, 286(34), 29922–29931. https://doi.org/10.1074/jbc.M111.233858

Williams, A. W., & Straley, S. C. (1998). YopD of Yersinia pestis plays a role in negative regulation of the low-calcium response in addition to its role in translocation of Yops. Journal of Bacteriology, 180(2), 350–358. https://doi.org/10.1128/JB.180.2.350-358.1998

Winter, S. E., Winter, M. G., Poon, V., Keestra, A. M., Sterzenbach, T., Faber, F., Costa, L. F., Cassou, F., Costa, E. A., Alves, G. E. S., Paixão, T. A., Santos, R. L., & Bäumler, A. J. (2014). Salmonella enterica Serovar Typhi conceals the invasion-associated type three secretion system from the innate immune system by gene regulation. PLoS Pathogens, 10(7), e1004207. https://doi.org/10.1371/journal.ppat.1004207

Woehrmann, M. H., Bray, W. M., Durbin, J. K., Nisam, S. C., Michael, A. K., Glassey, E., Stuart, J. M., & Lokey, R. S. (2013). Large-scale cytological profiling for functional analysis of bioactive compounds. Molecular BioSystems, 9(11), 2604–2617. https://doi.org/10.1039/c3mb70245f

Yang, F., Korban, S. S., Pusey, P. L., Elofsson, M., Sundin, G. W., & Zhao, Y. (2014). Small-molecule inhibitors suppress the expression of both type III secretion and amylovoran biosynthesis genes in Erwinia amylovora. Molecular Plant Pathology, 15(1), 44–57. https://doi.org/10.1111/mpp.12064

Young, B. M., & Young, G. M. (2002a). YplA Is Exported by the Ysc, Ysa, and Flagellar Type III Secretion Systems of Yersinia enterocolitica. Journal of Bacteriology, 184(5), 1324–1334. https://doi.org/10.1128/JB.184.5.1324-1334.2002

Young, B. M., & Young, G. M. (2002b). Evidence for targeting of Yop effectors by the chromosomally encoded Ysa type III secretion system of Yersinia enterocolitica. Journal of Bacteriology, 184(20), 5563–5571. https://doi.org/10.1128/JB.184.20.5563-5571.2002

Zambelloni, R., Connolly, J. P. R., Huerta Uribe, A., Burgess, K., Marquez, R., & Roe, A. J. (2017). Novel compounds targeting the enterohemorrhagic Escherichia coli type

three secretion system reveal insights into mechanisms of secretion inhibition. Molecular Microbiology, 105(4), 606–619. https://doi.org/10.1111/mmi.13719

Zetterström, C. E., Hasselgren, J., Salin, O., Davis, R. A., Quinn, R. J., Sundin, C., & Elofsson, M. (2013). The resveratrol tetramer (-)-hopeaphenol inhibits type III secretion in the gram-negative pathogens Yersinia pseudotuberculosis and Pseudomonas aeruginosa. PloS One, 8(12), e81969. https://doi.org/10.1371/journal.pone.0081969

Zhang, Y., Liu, Y., Qiu, J., Luo, Z.-Q., & Deng, X. (2018). The Herbal Compound Thymol Protects Mice From Lethal Infection by Salmonella Typhimurium. Frontiers in Microbiology, 9, 1022. https://doi.org/10.3389/fmicb.2018.01022

Zhang, Y., Liu, Y., Wang, T., Deng, X., & Chu, X. (2018). Natural compound sanguinarine chloride targets the type III secretion system of Salmonella enterica Serovar Typhimurium. Biochemistry and Biophysics Reports, 14, 149–154. https://doi.org/10.1016/j.bbrep.2018.04.011

Zhu, C., El Qaidi, S., McDonald, P., Roy, A., & Hardwidge, P. R. (2021). YM155 Inhibits NleB and SseK Arginine Glycosyltransferase Activity. Pathogens (Basel, Switzerland), 10(2), 253. https://doi.org/10.3390/pathogens10020253

Zigangirova, N. A., Kost, E. A., Didenko, L. V., Kapotina, L. N., Zayakin, E. S., Luyksaar, S. I., Morgunova, E. Y., Fedina, E. D., Artyukhova, O. A., Samorodov, A. V., & Kobets, N. V. (2016). A small-molecule compound belonging to a class of 2,4-disubstituted 1,3,4-thiadiazine-5-ones inhibits intracellular growth and persistence of Chlamydia trachomatis. Journal of Medical Microbiology, 65(1), 91–98. https://doi.org/10.1099/jmm.0.000189

Zigangirova, N. A., Nesterenko, L. N., Sheremet, A. B., Soloveva, A. V., Luyksaar, S. I., Zayakin, E. S., Balunets, D. V., & Gintsburg, A. L. (2021). Fluorothiazinon, a small-molecular inhibitor of T3SS, suppresses salmonella oral infection in mice. The Journal of Antibiotics, 74(4), 244–254. https://doi.org/10.1038/s41429-020-00396-w

Zuckermann, R. N., Kerr, J. M., Kent, S. B. H., & Moos, W. H. (1992). Efficient method for the preparation of peptoids [oligo(N-substituted glycines)] by submonomer solid-phase synthesis. Journal of the American Chemical Society, 114(26), 10646–10647. https://doi.org/10.1021/ja00052a076

FIGURE 4.1

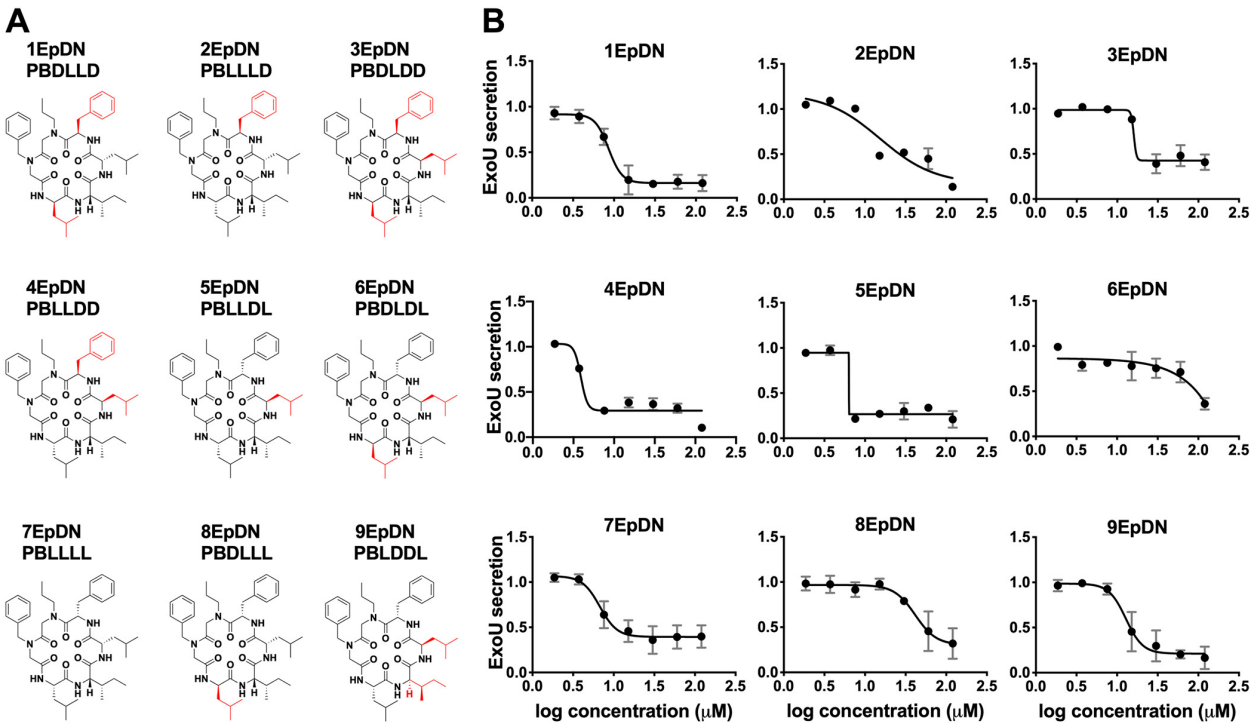

FIGURE 4.1. Stereochemistry scan of cyclic peptomers results in a more potent derivative, 4EpDN.

(A) Structures of 1EpDN stereoisomers. Isomers were generated from different combinations of four side chains at positions 3 to 6. Numbers preceding compounds were used to distinguish the different isomers and the conformation of the four side chains. The d-amino acid side chain is shown in red.

(B) WT *P. aeruginosa* PA103 was grown under T3SS-inducing conditions with increasing concentrations of cyclic peptomer isomers. Secretion of T3SS cargo into the culture supernatant was assessed by precipitating secreted proteins and visualizing them with Coomassie blue. ExoU band intensities were quantified and normalized to that of the DMSO control. The results are from at least two independent experiments. Nonlinear curve fitting is shown to depict the trend of inhibition. Error bars are standard errors of the mean.

FIGURE 4.2

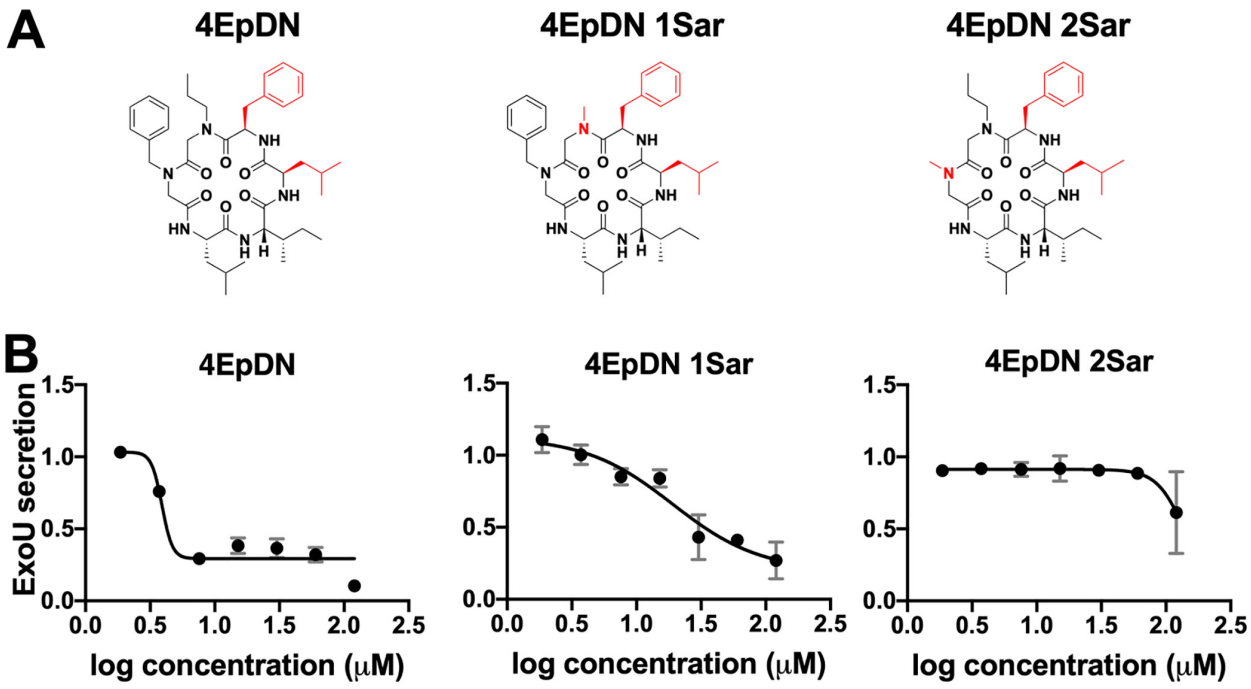

FIGURE 4.2. Sarcosine replacement of 4EpDN at position 1 or 2 eliminates activity.

(A) Structures of 4EpDN and its derivatives, 4EpDN 1Sar and 4EpDN 2Sar. The d-amino acid side chain is shown in red.

(B) WT *P. aeruginosa* PA103 was grown under T3SS-inducing conditions with increasing concentrations of compounds. Secretion of T3SS cargo into the culture supernatant was assessed on SDS-PAGE gel. ExoU band intensities were visualized with Coomassie blue, quantified, and normalized to that of the DMSO control. The results are from at least two independent experiments. Error bars are standard errors of the mean.

FIGURE 4.3

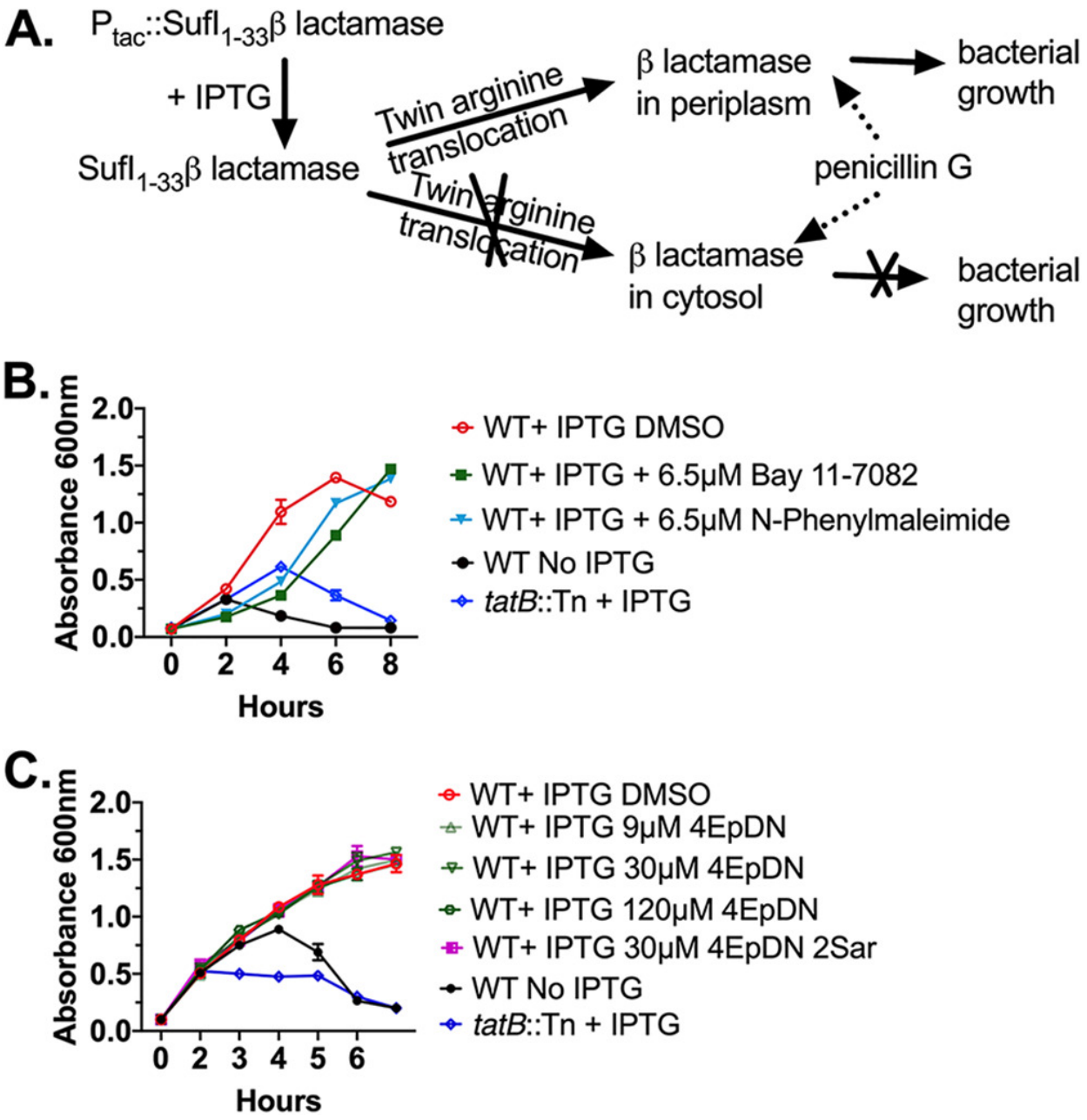

FIGURE 4.3. Cyclic peptomers do not affect the twin arginine translocation (Tat) system.

(A) *Y. pseudotuberculosis* expressing a SufI-β-lactamase Tat reporter incubated in the presence of penicillin G will only grow if the Tat system remains functional.

(B) *Y. pseudotuberculosis* SufI-β-lactamase reporters were treated with the Tat inhibitors Bay 11-7082, N-phenyl maleimide, or DMSO, and culture optical density was measured. WT refers to bacteria expressing a functional Tat secretion system. A mutant strain with a transposon insertion in the tatB gene serves as a control.

(C) The same assay as in panel B was repeated in the presence of cyclic peptomers or DMSO. The result was from two independent replicates. Error bars are standard errors of the mean.

FIGURE 4.4

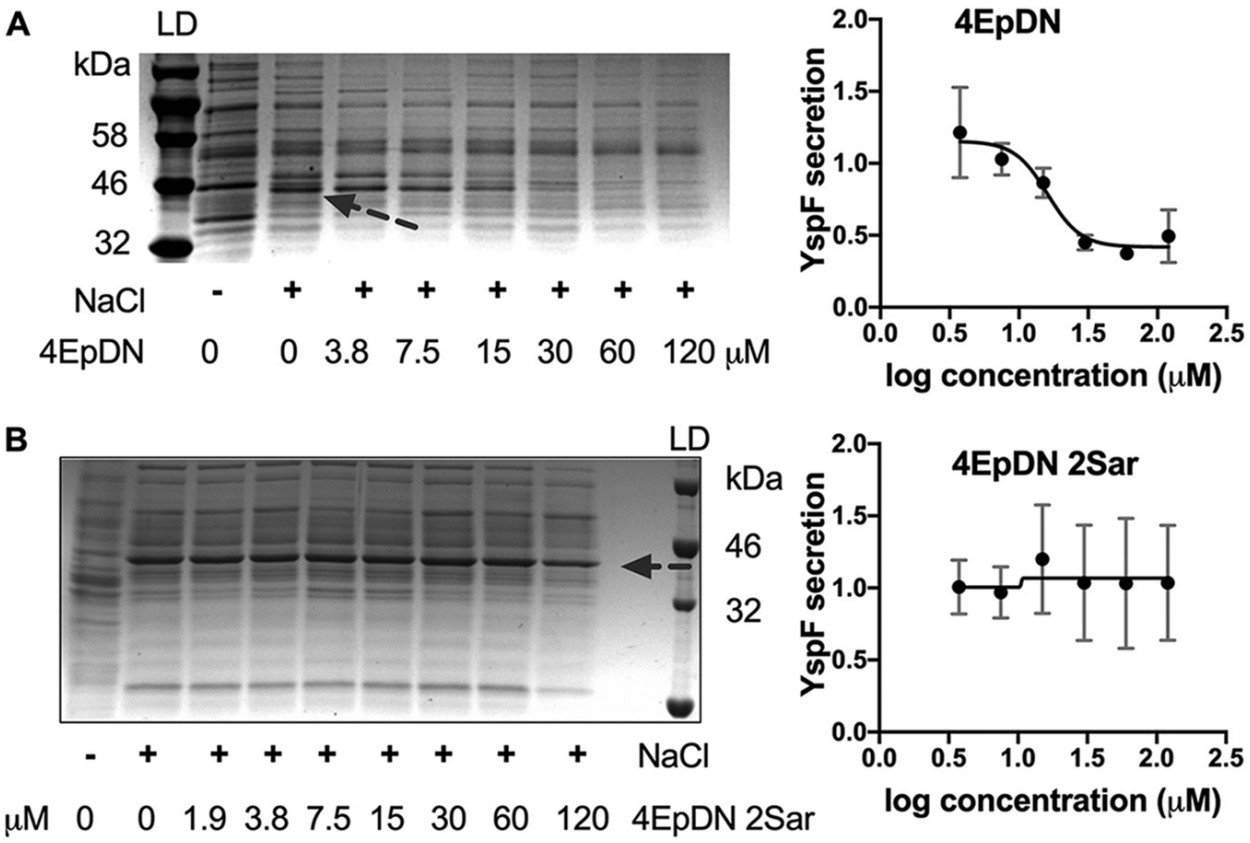

FIGURE 4.4. Effect of cyclic peptomers on secretion of *Yersinia* Ysa T3SS substrates.

(A and B) *Y. enterocolitica* serotype O:8 was grown under T3SS-inducing conditions with increasing concentrations of cyclic peptomer isomers, 4EpDN (A) and 4EpDN 2Sar (B). Secretion of T3SS cargo into the culture supernatant was assessed by precipitating secreted proteins and visualizing them with Coomassie blue. Arrow points to the YscF protein band. YspF band intensities were quantified and normalized to that of the DMSO control. Representative gel images and quantification of YspF are shown. The results are from two independent experiments. Error bars are standard errors of the mean.

FIGURE 4.5

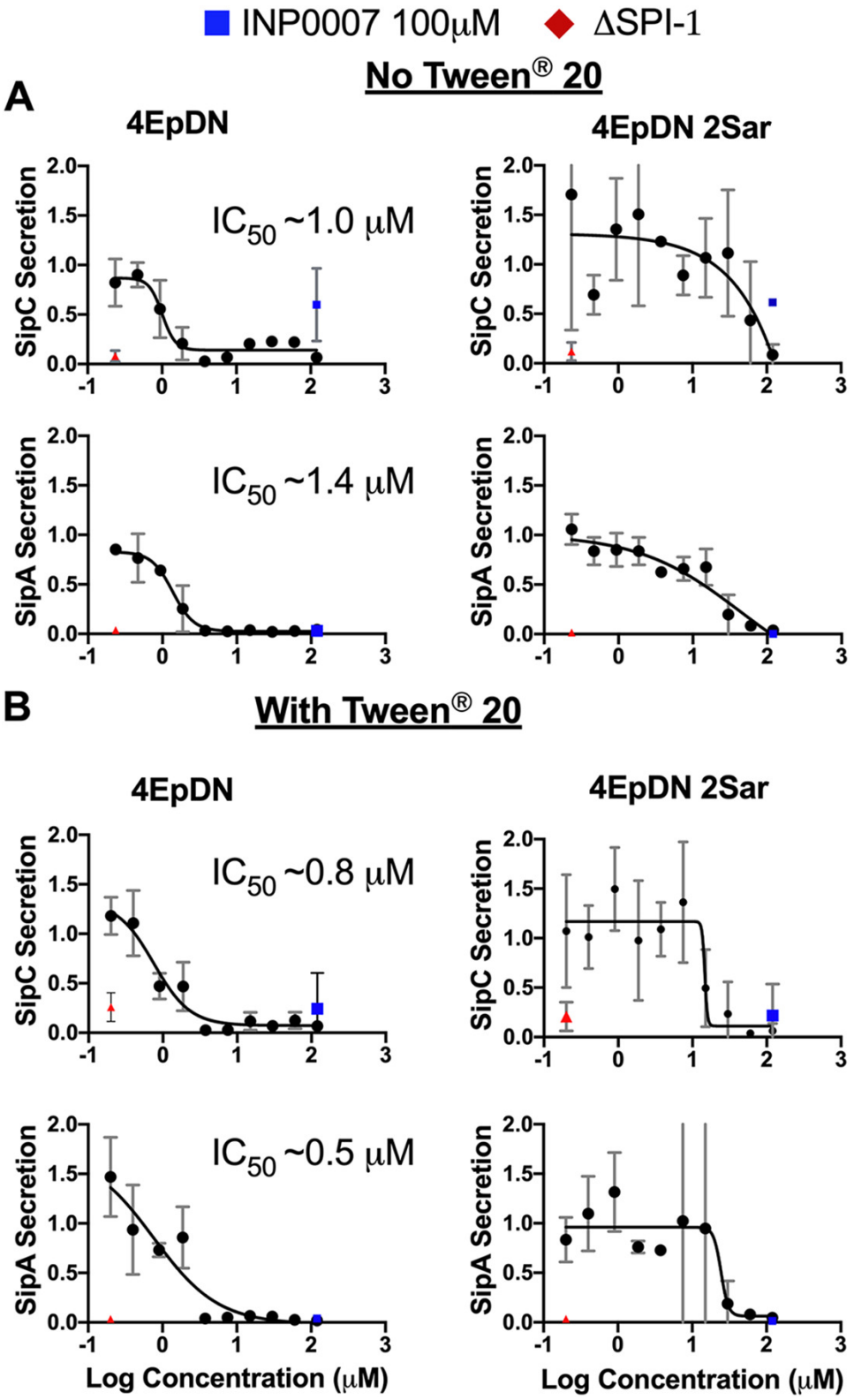
INP0007 100μM
ΔSPI-1
No Tween® 20
A
4EpDN
4EpDN 2Sar
SipC Secretion
SipA Secretion
IC50 ~1.0 μM
IC50 ~1.4 μM
B
With Tween® 20
4EpDN
4EpDN 2Sar
IC50 ~0.8 μM
IC50 ~0.5 μM
Log Concentration (μM)
Log Concentration (μM)

FIGURE 4.5. Cyclic peptomers inhibit the *Salmonella* SPI-1 T3SS.

Salmonella enterica Typhimurium was grown with increasing concentrations of cyclic peptomer isomers. Secretion of SPI-1 T3SS cargo into the culture supernatant was assessed by precipitating secreted proteins and visualizing them with Coomassie blue. SipA and SipC band intensities were quantified and normalized to that of the DMSO control. (A and B) The experiments were carried out without the detergent Tween 20 **(A)** or with Tween 20 **(B).** A ΔSPI-1 *Salmonella* mutant and INP0007, a known SPI-1 inhibitor, were used as controls. The results are from at least two independent experiments. Error bars are standard errors of the mean.

FIGURE 4.6

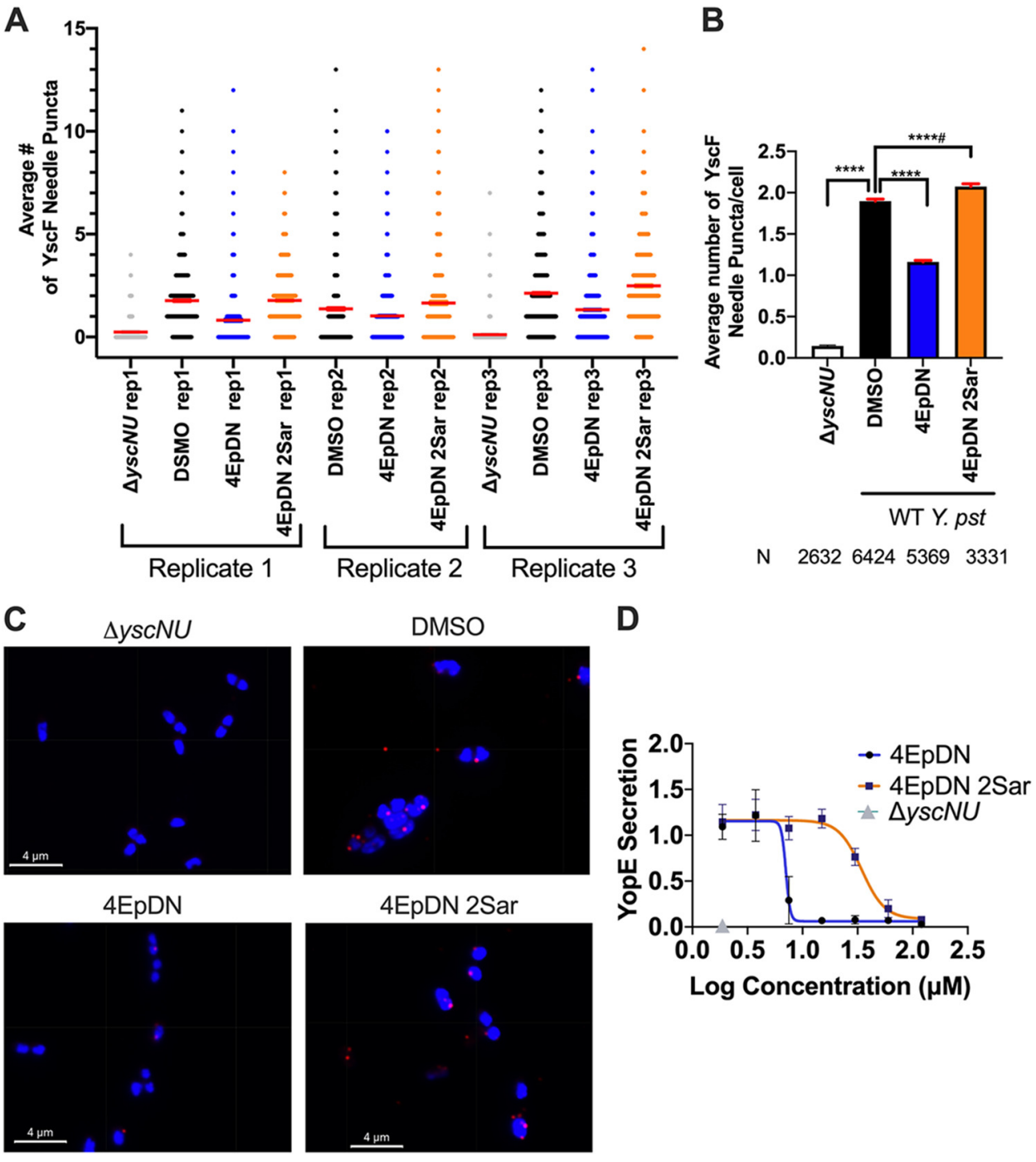
A
Average # of YscF Needle Puncta
15
10
5
0
ΔyscNU rep1
DSMO rep1
4EpDN rep1
4EpDN 2Sar rep1
DMSO rep2
4EpDN rep2
4EpDN 2Sar rep2
ΔyscNU rep3
DMSO rep3
4EpDN rep3
4EpDN 2Sar rep3
Replicate 1
Replicate 2
Replicate 3
B
Average number of YscF Needle Puncta/cell
2.5
2.0
1.5
1.0
0.5
0.0
****
****
****#
ΔyscNU
DMSO
4EpDN
4EpDN 2Sar
WT Y. pst
N 2632 6424 5369 3331
C
ΔyscNU
DMSO
4EpDN
4EpDN 2Sar
4 μm
D
YopE Secretion
2.0
1.5
1.0
0.5
0.0
0.0 0.5 1.0 1.5 2.0 2.5
Log Concentration (μM)
4EpDN
4EpDN 2Sar
ΔyscNU

FIGURE 4.6. YscF puncta visualization using immunofluorescence.

Y. pseudotuberculosis was grown under T3SS-inducing conditions (low Ca2+) in the presence of 60 μM cyclic peptomers or an equivalent volume of DMSO. A mutant lacking yscN and yscU was used as a negative control.

(A) Scatterplot of YscF puncta/cell for the three replicates. Means ± the standard error of the mean (SEM) are shown in red. The width of distribution of points is proportional to the number of data points at the Y value.

(B) Mean number of puncta/cell after treatment for all replicates combined ± SEM.

(C) Representative images of YscF puncta in different conditions. (Imaris software displays grid lines within the images; they are not physical lines on the samples.)

(D) Secretion of effector YopE in low-calcium medium on the presence of different concentrations of 4EpDN and 4EpDN 2Sar in WT *Y. pseudotuberculosis* stained with Coomassie stain and quantified. The data represent three independent experiments. The nonparametric Kruskal-Wallis test with Dunn's multiple-comparison test was used. ****, $P < 0.0001$; ****, $P < 0.0001$, but the trend is in the reversed direction.

FIGURE 4.7

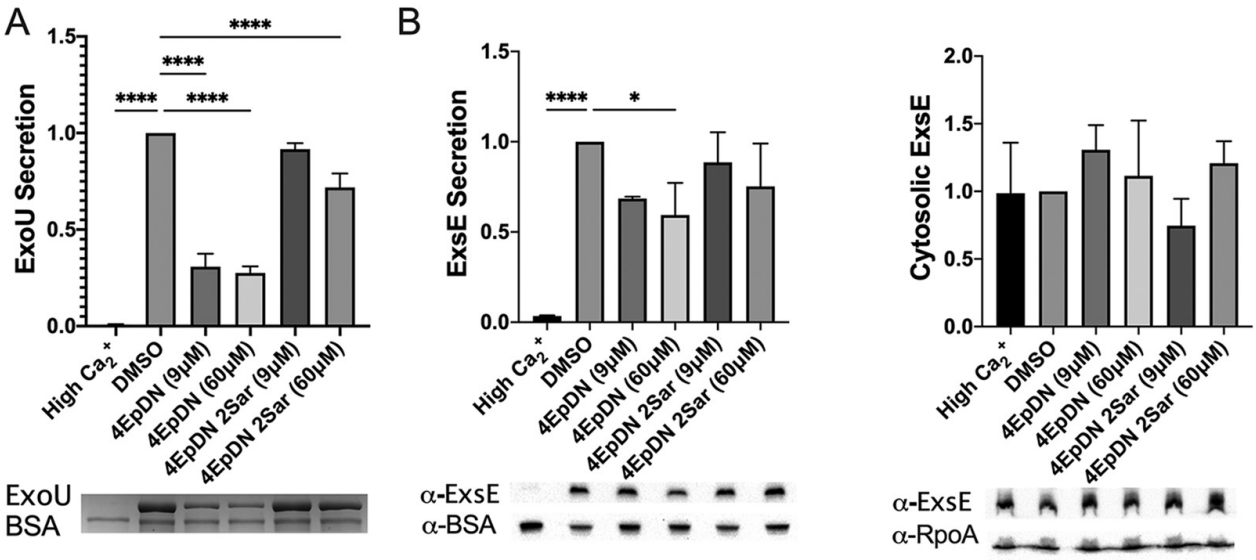

FIGURE 4.7. The cyclic peptomer 4EpDN inhibits secretion of the effector protein ExoU but not the regulator ExsE.

PA103 was grown under T3S-inducing conditions in the presence of 9 μM or 60 μM cyclic peptomers or DMSO.

(A) Secretion of ExoU was visualized using Coomassie blue and quantified.

(B) In the same samples, Western blotting was carried out for secreted ExsE in the supernatant and ExsE in the cell pellets. BSA and RpoA were used as loading controls. Data were from three independent experiments. One-way ANOVA with Dunnett's multiple-comparison test was used. *, $P < 0.05$; ****, $P < 0.0001$ compared to DMSO. Error bars are standard errors of the mean.

FIGURE 4.8

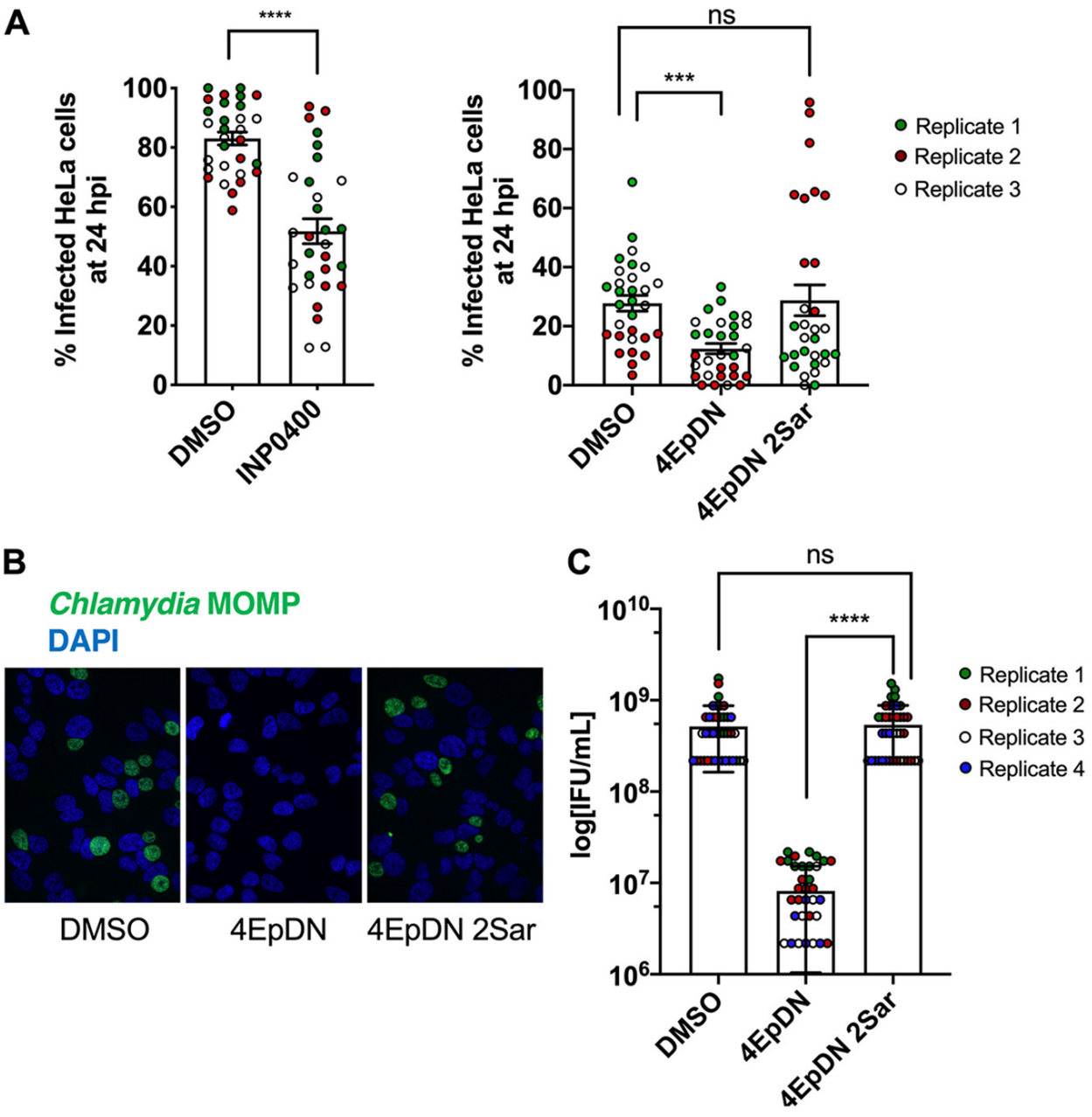
A
****
% Infected HeLa cells at 24 hpi
100
80
60
40
20
0
DMSO
INP0400
ns
***
% Infected HeLa cells at 24 hpi
DMSO
4EpDN
4EpDN 2Sar
Replicate 1
Replicate 2
Replicate 3
B
Chlamydia MOMP
DAPI
DMSO
4EpDN
4EpDN 2Sar
C
ns
****
log[IFU/mL]
10^{10}
10^{9}
10^{8}
10^{7}
10^{6}
DMSO
4EpDN
4EpDN 2Sar
Replicate 1
Replicate 2
Replicate 3
Replicate 4

FIGURE 4.8. The cyclic peptomer 4EpDN inhibits *Chlamydia* infection.

(A) HeLa cells were infected with *C. trachomatis* L2 at a multiplicity of infection (MOI) of 3 (left-hand panel) or 1 (right-hand panel) in the presence of 9 µM cyclic peptomers, 30 µM INP0400, or DMSO. Cells were stained for the *Chlamydia* major outer membrane protein (MOMP) and nucleic acids (DAPI) and imaged after 24 h of infection to determine the number of infected cells (primary infection). The Mann-Whitney test was used.

(B and C) Infectious elementary bodies (EB) were harvested after 48 h of HeLa cell infection in the presence of inhibitors and were used to infect fresh HeLa cells without applying inhibitors (secondary infection). After 24 h, cells were imaged as in panel A. Representative images (B) and infectious units/ml (C) are shown from three to four independent experiments. Error bars are standard errors of the mean. The Kruskal-Wallis test with Dunn's multiple-comparison test was used. ***, $P < 0.0005$; ****, $P < 0.0001$; ns: not significant.

FIGURE 4.9

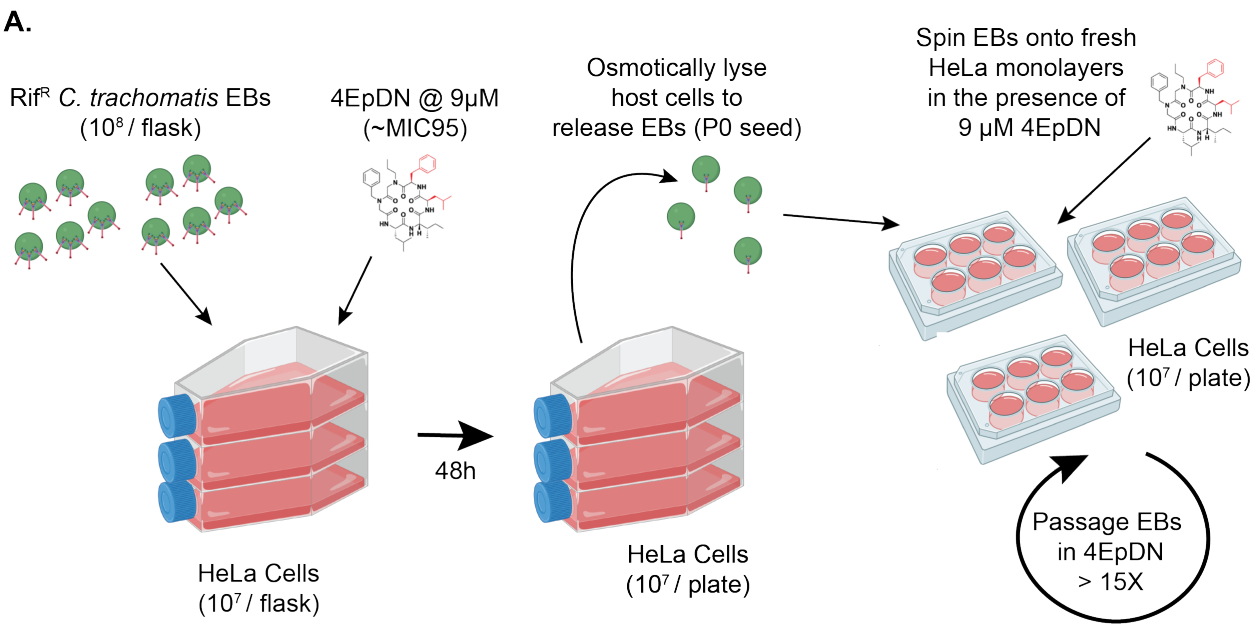
A.
Rif^R *C. trachomatis* EBs
(10^8 / flask)
4EpDN @ 9μM
(~MIC95)
Osmotically lyse
host cells to
release EBs (P0 seed)
Spin EBs onto fresh
HeLa monolayers
in the presence of
9 μM 4EpDN
HeLa Cells
(10^7 / plate)
48h
HeLa Cells
(10^7 / flask)
HeLa Cells
(10^7 / plate)
Passage EBs
in 4EpDN
> 15X

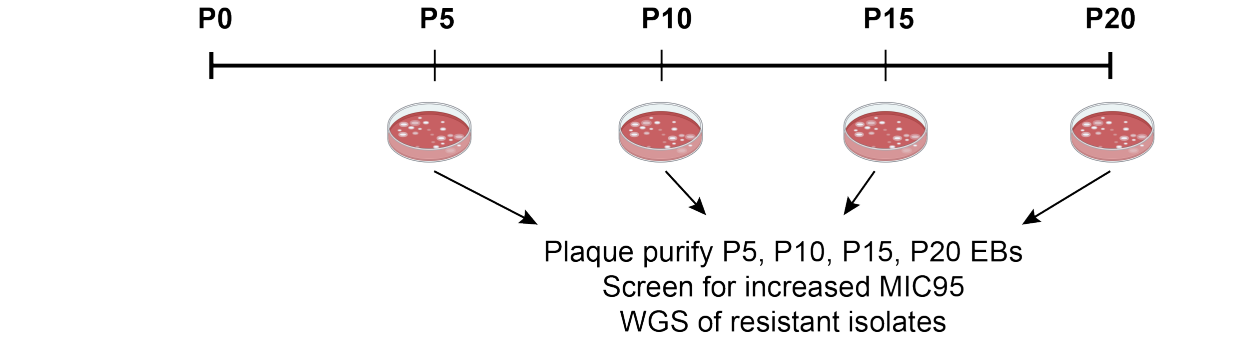
B.
P0
P5
P10
P15
P20
Plaque purify P5, P10, P15, P20 EBs
Screen for increased MIC95
WGS of resistant isolates

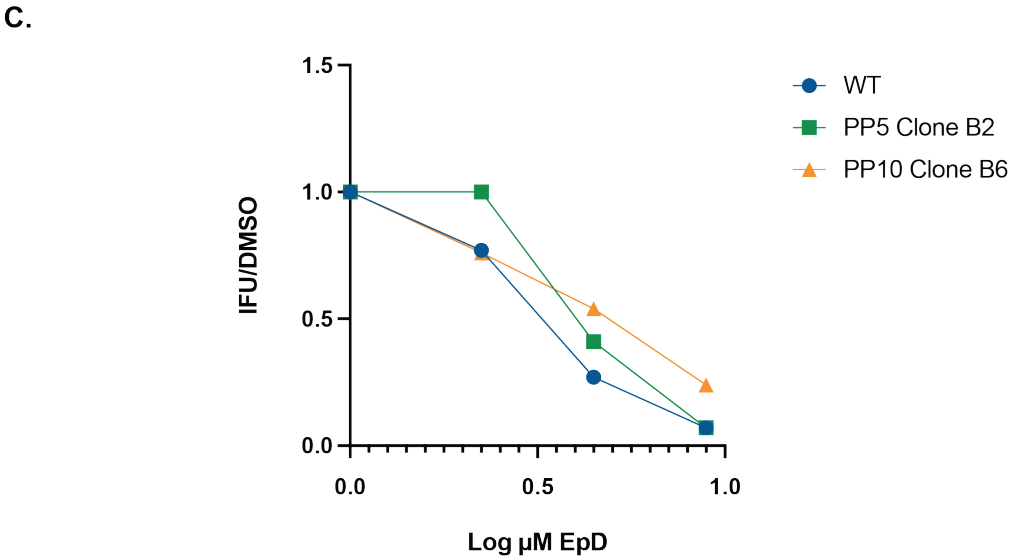
C.
1.5
1.0
0.5
0.0
IFU/DMSO
0.0
0.5
1.0
Log μM EpD
WT
PP5 Clone B2
PP10 Clone B6

FIGURE 4.9. Strategy for using the obligate intracellular pathogen *C. trachomatis* to identify T3SS mutants.

To use *C. trachomatis* to identify mutants resistant to 4EpDN, the MIC95 for 4EpDN was first determined to be 9μM during *C. trachomatis* re-infection assay.

(A) $3x10^8$ Rifampin-resistant *C. trachomatis* EBs were incubated with 9 μM 4EpDN and added to HeLa cells. Infections were incubated with 9 μM 4EpDN for 48 hours, and were osmotically lysed to release EBs (P0 seed). These EBs were then incubated with 9μM 4EpDN and centrifuged onto a fresh HeLa monolayer. Infections again were allowed to proceed 48-60 hours (to allow EBs the maximum time to replicate) in the presence of 9 μM 4EpDN, and were subsequently osmotically lysed. EBs were passaged in the presence of 4EpDN at least 20 times.

(B) At P5, P10, P15, and P20 15% of EBs were plaque purified and clonal populations were isolated.

(C) Mutant populations were then screened for increased resistance to 4EpDN by reinfection assay. The starting pool of wild-type RifR C. trachomatis (blue circles) was assayed along-side a surviving P5 clone (green squares) and a surviving P10 clone (orange triangles). All clones exhibiting increased resistance will be sequenced to identify mutations that confer resistance to 4EpDN.

FIGURE S4.1

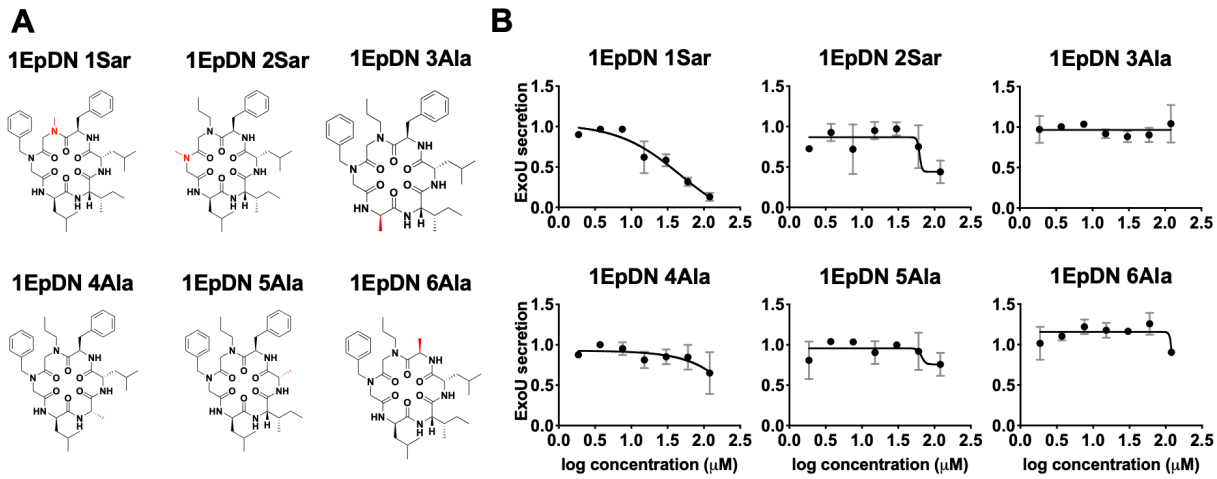

FIGURE S4.1. EpDN alanine/Sarcosine scan suggests peptoid sidechains are important for biological activity.

(A) Structures of 1EpDN alanine derivatives. D-form of side chain is shown in red.

(B) WT *P. aeruginosa* PA103 was grown under T3SS-inducing conditions with increasing concentrations of cyclic peptomers. Secretion of T3SS cargo into the culture supernatant was assessed by precipitating secreted proteins and visualizing them with Coomassie blue. ExoU band intensities were quantified and normalized to that of the DMSO control. The results are from at least two independent experiments. Error bars are standard errors of the mean. Nonlinear curve fitting is shown to depict the trend of inhibition.

FIGURE S4.2

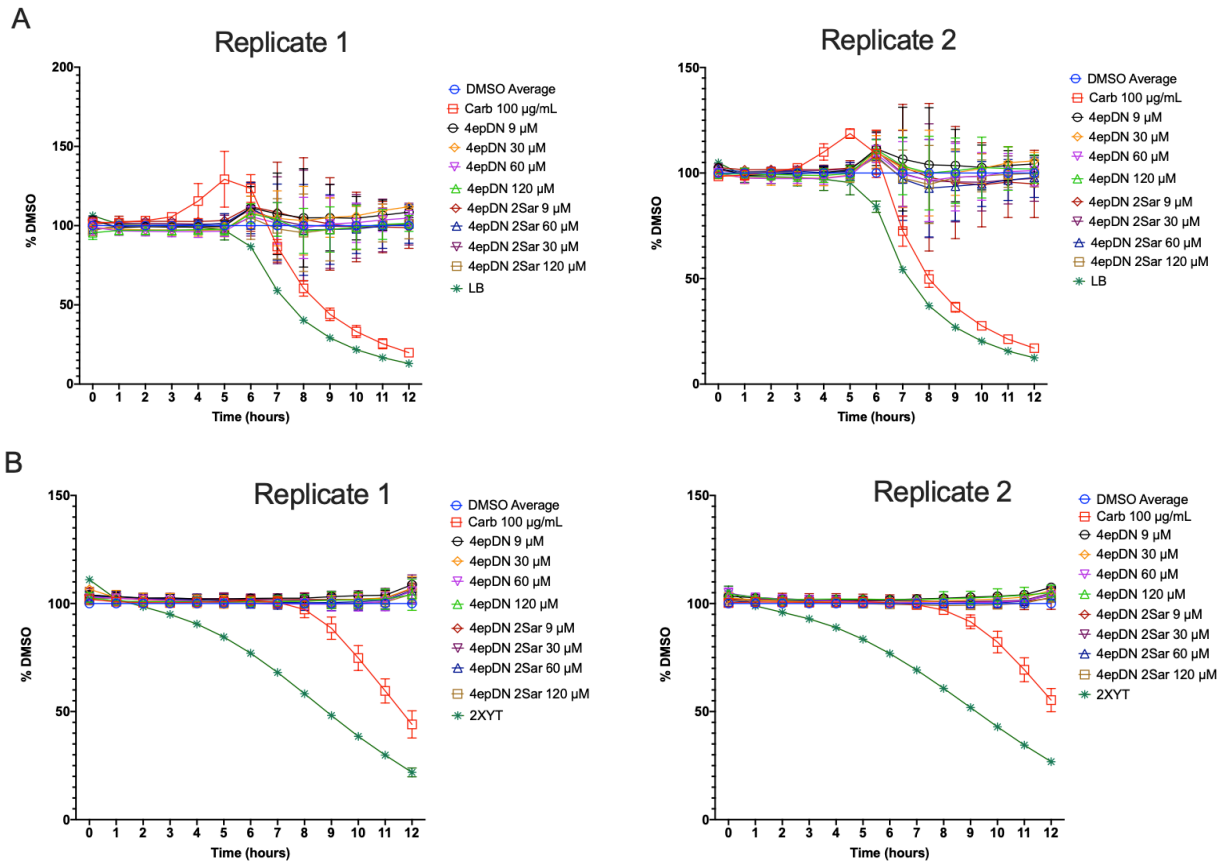

FIGURE S4.2. Cyclic peptomers do not affect bacterial viability.

P. aeruginosa PA01 **(A)** or *Y. pseudotuberculosis* **(B)** was grown in LB or 2xYT medium at 37℃ or 26℃ in the presence of cyclic peptomers at 9 µM, 30 µM, 60 µM and 120 µM, equivalent volume of DMSO or Carbenicillin (100 µg/mL). Resazurin-based alamarBlue HS cell viability reagent was used to monitor metabolic activity of the bacteria over a period of 12 hrs. Fluorescence of treatment over control was plotted over time. Media only served as a control for bacterial growth. The experiment was carried out in two biological replicates with three technical replicate each.

FIGURE S4.3

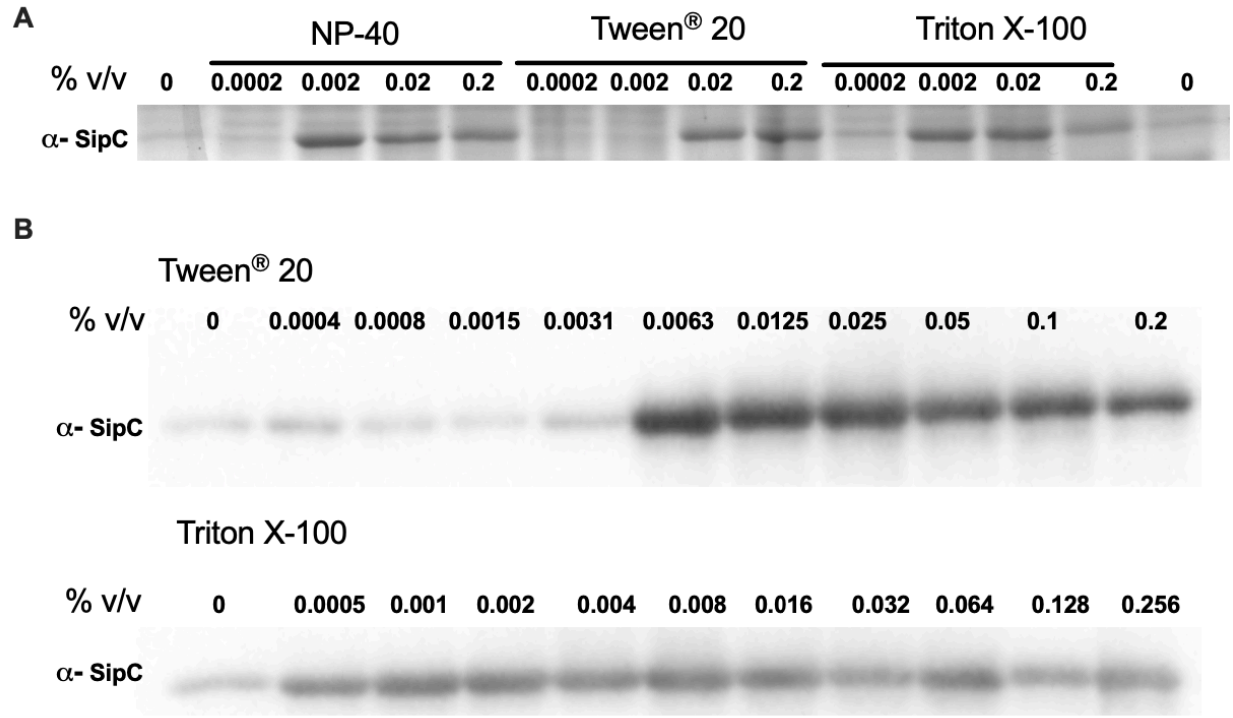

FIGURE S4.3. Secretion of *Salmonella* T3SS substrate in the presence of non-ionic detergents.

Detergents without T3SS inhibitors were used to determine the highest concentration of detergent that can be added to the cultures without causing an observable effect on the T3SS.

(A) *Salmonella enterica* Typhimurium was grown in LB with increasing concentrations of NP-40, Tween® 20, or Triton X-100. Secretion of SPI-1 T3SS effector SipC into the culture supernatant was assessed by precipitating secreted proteins and visualizing them with Coomassie blue.

(B) Secretion of SipC in the presence of increasing concentrations of Tween® 20 or Triton X-100 was detected by Western Blot.

FIGURE S4.4

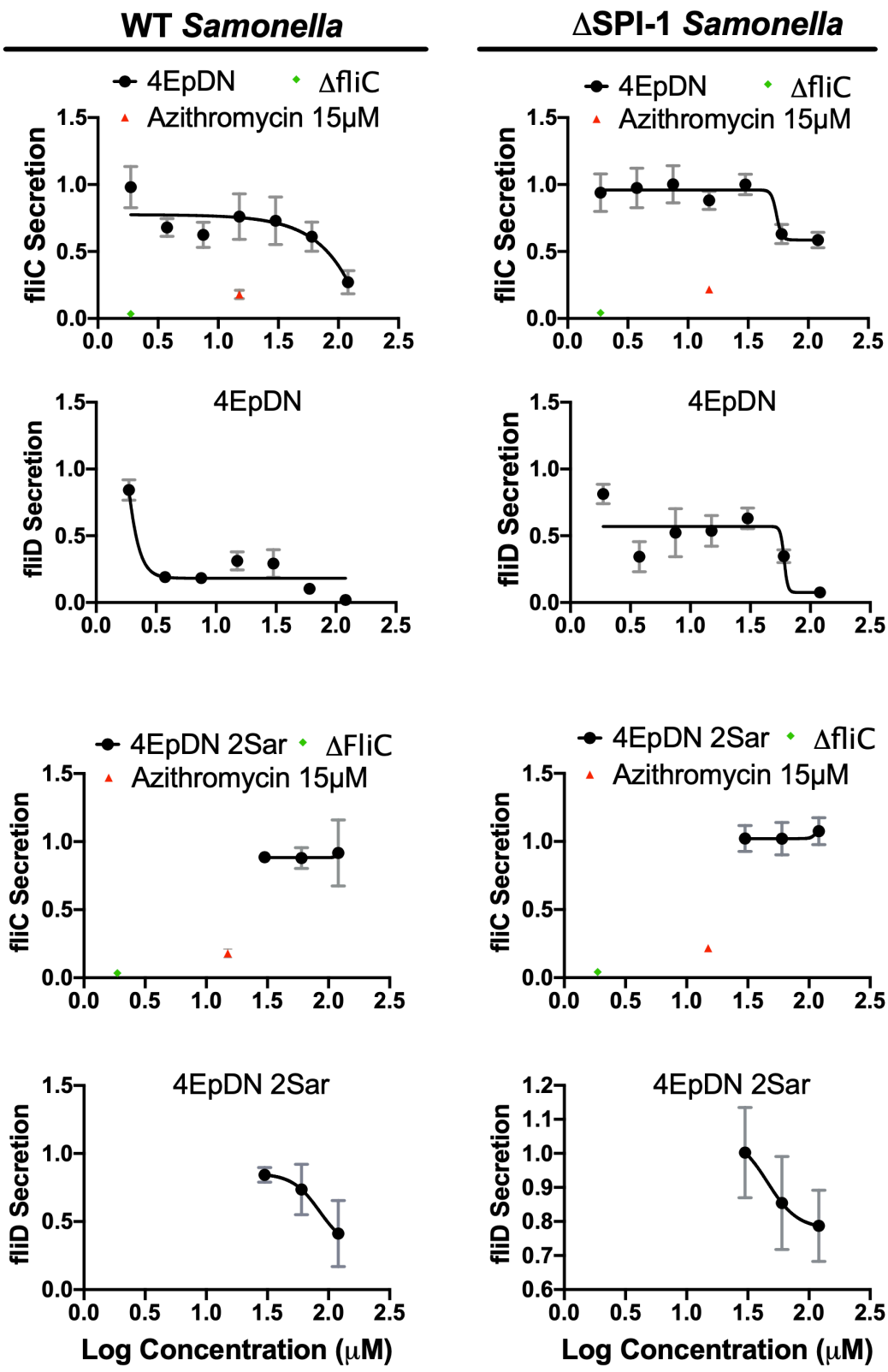
WT Samonella
ΔSPI-1 Samonella
4EpDN
ΔfliC
Azithromycin 15μM
fliC Secretion
fliD Secretion
4EpDN 2Sar
ΔFliC
Log Concentration (μM)

FIGURE S4.4. Cyclic peptomers do not affect secretion of flagellar proteins.

Salmonella enterica Typhimurium was grown in LB with increasing concentrations of cyclic peptomers. Secretion of flagellar structural proteins FliC and FliD were assessed by precipitating the secreted proteins and visualizing them with Coomassie blue. A ΔfliC mutant and azithromycin, which inhibits flagellin secretion, were used as controls. The SPI-1 mutant and WT *Salmonella* were both tested, as flagella substrates can be secreted through both flagellar and SPI-1 T3SS systems. The results are from at least two independent experiments. Error bars are standard errors of the mean.

FIGURE S4.5

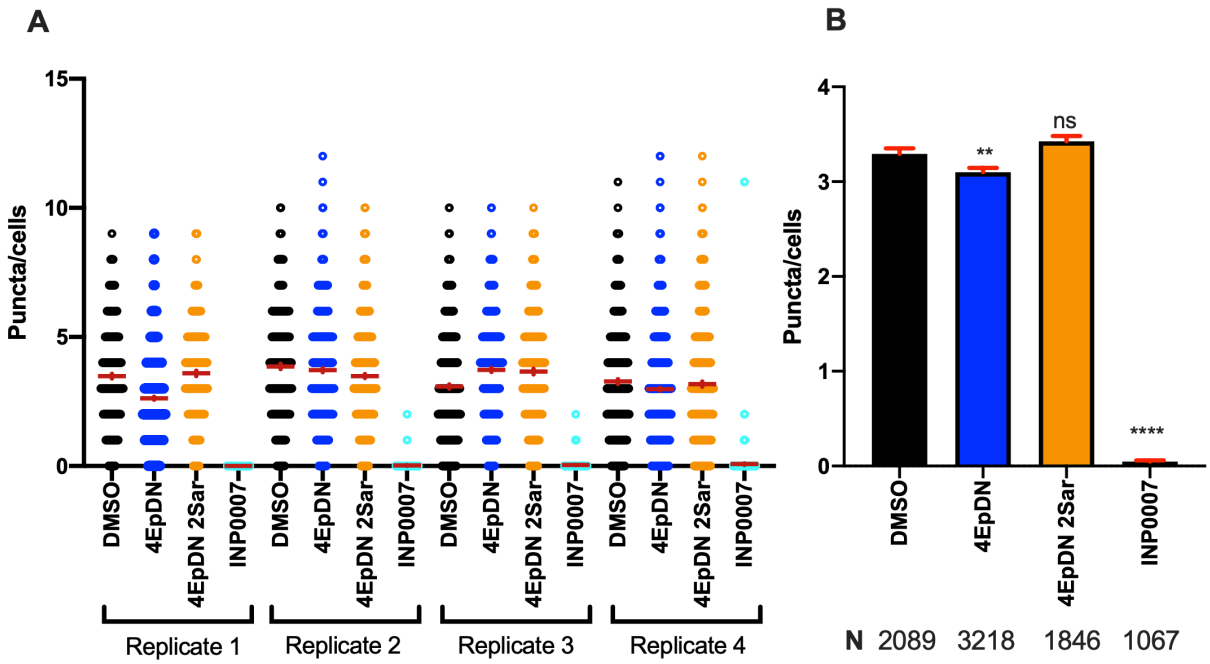

FIGURE S4.5. The cyclic peptomer 4EpDN effect on localization of the *Yersinia* T3SS basal body component YscD.

Y. enterocolitica expressing YscD-EGFP was grown under T3SS inducing condition (low Ca2+) in the presence of 9 μM cyclic peptomers, 50 μM INP0007, or DMSO.

(A) Scatter plot of YscD puncta/cell for four replicates. Mean ±SEM was shown in red. Width of distribution of points is proportional to the number of data points at the Y value.

(B) Mean number of puncta/cell after treatment for all replicates combined ±SEM. Data represents four independent experiments. Non- parametric Kruskal-Wallis test with Dunn's multiple-comparison test was used. ****, $P < 0.0001$; **, $P < 0.005$; ns: not significant.

FIGURE S4.6

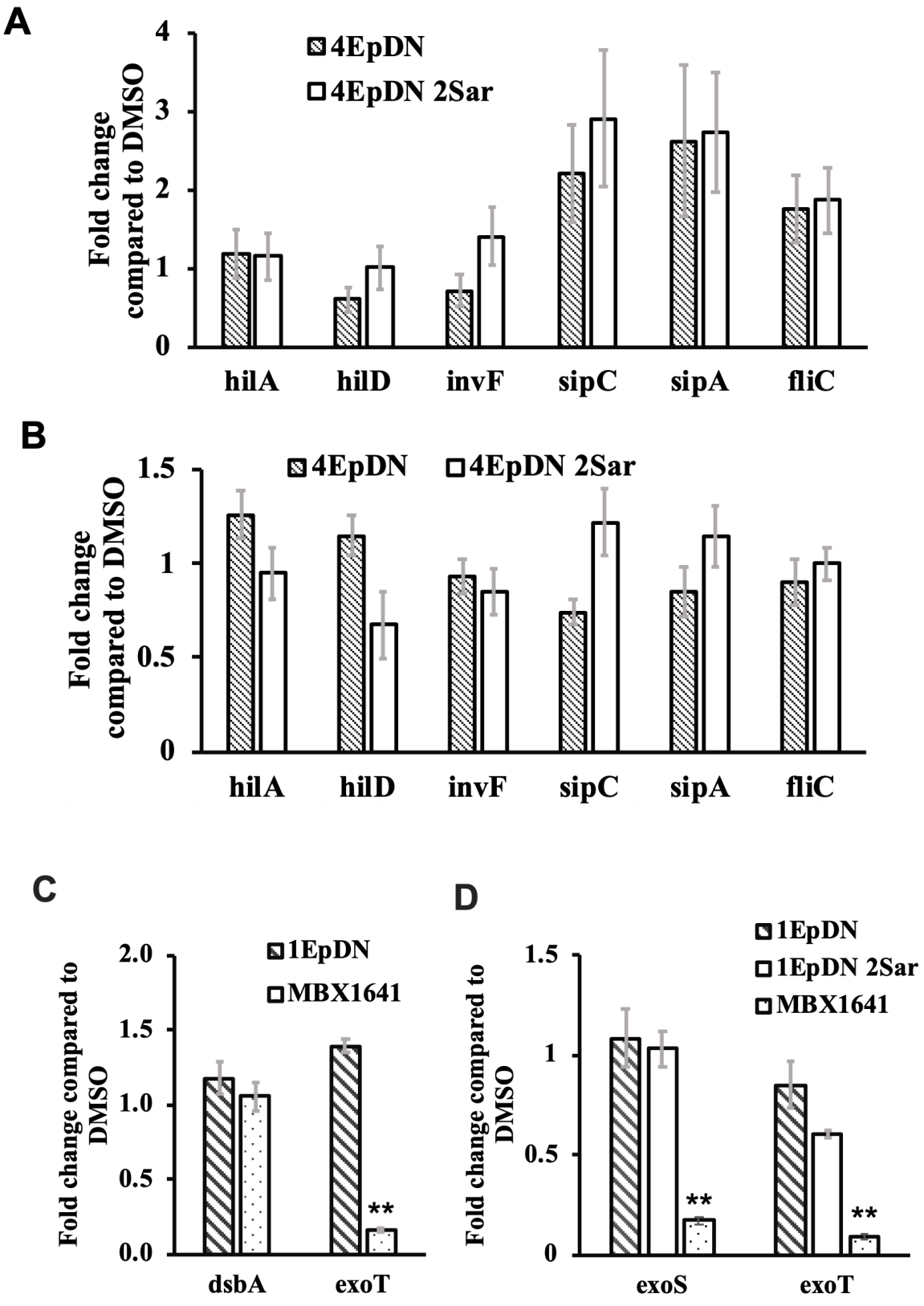
A
4EpDN
4EpDN 2Sar
Fold change compared to DMSO
0
1
2
3
4
hilA
hilD
invF
sipC
sipA
fliC
B
4EpDN
4EpDN 2Sar
Fold change compared to DMSO
0
0.5
1
1.5
hilA
hilD
invF
sipC
sipA
fliC
C
1EpDN
MBX1641
Fold change compared to DMSO
0.0
0.5
1.0
1.5
2.0
**
dsbA
exoT
D
1EpDN
1EpDN 2Sar
MBX1641
Fold change compared to DMSO
0
0.5
1
1.5
**
**
exoS
exoT

FIGURE S4.6. Cyclic peptomers do not affect transcription of T3SS genes in *Salmonella* and *P. aeruginosa*.

Salmonella enterica Typhimurium was grown in LB with 300 mM NaCl in the presence of 9 μM cyclic peptomers or DMSO. Samples were taken 2 hrs **(A)** and 4 hrs **(B)** after addition of compounds at 37oC and expression of flagellar (fliC) and injectisome T3SS (hilA, hilD, invF, sipC, sipA) genes were assessed using qPCR.

P. aeruginosa PA103 **(C)** or PA01 **(D)** was grown in low calcium media in the presence of 60M cyclic peptomers or DMSO. Samples were collected 3 hrs after induction for qPCR analysis. The phenoxyacetamide MBX1641, a known T3SS inhibitor predicted to inhibit type III secretion by binding to the T3SS needle subunit, was used as a control. Data are from two to three replicates, analyzed by one-way ANOVA with Dunnett's multiple-comparison test. **, $P < 0.01$.

FIGURE S4.7

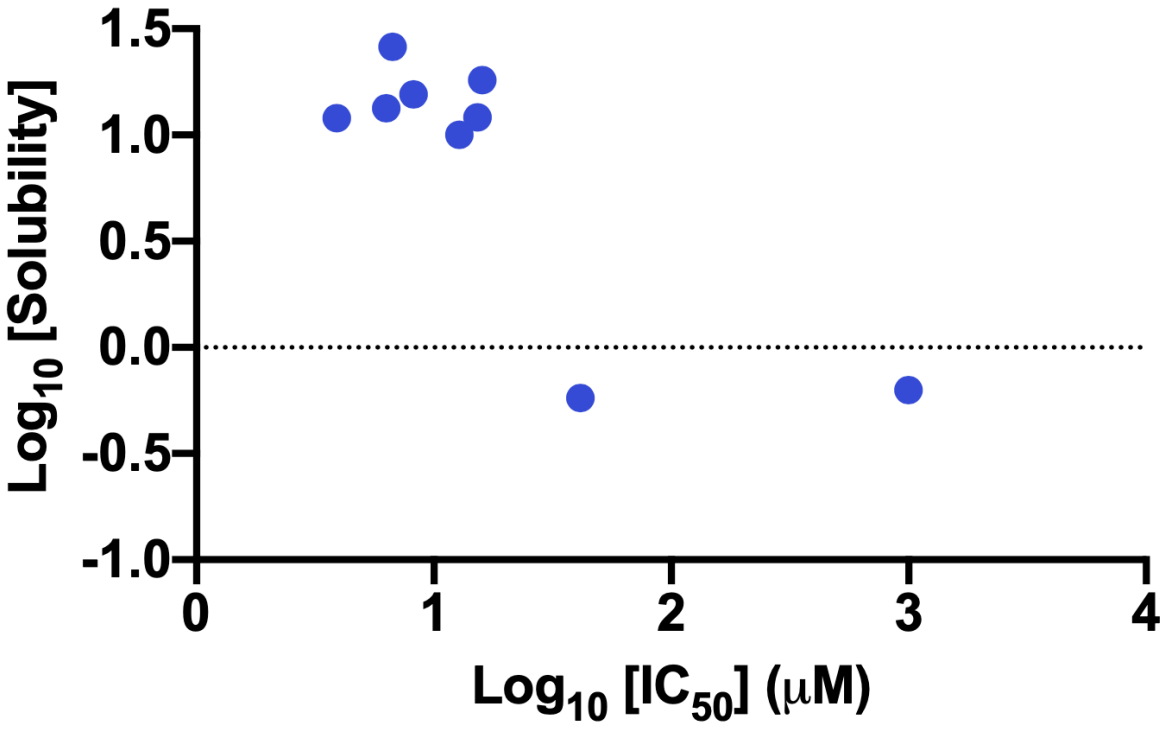

FIGURE S4.7. Relationship between solubility and activity of cyclic peptomers.

IC50 of stereoisomers and their solubility (table S1) were plotted on a log10 scale. Average solubility was used when the solubility was measured in different conditions.

FIGURE S4.8

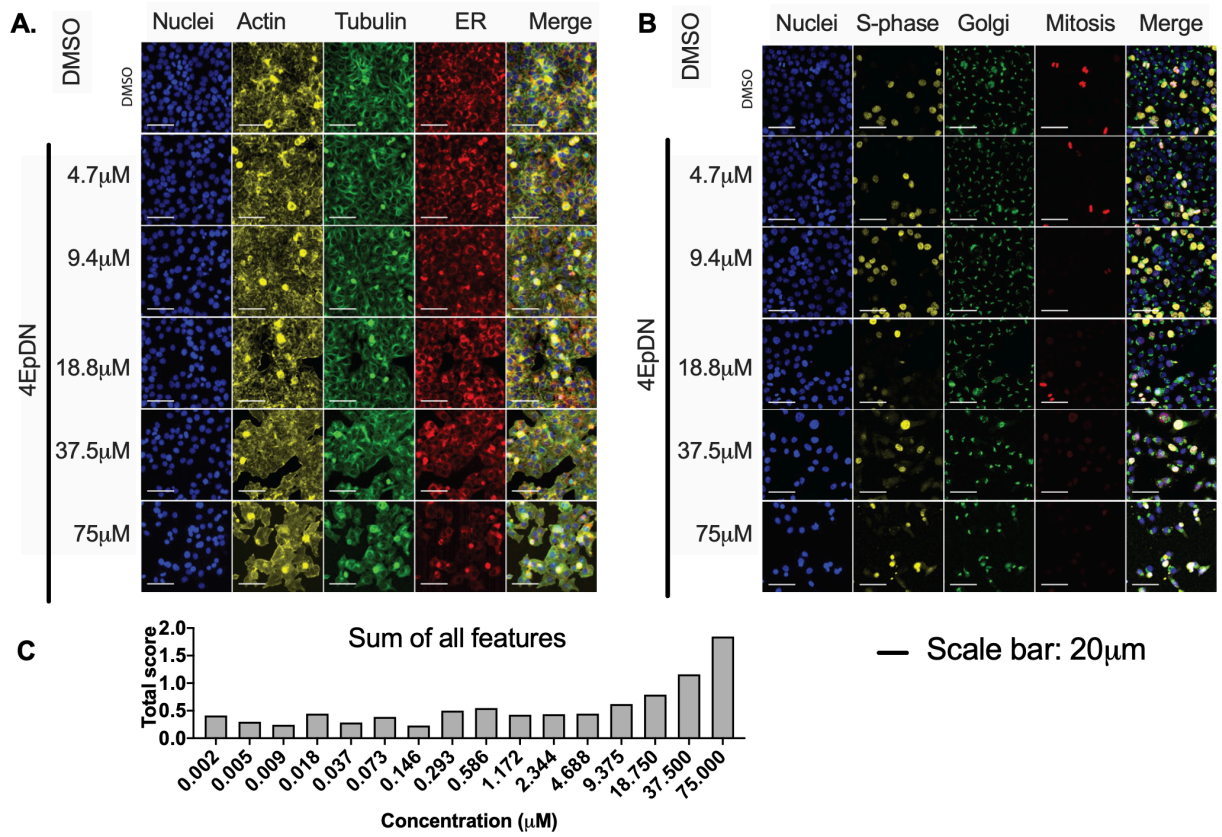

FIGURE S4.8. Effect of cyclic peptomers on HeLa cells.

HeLa cells were incubated with compounds for 48 hrs. Cells were then stained with: **(A)** Stain Set 1: Hoechst, FITC-alpha tubulin, rhodamine-phalloidin (actin), and Calnexin (ER induced protein); or **(B)** Stain set 2: Hoechst, EdU-rhodamine (S-phase detection), anti-Phosphohistone H3 (mitosis marker), and GM130 (Golgi matrix protein). Representative images of cells treated with different concentrations of 4EpDN or DMSO are shown.

(C) Quantification of all cell features for 4EpDN-treated cells. The total CP score is the square root of sum of square of the difference between treatment and DMSO for all measured features.

CHAPTER FIVE

CONCLUSIONS

“Coming back to where you started is not the same as never leaving.”
- Terry Pratchett

All *Chlamydia* species share a common dimorphic obligate intracellular life cycle that requires them to (i) gain entry into non-phagocytic host cells, such as the epithelial layers that line the genital tract, lungs, digestive system, and eyes, (ii) reprogram host vesicular trafficking pathways to avoid phagolysosomal fusion, access nutrients, and establish a protected robust replicative niche, (iii) avoid immune surveillance while maintaining host viability, and (iv) exit to disseminate (reviewed in Elwell et. al., 2016). *C. trachomatis* encodes approximately 100 secreted effectors, a surprisingly large number given its reduced genome (Betts-Hampikian & Fields, 2010; Stephens et al., 1998). The majority of these effectors are secreted by the needle-like type III secretion system (T3SS). In addition to the more canonical T3SS effectors that are translocated from the bacteria across the inclusion membrane to the host cell cytoplasm, *Chlamydiae* encode a unique class of T3SS effectors, the Inclusion membrane (Inc) proteins. These effectors are translocated across and inserted into the inclusion membrane at various times during infection, where they are ideally positioned to mediate host-pathogen interactions. The T3SS effectors, including the Incs, are likely critical for the success of *Chlamydia* in creating a unique replicative niche to survive in the hostile intracellular environment.

In this thesis work, we show how unbiased proteomic screens and targeted genetic manipulation of this pathogen have provided new insights into how *Chlamydia* subverts the host cell and causes disease. We have identified a *C. trachomatis* effector, Dre1, that binds host dynactin, not to facilitate intracellular transport of the pathogen, but rather to reposition organelles including the centrosome, mitotic spindle, and GA around the growing inclusion. Our data suggest that Dre1 binds dynactin complexes stably

associated with organelles that nucleate and organize MTs, and that Dre1 might target dynactin subpopulations that are specifically involved in mediating organelle positioning within the cell. This selectivity would allow *C. trachomatis* to override host mechanisms for organelle positioning and create a replicative niche without globally altering trafficking or organelle function. Our work highlights how a single pathogen effector can facilitate specific, large scale changes in host cell architecture by interacting with a single, ubiquitous host protein complex.

We used cross-linking mass-spectrometry to elucidate the molecular basis of Dre1:dynactin interaction in order and provide insight into the regulation and activities of this essential host protein complex. We have preliminary evidence that Dre1 binds to the actin-like filament of dynactin. This filament mediates interaction with the motor dynein, as well as various adaptors that specify cargo-binding and enhance processivity of the complex along MTs. We hypothesize that binding the interface between dynactin and various regulators provides the mechanism by which Dre1 discriminates different subpopulations or regulatory states of dynactin. As this project continues, it will shed light on the varied functions of this essential host protein complex and may provide the molecular basis by which a pathogen effector selectively subverts host processes.

Overall, this work highlights strategies by which C. trachomatis selectively engages with host cell pathways, structures, and proteins to establish and maintain its intracellular niche while maintaining host cell viability. Decoding how microbial effectors modulate host cell pathways has broad implications in cell biology and human disease.

REFERENCES

Betts-Hampikian, H. J., & Fields, K. A. (2010). The Chlamydial Type III Secretion Mechanism: Revealing Cracks in a Tough Nut. Frontiers in Microbiology, 1, 114. https://doi.org/10.3389/fmicb.2010.00114

Elwell, C., Mirrashidi, K., & Engel, J. (2016). Chlamydia cell biology and pathogenesis. Nature Reviews Microbiology, 14(6), 385–400. https://doi.org/10.1038/nrmicro.2016.30

Mirrashidi, K. M., Elwell, C. A., Verschueren, E., Johnson, J. R., Frando, A., Von Dollen, J., Rosenberg, O., Gulbahce, N., Jang, G., Johnson, T., Jäger, S., Gopalakrishnan, A. M., Sherry, J., Dunn, J. D., Olive, A., Penn, B., Shales, M., Cox, J. S., Starnbach, M. N., … Engel, J. (2015). Global Mapping of the Inc-Human Interactome Reveals that Retromer Restricts Chlamydia Infection. Cell Host & Microbe, 18(1), 109–121. https://doi.org/10.1016/j.chom.2015.06.004

Stephens, R. S., Kalman, S., Lammel, C., Fan, J., Marathe, R., Aravind, L., Mitchell, W., Olinger, L., Tatusov, R. L., Zhao, Q., Koonin, E. V., & Davis, R. W. (1998). Genome sequence of an obligate intracellular pathogen of humans: Chlamydia trachomatis. Science (New York, N.Y.), 282(5389), 754–759. https://doi.org/10.1126/science.282.5389.754

Publishing Agreement

It is the policy of the University to encourage open access and broad distribution of all theses, dissertations, and manuscripts. The Graduate Division will facilitate the distribution of UCSF theses, dissertations, and manuscripts to the UCSF Library for open access and distribution. UCSF will make such theses, dissertations, and manuscripts accessible to the public and will take reasonable steps to preserve these works in perpetuity.

I hereby grant the non-exclusive, perpetual right to The Regents of the University of California to reproduce, publicly display, distribute, preserve, and publish copies of my thesis, dissertation, or manuscript in any form or media, now existing or later derived, including access online for teaching, research, and public service purposes.

DocuSigned by:
Jessica Sherry
506053C660934E7...
Author Signature

9/2/2021
Date